AL-Kitab Journal For Pure Sciences

Volume : 6 (2022)

Issue: 2

ISSN: 2617-1260 (print)

ISSN: 2617-8141 (online)

DOI: http://10.32441/kjps

Deposit number at the Notional House of Books and Archives, Iraq, 2271 in 2017

Al-Kitab Journal for Pure Science

KJPS

ISSN: 2617-1260 (print), 2617-8141(online)
DOI: http://10.32441/kjps
https://isnra.net/index.php/kjps

An Academic Semi-Annual Journal

Volume: 6 Issue: 2 Dec. 2022

University Website: www.uoalkitab.edu.iq
Journal Website: https://isnra.net/index.php/kjps
E-mail: kjps@uoalkitab.edu.iq

Editors

Authors Guidelines

Rules and Instructions for Publication in Al-Kitab Journal for Pure Sciences

First: General requirements

1. The paper is submitted to the Editorial Secretariat directly in four copies with CD-ROM or E-mail of the magazine in MS Word and PDF files.
2. Research before being sent to scientific evaluators is subject to the quotation Turnitin program.
3. Research shall be accepted for publication after being judged by scientific evaluators and according to the rules.
4. The publication fee is (50$) for researchers from Iraqi Universities and (free of charge) for foreign researchers.

Second: To prepare research for publication, authors must follow the following procedures.

1. **The article:**

   The article needs to be typed on one side of A4 paper (Right margin =2.5 cm, left margin =2.5 cm, and 2cm for the top and bottom) with 1.5 space, and the pages must be numbered.

2. **The content organization:**

   MS Word is to be used as follows: "Simplified Arabic" font for the Arabic articles, and "Times New Roman" for the English articles. The Size of the title is 18 bold. The name of the authors will be typed in 11 bold in Arabic and 11 bold in English. Abbreviations, keywords, the main headings, the reference, and the acknowledgment will be typed in 14. Subheadings will be in 12 bold. The abstract will be size 12. The body of the article/paper is in size 12. The order of the content of the paper will be as follows: The article heading, the names of authors and their addresses, and the abstract (Both in Arabic and English).

3. **Research paper title:**

   The title must be as short as possible and indicates the contents of the subject together with the name (names) of the authors. The names of the authors to whom correspondence is to be made should be indicated with (*) and show his / her email.

4. **The size:**

The paper should contain no more than 15 pages of journal pages including charts and diagrams. Extra pages will be charged at (3$) each.

5. **Abstract:**

The abstract should include the purpose and the means of the founding results and the conclusions. It should also contain the knowledge values of the subject of research. It is meant to be no more than 250 words. It should also emphasize the content of the subject and includes the keywords used throughout the paper.

6. **Diagrams:**

Figures and diagrams must be given following the explanation referring to the diagram. Each diagram must contain its title below the diagram at the first size of 12. The diagram should be editable in terms of enlargement or reduction within the margins of the paper size. The parts of each diagram must be grouped into drawing parts.

7. **Tables:**

The tables should follow the parts of the main body and should be located below the indicated part of the text. Tables must have titles with a text size of 12. The text used inside the tables should be of size 12 and kept within the cells of the table.

8. **References:**

The references used in the paper must be given in order and their numbers given inside the square bracket [ ]. The following instructions are to be followed:

If the reference is a book, the First name of the reference must be given first followed by the other names. Then the title (bold and Italic) of the book, edition, year of publication, the publisher, and place of publication (year of publication).

Example: [1] P. Ring and P. Schuck, "**The Nuclear Many-Body Problem**", First Edition, Springer-Varlag, New York (1980).

(b) If the reference is a research paper or an article in a journal: The name of the author must be given first, the title of the article, the name of the journal, the volume (issue), page (Year). **Example:** [1] Ali H. Taqi, R. A. Radhi, and Adil M. Hussein, **"Electroexcitation of Low-lying Particle-Hole RPA States of ^{16}O with WBP Interaction"**, Communication

Theoretical Physics, 62(6), 839 (2014).

c) If the reference is an M.Sc. or Ph.D. thesis, the name of the anther must be written with the first name first followed by the surname, title of the thesis, the name of the university, and Country (Year).

Example: [1] R. A. Radhi, **"Calculations of Elastic and Inelastic Electron Scattering in Light Nuclei with Shell-Model Wave Functions"**, Ph.D. Thesis, Michigan State University, USA (1983).

(d) If the reference is from the conference. Authors Name, "**Paper Title**", Conference, Country, Publisher, volume, page (Year).

Example: [1] Ali H. Taqi and Sarah S. Darwesh, **"Charge-Changing Particle-Hole Excitation of ^{16}N and ^{16}F Nuclei"**, 3rdInternational Advances in Applied Physics and Materials Science Congress, Turkey, AIP Conf. Proc., 1569, 27 (2013)

Third: Privacy Statement

1. The names and e-mail addresses entered into the journal's website will be used exclusively for the purposes stated in this journal and will not be provided for any other purpose or to any other party.
2. The editor of the journal has the right to change any statement or phrase of the research content he may find necessary in order of expressing the work suitable to the general style of the journal.
3. After publishing the paper and its presentation on the journal page, the editors' team will destroy all the scrap papers. The author has no right to ask for them in any case.

Fourth: Modernity of sources:

The percentage of modern references used in the research should not be less than 50% of the total references used in the research. Modernity is measured within the last ten years of the year of submission of the research. For example, when submitting the research in 2018, the references should be from 2008 upwards and not less than 50%. The journal prefers to have at least one of the reference types of research published in the previous journal issues.

Note: For more information, visit:

Al-Kitab University Website: www.uoalkitab.edu.iq

Or Journal Website: https://isnra.net/index.php/kjps

The Journal can also be e-mailed to kjps@uoalkitab.edu.iq

Table of Contents

Volume: 6 Issue: 2 Dec. 2022

Al-Kitab Journal for Pure Sciences (2022); 6(2):1-13.

https://doi.org/10.32441/kjps.06.02.p1

Al-Kitab Journal for Pure Sciences
ISSN: 2617-1260 (print), 2617-8141(online)
www.kjps.isnra.org

Performance Evaluation of Dispersion Compensation Fiber-based Coherent Optical OFDM-WDM for Long Haul RoF

Raghad Zuhair Yousif *[1], Yazen Saifuldeen Almashhadani[2] , Basud Mohammed Rasool [1]

[1]Salahaddin University-Erbil, College of Science, Iraq.
[2]Gihan University, College of Engineering, Iraq.

*Corresponding Author: Raghad.yousif@su.edu.krd

Citation: Yousif R., Saifuldeen Y., Rasool B. Performance Evaluation of Dispersion Compensation Fiber based Coherent Optical OFDM-WDM for Long Haul RoF. Al-Kitab Journal for Pure Sciences (2022); 6(2): 1-13. DOI: https://doi.org/10.32441/kjps.06.02.p1.

Keyword
DCF, WDM, CO-OFDM, MZM, OFDM.

Article History

Received	25 July 2022
Accepted	21 Sep. 2022
Available online	03 Nov. 2022

Abstract:

Demanding extra Bandwidth and high data rates has been meet by the integration both of wired and wireless communication systems. For that the Radio over Fiber (RoF) technology has gained a traction. In this article a Coherent Optical Orthogonal Frequency Division Multiplexing (CO-OFDM) is proposed as the main wired system for transmitting data at high rates suffers from the polarization mode dispersion and chromatic dispersion of the optical channel which mitigates the data rates. Thus, to combat these limitations a Desperation Compensation Fiber (DCF) which adds negative attenuation to the optical signals transmitted in optical fiber is suggested. Moreover, the addition of Wavelength- Division- Multiplexing (WDM) to the system of transmission provides better bandwidth saving, high data rates, and better spectral efficiency, and power utilization. The efficiency of high data rate CO-OFDM integrated with RoF for long haul transmission between 100km and 450km with data rates up to 10 Gbps have been investigated in this article with SMF-DCF with 16 DPSK and 16-QAM modulations schemes

respectively. The simulation results showed that the proposed system can achieve a high data rate up to 55 Gbps but when integrated with WDM, with a fiber link length can be increased to up to 6600 kilometers, with highest data rate up to 1.65 Tbps.

Keywords: DCF, WDM, CO-OFDM, MZM, OFDM

تقييم أداء تعويض التشتت البصري لنظام الموجات الرادوية عبر الألياف البصرية لمسافات طويلة باستخدام نظام *OFDM-WDM* البصري

رغد زهير يوسف[1*], يزن سيف الدين المشهداني[2], بسود محمد رسول[1]

[1]جامعة صلاح الدين–أربيل كلية العلوم، العراق.

[2]جامعة جيهان كلية الهندسة، العراق.

*Corresponding Author: Raghad.yousif@su.edu.krd

الخلاصة:

المطالبة بنطاق ترددي إضافي ومعدلات بيانات عالية يتم من خلال تكامل كل من أنظمة الاتصالات السلكية واللاسلكية. لذلك اكتسبت تقنية الراديو عبر الألياف (RoF) قوة دفع. في هذه المقالة ، يُقترح تعدد الإرسال بتقسيم التردد البصري المتعامد المتماسك (CO-OFDM) باعتباره النظام السلكي الرئيسي لنقل البيانات بمعدلات عالية يعاني من تشتت وضع الاستقطاب والتشتت اللوني للقناة الضوئية مما يخفف من معدلات البيانات. وبالتالي لمكافحة هذه القيود ، يُقترح استخدام ألياف تعويض اليأس (DCF) التي تضيف توهينًا سلبيًا للإشارات الضوئية المرسلة في الألياف الضوئية. علاوة على ذلك ، فإن إضافة الطول الموجي - التقسيم - المضاعفة (WDM) إلى نظام الإرسال يوفر أفضل عرض النطاق الترددي ، ومعدلات بيانات عالية ، وكفاءة طيفية أفضل ، واستخدام للطاقة. تم التحقيق في كفاءة معدل البيانات المرتفع CO-OFDM المدمج مع RoF للإرسال لمسافات طويلة بين ١٠٠ كم و٤٥٠ كم بمعدلات بيانات تصل إلى ١٠ جيجابيت في الثانية في هذه المقالة باستخدام SMF-DCF مع مخططات تعديل DPSK١٦ و١٦-QAM على التوالي. أظهرت نتائج المحاكاة أن النظام المقترح يمكنه تحقيق معدل بيانات مرتفع يصل إلى ٥٥ جيجابيت في الثانية، ولكن عند تكامله مع WDM ، يمكن زيادة طول ارتباط الألياف إلى ٦٦٠٠ كيلومتر ، مع أعلى معدل بيانات يصل إلى ١,٦٥ تيرا بايت في الثانية.

الكلمات المفتاحية: ألياف تعويض التشتت، إرسال متعدد بتقسيم طول الموجة، تعدد الإرسال بتقسيم متعامد بصري متماسك، المضمن البصري ماخ – مازندر، مضاعفة قسم التردد المتعامد.

1. INTRODUCTION:

As the internet's data traffic grows, data transmission rates over optical fiber networks must increase, from 1-Gb/s to 10-Gb/s to today's 1 Tb/s. The internet has been steadily expanding, and to meet the demand for bandwidth [1]. To overcome losses in a transmission medium,

scientists developed a medium with low attenuation and no electromagnetic interference by adding DCF because it's ability to combat the chromatic dispersion and polarization mode dispersion problems. To combat the problem of long-haul transmission the CO-OFDM is suggested. In addition, the use of WDM is to increase the bandwidth utilization. As a result, the first goal of this article is to investigate the performance of integrated CO-OFDM with RoF framework for a single user[2]. The second goal is to determine the best form of dispersion compensation fiber (DCF) to compensate for fiber connection losses, and the third goal is to achieve long-haul transmission over a distance up to 6600 kilometers based on pervious system elements described in the first and second goals based on Opti system 14 software. Finally, the fourth goal is to look into the rendering of the proposed CO-OFDM WDM system along to RoF for long haul transmission over distances of up to 6600km and data rates of up to 1.65Tbps. The analysis of the comprehensive proposed system is based on the construction of a constellation diagram for both transmitter and receiver, along with studying the relationship between Q - Factor and input power, as well as finding the relation between RF signal power and optical fiber length. Furthermore, the influence of optical fiber length on the Optical Signal to Noise Ratio (OSNR) and Bit Error rate (BER) were depicted. The literature review begins with a transmitted OFDM modulated radio signal over SMF (Wong 2012). (Single Mode Fiber). Then, using CO-OFDM and WDM RoF, multiple RF signals were modulated and multiplexed. The device is capable of transmitting data at up to 10 Gbps using 4-QAM (2-bits per symbol for each channel) and OFDM. Wong demonstrates that as the higher the fiber transmission distance, the transmitted signal power is reduced[3]. On the other side, Almasoudi in 2013, looked at high data rates of RoF for long-haul optical fiber. It has been demonstrated that RoF is a powerful tool for mitigating chromatic dispersion, polarization mode, and modal dispersion, resulting in increased versatility and coverage area with reasonable device complexity and expense, as well as high data rates up to 1.4 Tbps and transmission distances of 6600 km [4]. Atta Takhum Jaber and colleagues, in 2020. For long path transmissions, a comprehensive solution of higher data rates using Direct and CO-OFDM was proposed. In this study a single user was investigated, along with multiusers by integrating OFDM – WDM which leads to attain a data rate up to 100 Gbps. The Opti system simulation tool was used for the system's design and implementation. The OFDM signal is modulated with QAM, and I/Q modulation was used, with Coherent and Direct detection used at the receiving end. Saifur Rahman et al. in 2020 stated (RoF) transport-based fronthaul as efficient candidate for C-RAN framework, but the related issues of nonlinear impairments (NLIs) from power amplifiers, linear distortions (LDs) from modulating lasers, and high peak to average power ratio (PAPR) of (OFDM) signals

must be Alatawi et al. in 2013tackled. Thus a variety of input power values, different (QAM) formats for the OFDM signal, high accuracy filtering at the receiver end, and varying channel spacing among the optical WDM channels have been employed[5]. Adnan Hussein et al in 2019, proposed in their article uses an integrated CO-OFDM and WDM schemes to transmit and receive data streams across a long distance through the optical fiber and optimized the constellation diagram by testing various modulation schemes[6]. Alatawi et al. in 2013 proposed a study for the performance of direct detection optical orthogonal frequency division multiplexing (DD-OFDM) along with (WDM) was proposed by [7]. The proposed system succeeded to attain 1050 Tb / s over distance of 3600 km using a Single Mode Fiber (SMF) by multiplexing 30 signals of OFDM, each with 35 Gb / s. Almasoudi et al, in 2013 used RoF in the case of Passive Optical Network (PON) with SMF in the last mile of a wireless system with 100 km, 140 km, and 288 km[8]. Almashhadani et al 2017, pointed out the influence of the cyclic prefix and the length of the cyclic prefix on the OFDM system. Also, compared the system's performance with and without the cyclic prefix. The simulations ran on AWGN and Rayleigh fading channels marked the importance of cyclic prefix[9]. Aloff in 2014 had simulate (CO-OFDM). compared the two systems by simulating the (DD- OFDM) and (CO-OFDM) using the same parameters as before. Then, he realized that increasing optical fiber length must be done by using Dispersion Compensating Fiber (DCF)[10].By multiplexing four 12Gbps OFDM channels over more than 80km from (SMF), Das and Zahir in 2014 investigated a hybrid system made up of (CO-OFDM) and (WDM-RoF) with DCF technique to achieve a 48Gbps for a distance up to 80km from (SMF). A Fiber Bragg Grating (FBG) has been applied to this device proposal to counteract the effect of dispersion. By comparing the Q-factor, BER, and constellation diagram of CO-OFDM/WDM-RoF systems with and without FBG, it was determined that using FBG in the CO-OFDM/WDM-RoF system dramatically improves system efficiency[11]. Sarup and Gupta in 2014 showed how to use the RoF method in synchronism with the dense wavelength division multiplexing (DWDM) technique to increase the system band width and achieve ultra-high-speed communication. With a 40-channel DWDM-RoF system, each channel transmits 25 Gbps, and hence the overall speed attained is 1Tbps with different wavelengths of 0.1 nm and 0.2 nm. The Erbium Doped Fiber Amplifier (EDFA) and Semiconductor Optical Amplifier (SOA) were used to achieve highly narrow channel spacing. When used as a post amplifier, SOA is found to perform linearly and better than EDFA[12]. Abdul-Rahaim, Murdas, et al. in 2015 demonstrated a Polarization Division Multiplexing Coherent Optical Orthogonal Frequency-Division Multiplexing (PDM CO-OFDM) scheme with the modulation formats of (QPSK and 16-QAM) at bit rates of 40 and 100 Gb/s. To

investigate the output, the device is essentially simulated assuming a single channel. After that, 8 WDM channels with 50 GHz channel spacing were simulated. PDM CO-OFDM QPSK was recommended for high-capacity networks because of its superior efficiency. Because of the advantages of PDM CO-OFDM 16-QAM (improved spectral performance, reduced electrical bandwidth), the optimal input power is reduced. At a maximum distance of 1760 km, the single channel's optimum input power was -4dBm and -1dBm. The 8-WDM system's optimum input power was between -8dBm and -4dBm**[13]**. Sinan M. Abdul Satar, in 2015 investigate the use of a (CO-OFDM) system with (DWDM) and the achievement of 1.60 Tb/s data rates over a 4500 km SMF by multiplexing 16 CO-OFDM signals, each of 100 Gb/s**[14]**. According to Pawar and Umbardand in 2016), a rate of 100Gb/s for fiber length of 360 km using (SMF), can be achieved when (CO-OFDM) combined with Dual –Polarization Quadrature Phase Shift Keying (DP-QPSK) modulation**[15]**. M. Sofien et al. in 2018 have examined many regression methods for fiber non-linearity mitigation**[16].** The remainder of this work is structured as follows. Section 2 Proposed WDM CO-OFDM-ROF with Dispersion Compensation Fiber; Section 3 Results and Calculations; Section 4 Comparison with peer Literatures ; Finally, conclusions are brought in Section 5.

2. Proposed WDM CO-OFDM-ROF with Dispersion Compensation Fiber

Fig. 1. shows the proposed system named WDM CO-OFDM RoF with SMF-DCF. The First stage from the proposed scheme is pseudo random binary sequence (PRBS) which generates semi-random binary data stream which modulated using QAM modulator. The modulated signal is then converted from serial to parallel to frame of 512 subcarriers and 1024 Fast Fourier Transform (FFT) points OFDM modulator. Then the output of OFDM modulator include two types of signals, the in - phase(I) and quadrature phase(Q) signals are modulated by optical I/Q modulator which consists of two Mach-Zehnder (MZM) lithium Niobate (LiNb) modulators using an optical carrier. The output of each CO-OFDM system is then transmitted via one of the available channels of (WDM). Thus, the capacity of the overall is improved. The WDM maps the optical spectrum into smaller channels, employed to transmit and receive data simultaneously. Due to available very high-speed electronics, the WDM can support up to 55Gbps for each channel. The multiplexed optical signal resulted from WDM MUX is transmitted via SMF-DCF. In the optical channels, DCF can be used for fiber dispersion compensation, and an (EDFA) is being used for the signal amplification and for compensate the losses. At recover side the WDM DEMUX is split the received optical signal through the

optical fiber into multiple wavelengths and make each wavelength is manipulated by its receiver which is to be designed. The signals that resulted from the MZMs (optical demodulators) are then provided to the OFDM demodulator before it demodulated by QAM demodulator. Eventually the original digital signals are reconstructed. The parameters used in this article simulation have to be summarized in the next part. Thus, the optical link used in this research is SMF with the nonlinearity coefficient of 2.6 * 10−20 and 0.2dBm/km the attenuation per kilometer.

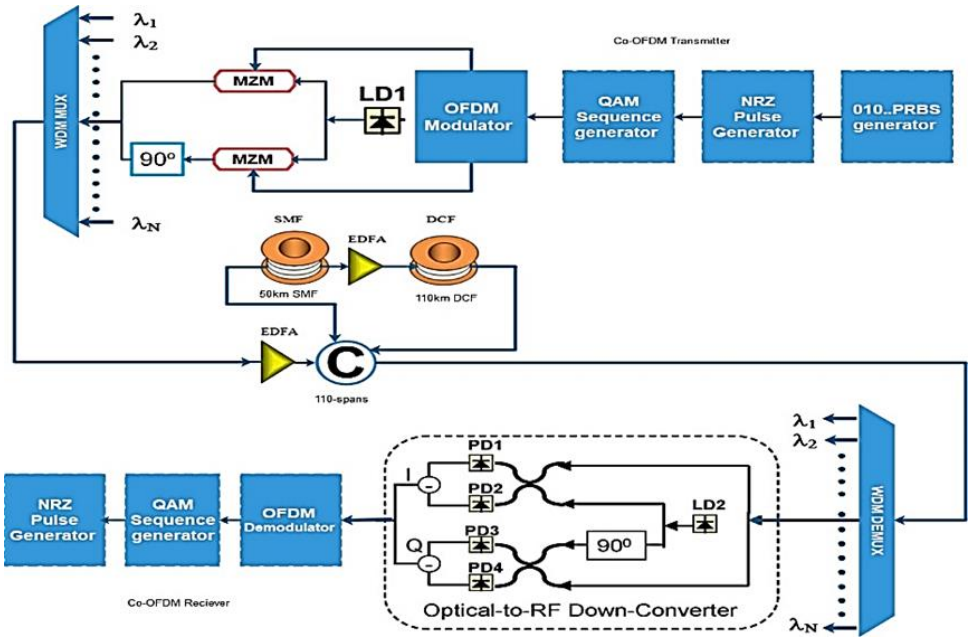

Fig. 1: CO-OFDM WDM RoF system with SMF-DCF (Block diagram).

The dispersion factor is 16 ps/nm/km with slope of 0.08ps/nm ^{2}/km while the DCF attenuation is assumed to be 0.4dB/ km. To amplify the optical power signal, the (EDFA) can be employed on the SMF link. The resulting filtered optical signals from the two LiNb MZM are Subsequently transmitted via SMF-DCF. Thus, a 50 km length SMF fiber will result in a dispersion of 16 × 50 = 800ps/nm. Consequently, a 10 km long of DCF with a dispersion factor -80 ps / nm / km is required to combat the dispersion of 50 km SMF length yielding a dispersion of 80 × 10 = 800ps/nm. An EDFA employed has a power gain of 20 dB power. Then a pair of local oscillators (LO) behave as a balanced coherent detector exploited for I/Q optical- to electrical conversion and for canceling the noise of the optical signal contaminated. Each detector is made up of pair of couplers with pair of PIN photodetectors with a 10 nA of the current, 1 A/W responsively, and 10×10^{-24}W/Hz of the thermal noise. In the proposed system, up to 1.65Tbps rate has been attained by multiplexing thirty CO-OFDM channels. The optical

carrier which has a laser frequency begins from 193.05 until 194.5 THz. It's up to1.65 Tbps generated by multiplexing thirty OFDM channels and optical carrier with laser frequency begins from 193.05 until 194.5 THz. **Fig 2.** shows the structure of each OFDM channel while **Fig.3** shows the multiplexed CO-OFDM channels spectrums (after being multiplexed by WDM). The spectrum starts at 193.05 THz up to 194.5 THz with 50GHz of the channel guard band.

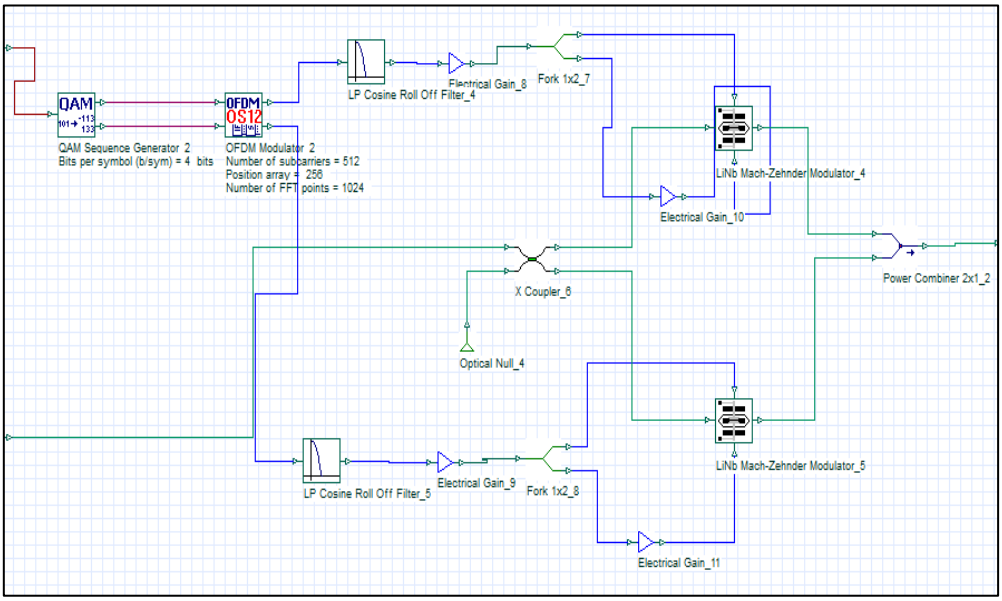

Fig.2: CO-OFDM Channel structure.

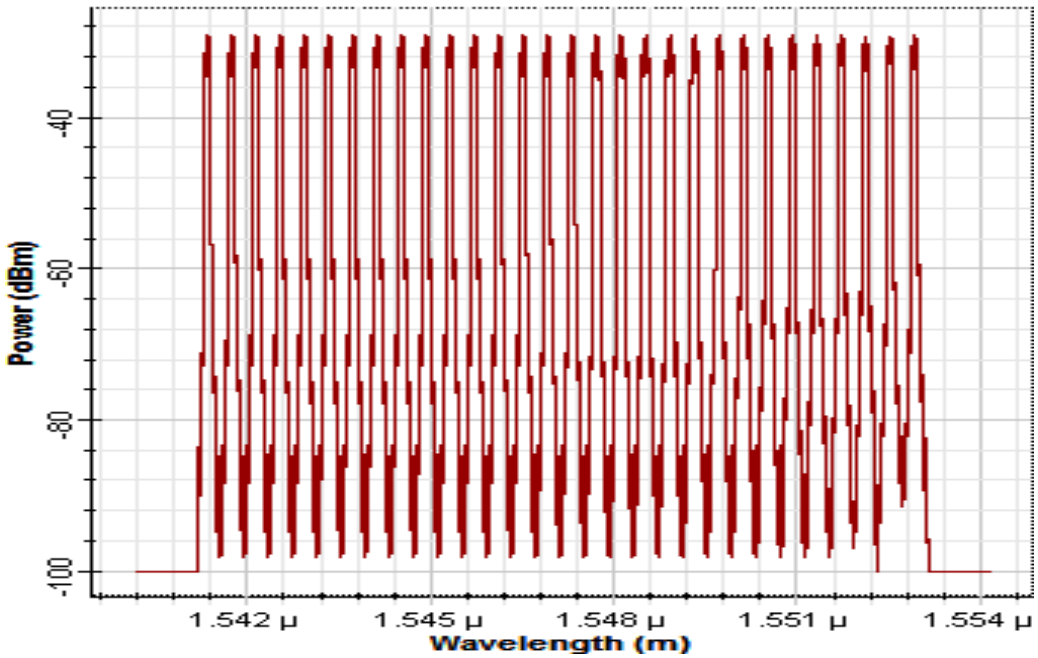

Fig. 3: A 30 CO-OFMD multiplexed channel spectrum at the output of WDM.

3. Results and Calculations

The simulation results are mainly divided in to two parts: the first part depicts the results of CO-OFDM RoF with dispersion compensation fiber. Whereas the second part illustrates the results of the proposed system.

Part A

Fig 4 shows the relation between input power in dBm and the Q-factor. It's clear that input laser power, and Q-factor values are directly related, hence the signal power increased at the receiver end, but after exceeding 5dBm (input power at which the Q-factor is maximum) the system performance begin to decline with grow happened in input power.

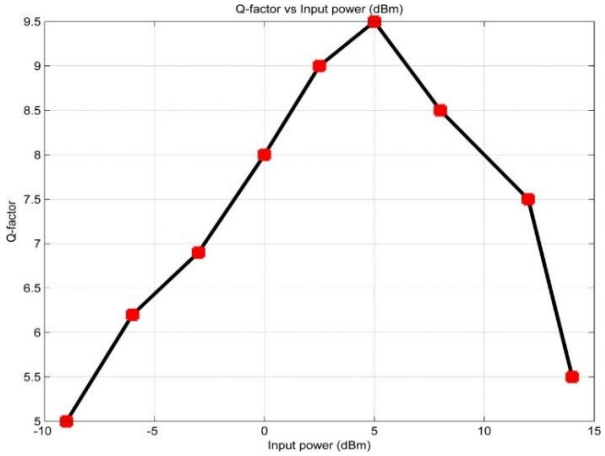

Fig. 4: Input power vs to Q-Factor.

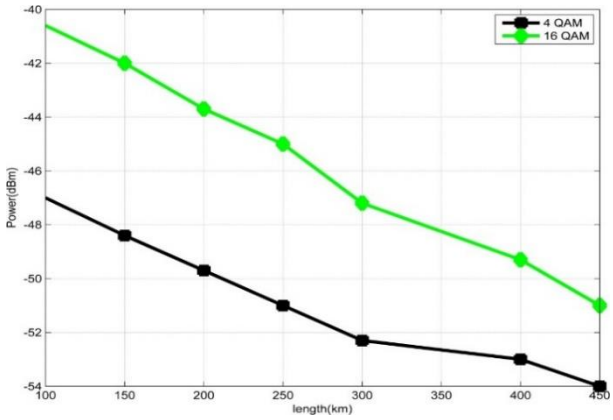

Fig. 5: Power versus the length of optical fiber.

The received power for 4-QAM and 16-QAM respectively with OFDM technique versus fiber length is depicted in **Fig. 5**. As the length of fiber increases the RF power decreases. The RF signal power with 16-QAM is higher than the RF signal power for this system using 4-QAM. It can be concluded that There is a direct relation between the RF signal received power value with the level M-ary QAM selected for the same bit error rate. **Fig 6** shows that both of symmetrical and post configuration give a comparable result in case of relatively short fiber distance but as distance increases above 100km (long distance) post configuration is preferable. Using DCF along with SMF mitigates the distortion level on the propagated optical signal for a longer SMF length. By investigation **Fig. 6** which depicted the relation between Q –factor and fiber length for different DCF types. It's clear that the quality factor (Q-factor) of 12 can be achieved at fiber length doesn't exceed 50 km without using fiber while the same Q-factor

can be achieved at fiber length of 140km, 200 km,225 km corresponding to pre DCF, symmetrical DCF, post DCF respectively before noticing any reduction in Q-factor values.

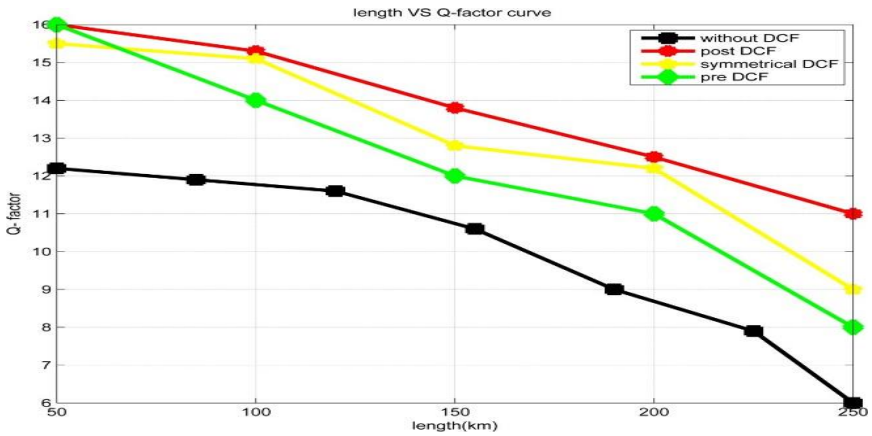

Fig. 6: The Variation in Q-Factor.

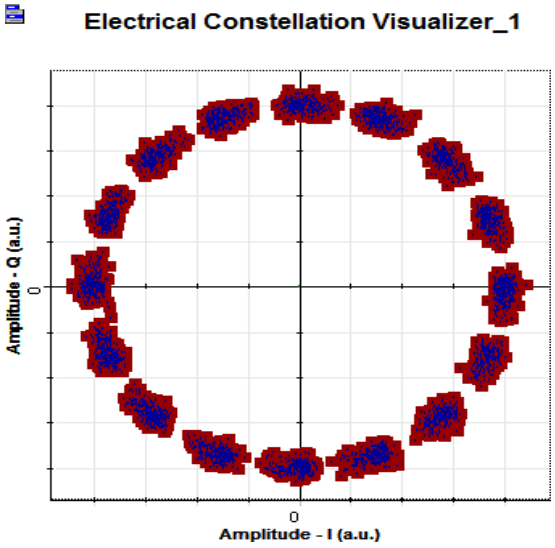

Fig. 7: Constellation diagram of 16-DPSK.

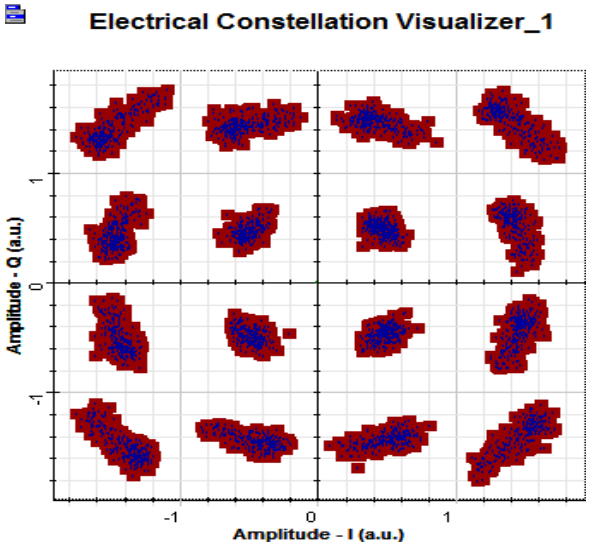

Fig. 8: Constellation diagram of 16-QAM

Part B

In this part, the performance CO-OFDM-RoF integrated with WDM and DCF would be investigated. From simulation results it's found that the maximum data rate of 1.65 Tbps can be attained over 6600 SMF- DCF, considering 16-DPSK, and 16-QAM modulation schemes. Thus, **Fig.7** illustrates the constellation diagram of 16-DPSK based system taking place on the receiver side for 6600 km fiber length with SMF-DCF, whereas **Fig.8** depicts that the constellation diagram of 16-QAM based system revived signal with 6600 km fiber length employing SMF-DCF. From these two **Figures (7,8)** it's obvious that achieving a 1.65Tbps rate it was possible by using 30-channels (Dense Wavelength Division Multiplexing) DWDM

integrated with 16-QAM modulation which outperform the 16-DPSK modulator by reducing the noise and distortion levels. **Fig.9** shows the relation between BER with different transmission distances. It's clear from **Fig.9,** that the BER has been declined as increasing the transmission distance, hence increasing the fiber length to cover longer distance come with the cost of increasing fiber loss. **Fig.10** demonstrates the behavior of the BER related with the OSNR considering different distances of transmission. From this figure an inverse relation between the OSNR and the BER has been discovered, so to attain a BER less than 10−13, the OSNR must be raised to 55 dB with transmission distance 6600 km while for transmission distance of 3120 km OSNR must be greater than 46dB which is 16 dB less than transmission distance 6600 to achieve BER less than10−14. However, the OSNR increment must be compromised with the input power increment, because any increase in the input power will results of increasing in the nonlinear effect of the fiber which lead to detritions in system

performance.

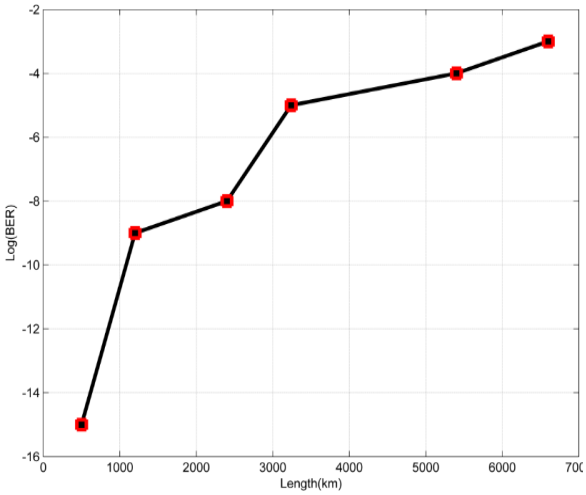

Fig.9: BER vs. transmission distance for 1.65Tbps data rate.

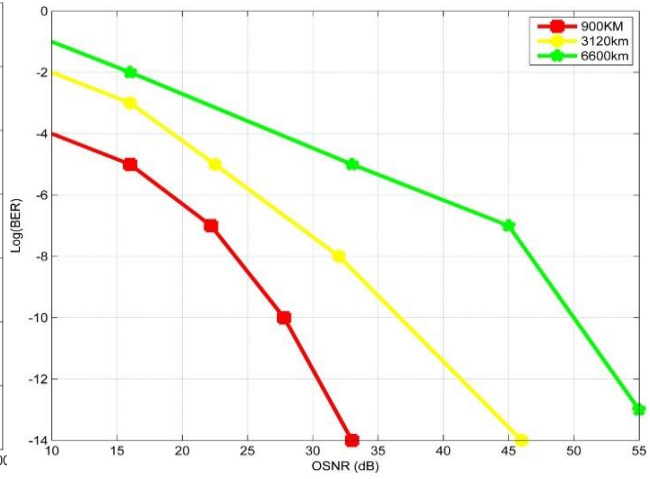

Fig 10: BER vs. OSNR for different transmission distances at 1.65Tbps data rate.

4. Comparison with peer Literatures:

To compare the proposed system model with other articles such as the thesis of khaled alatawi **[5]**. Our proposed system successes to transmit data up to 6600 km rather than that proposed by alatawi which was 6000 km, using 16-QAM compared to alatawei he had used 4-QAM. The proposed system has obtained higher data rate of 1.65Tbps, while in Khaled Alatwi's

article only 1Tbps has been attained. **Table 1** shows the distance gain and rate gain proposed by the proposed model compared to alatawei.

Table 1: Comparison present work to other articles

Author/year	Types of QAM	Types of OFDM	Maximum transmission distance	Maximum data rate
Ass. Prof. Dr. sinan	16 QAM	CO-OFDM	6600 km	1.65 Tbps
M. Abdul Satar/2015	64 QAM	CO-OFDM	4500 km	1.6 Tbps
Aloff, N.M.A,2014	4 QAM	CO-OFDM and OOFDM	6600 km	48 Gbps
Fahad Mobarak Almasoudi/2013	4 QAM	DD-OFDM	6600 km	1.4 Tbps
Alatawi. K. S. (2013)	4 QAM	CO-OFDM	6000 km	1 Tbps
Alatawi, Almasoudi et al.2013)	4 QAM	CO-OFDM	1800 km	1 Tbps

5. Conclusions

In the case of a single user system, it is concluded that rising the input the power from -9dBm to 5 dBm leads to distortion mitigation and hence improving the Q-factor of received signal. But after 5dBm the relation is inversed such that a deterioration of the transmitted signal has been observed which corresponds to disprove in Q-factor. There is a direct relation between the positive dispersion is and the transmission distance. Increasing the number of spans till 450km leads to increasing received signal distortion due to broadening of the sent signal caused by signal dispersion for long distance besides the increasing fading due to channel attenuation. With transmission distance up to 550 km SMF employing EDFA power of 60 dB and in case if the power gain of EDFA is increased beyond 60 dB, the received signal distortion level doesn't improve. Thus, the power gain of the EDFA cannot improve the quality of the signal over SMF length beyond 550km since it cannot compensate for the power loss. It's observed that the amount of distortion in the transmitted signal is decreased using DCF as compared to the case of without DCF; also, the type of DCF has its effect on transmitted signal distortion. It's clear from the results that post compensation gives better results as compared to pre or symmetrical compensation. Symmetrical and post configuration gives a comparable result in case of relatively short distance but as distance increases above 100km (long distance) post configuration is preferable. By using DWDM (Multiuser system), in applying 16-QAM the data rate of the system is improved from 10 Gbps to 55 Gbps whereas in using of 4-QAM the high data rate of 55 Gbps cannot be supported. The signal is distorted and corporate due to the high

data rate even if the EDFAs power is increases. So, the signal does not improve. Using DWDM is the main reason for increasing the system capacity and attaining high rate up to 1Tbps compared with a single user rate which is less than 65Gbps. Therefore. In this research, a data rate of 1.65 Tbps over 6600 km has been achieved by multiplexing 30-channel. These results showed a good performance curve between OSNR and BER. The system gives superior performance in term of very low BER of 10^{-13}at OSNR of 55 dB. Finally, the resulting data verified the superiority in the performance of CO-OFDM WDM-RoF in attaining higher data rates. The proposed system successes to transmit data up to 6600 km rather than that proposed by Alatawi **[17]**which was 6000 km, using 16-QAM compared to alatawei he had used 4-QAM.We achieve higher data rate up to 1.65 Tbps while in khaled alatwi the maximum rate was 1Tbps. Also, the proposed system outperforms the results conducted by Dr. Sinan M. Abdul **[14]**which was attained a data rate 1.6 Tbps but with shorter transmission length of 4500 km.

References

[1] A. Sano *et al.*, "102.3-Tb/s (224 {\texttimes} 548-Gb/s) C- and Extended L-band All-Raman Transmission over 240 km Using PDM-64QAM Single Carrier FDM with Digital Pilot Tone," in *National Fiber Optic Engineers Conference*, 2012, p. PDP5C.3.

[2] A. T. Jaber, S. S. Ahmed, and S. A. Kadhim, "Next Generation of High-Speed Optical Communications Networks Using OFDM Technology," *J. Phys. Conf. Ser.*, vol. 1591, no. 1, 2020.

[3] S. W. Wong, "Development of OFDM in WDM-radio over fiber access network." Universiti Tun Hussein Onn Malaysia, 2012.

[4] A. Khaled, "High Data Rate Coherent Optical Ofdm System for Long Haul Transmission," *Thesis*, no. November, 2013.

[5] S. Rahman *et al.*, "Mitigation of nonlinear distortions for a 100 gb/s radio-over-fiber-based wdm network," *Electron.*, vol. 9, no. 11, pp. 1–17, 2020.

[6] A. H. Ali, H. J. Alhamdane, and B. S. Hassen, "Design analysis and performance evaluation of the WDM integration with CO-OFDM system for radio over fiber system," *Indones. J. Electr. Eng. Comput. Sci.*, vol. 15, no. 2, pp. 870–878, 2019.

[7] K. Alatawi, F. Almasoudi, and M. Matin, *Performance Study of 1 Tbits/s WDM Coherent Optical OFDM System*, vol. 03. 2013.

[8] F. M. Almasoudi, "Integration of OOFDM with RoF for High Data Rates Long-Haul Optical Communications," 2013.

[9] Y. Almashhadani, H. Alqaysi, and G. Qasmarrogy, "Performance Analysis of OFDM with Different Cyclic Prefix Length," no. July, 2017.

[10] A. Aloff and N. Mansor, "Coherent OFDM for Optical Communication systems," 2014.

[11] S. Das and E. Zahir, "Performance Evaluation of WDM-ROF System Based on CO-OFDM using Dispersion Compensation Technique," *Int. J. Electron. Electr. Comput. Syst.*, vol. 3, pp. 7230–7236, 2014.

[12] V. Sarup and A. Gupta, *Performance analysis of an ultra high capacity 1 Tbps DWDM-RoF system for very narrow channel spacing*. 2014.

[13] L. Abdul-Rahaim, *Performance of Coherent Optical OFDM in WDM System Based on QPSK and 16-QAM Modulation through Super channels*, vol. 5. 2015.

[14] S. M. A. Satar, M. J. Abdul-Razzak, and M. M. N. Abdul-kareem, "Coherent Optical-OFDM using 64QAM to high data rates 1.60 Tb/s over 4500 km," *Int. J. Sci. Res. Publ.*, vol. 5, no. 9, p. 1, 2015.

[15] V. Pawar and A. U. Umbardand, "Performance evaluation of high speed coherent optical OFDM system," *Int. J. Curr. Trends Eng. Res.(IJCTER)*, vol. 2, no. 7, pp. 129–142, 2016.

[16] R. S. Asha, V. K. Jayasree, and M. Sofien, "Chromatic Dispersion Compensation in 80Gbps Ultra High Bit Rate Long-Haul Transmission with Travelling Wave Semiconductor Optical Amplifier," 2018.

[17] K. Alatawi, "High Data Rate Coherent Optical OFDM System for Long-Haul Transmission," 2013.

Al-Kitab Journal for Pure Sciences
ISSN: 2617-1260 (print), 2617-8141(online)
www.kjps.isnra.org

Uterine artery pulsatility index among polycystic ovary disease; case control study

Salah Mohi Salih*, Sarab K. Abedalrahman, Usama Nahi Hamdi

Salaheddin Health Directorate -Iraq.

*Corresponding Author: sara.k.abed@gmail.com

Citation: Salih S. M., Abedalrahman S. K., Hamdi U. N. Uterine artery pulsatility index among polycystic ovary disease; case control study. Al-Kitab Journal for Pure Sciences (2022); Doi: https://doi.org/10.32441/kjps.06.02.p2 .

Keyword
Uterine artery pulsatility index in PCOS; case control study, Uterine artery pulsatility index in PCOS.

Article History

Received	20 Aug. 2022
Accepted	25 Sep. 2022
Available online	15 Nov. 2022

Abstract:

Introduction: Polycystic ovarian syndrome is a multiple organ disorder affects 5 to 10 % female population. The world occurrence of PCOS is 105 million in the age ranges from 15 to 45. The polycystic ovarian syndrome is a set of disorders like amenorrhea, infertility, polycystic ovaries, hyperinsulinemia, hirsutism, acne vulgaris and other symptoms of hyperandrogenism. Color Doppler and Pulse Doppler play a major role in evaluation of uterine artery Resistive index for access correlation with PCOS. PCOS patients suffer from primary and secondary infertility. This study aimed to show assess uterine blood flow and whether there is a correlation between these patterns and specific hormonal parameters.

A case control study done in Salah Al-Deen governorate during the period of 1st May–1st October 2022. Twenty-five patients with polycystic ovary disease compared with 25 normal healthy women. The ultrasound and Doppler analyses were performed for all women during the

follicular phase of the menstrual cycle. Uterine artery blood flow velocities were analyzed and the pulsatility index, were calculated .

The current study showed that oligomenorrhea found among (72%) of the patients, clinical/biochemical signs of hyperandrogenism found among (76%). The mean LH (mIU/L) was significantly higher among PCO disease cases and also that the mean FSH (mIU/L) was significantly lower among PCO disease cases than control group. There was at increased ovarian volume of > 10 cm3 found among (80%), and ≥12 follicles measuring 2-9 mm found in (84%) of the PCO disease patients. The mean Uterine artery PI was significantly higher among PCO disease cases 2.3 ± 0.5 than control group 1.8 ± 0.4 (P value <0.05).

The mean ovarian volume was significantly higher among PCO disease cases than control group. The mean Uterine artery PI was significantly higher among PCO disease cases than control group.

Keywords: PCOS, uterine resistant index, RI, Doppler study of polycystic ovary.

مؤشر نبض الشريان الرحمي بين مرض تكيس المبايض. دراسة الحالات والشواهد

صلاح محي صالح *, سراب قحطان عبد الرحمن, أسامة ناهي حمدي

دائرة صحة صلاح الدين ، العراق.

*Corresponding Author: sara.k.abed@gmail.com

الخلاصة:

متلازمة تكيس المبايض هي اضطراب متعدد الأعضاء يصيب ٥ إلى ١٠٪ من الإناث. يبلغ معدل حدوث متلازمة تكيس المبايض في العالم ١٠٥ ملايين في الفئة العمرية من ١٥ إلى ٤٥. متلازمة تكيس المبايض هي مجموعة من الاضطرابات مثل انقطاع الطمث ، والعقم ، وتكيس المبايض ، وفرط أنسولين الدم ، والشعرانية ، وحب الشباب ، وأعراض أخرى لفرط الأندروجين. يلعب دوبلر اللون والدوبلر النبضي دورًا رئيسيًا في تقييم مؤشر مقاومة الشريان الرحمي من أجل ارتباط الوصول مع متلازمة تكيس المبايض. يعاني مرضى متلازمة تكيس المبايض من العقم الأولي والثانوي. هدفت هذه الدراسة إلى إظهار تقييم تدفق الدم في الرحم وما إذا كان هناك ارتباط بين هذه الأنماط والمعايير الهرمونية المحددة.

دراسة حالة تم إجراؤها في محافظة صلاح الدين خلال الفترة من ١ مايو إلى ١ أكتوبر ٢٠٢٢. خمسة وعشرون مريضة مصابة بمرض تكيس المبايض مقارنة مع ٢٥ امرأة سليمة طبيعية. تم إجراء تحاليل الموجات فوق الصوتية والدوبلر لجميع النساء خلال المرحلة الجرابية من الدورة الشهرية. تم تحليل سرعات تدفق الدم في الشريان الرحمي وحساب مؤشر النبض.

أظهرت الدراسة الحالية أن قلة الطمث وجدت لدى (٧٢٪) من المرضى علامات سريرية / بيوكيميائية لفرط الأندروجين عند (٧٦٪). كان متوسط LH (mIU / L) أعلى بشكل ملحوظ بين حالات مرض PCO وأيضًا أن متوسط FSH (mIU / L) كان أقل بشكل ملحوظ بين حالات مرض PCO من المجموعة الضابطة. كان هناك زيادة في حجم المبيض> ١٠ سم ٣ بين (٨٠٪) ، و١٢ بصيلة مقاس ٢-٩ ملم وجدت في (٨٤٪) من مرضى PCO. كان متوسط الشريان الرحمي PI أعلى بشكل ملحوظ بين حالات مرض PCO 2.3 ± 0.5 من مجموعة التحكم ١,٨ ± ٠,٤ (قيمة P <0.05).

كان متوسط حجم المبيض أعلى بشكل ملحوظ في حالات مرض PCO منه في مجموعة السيطرة. كان متوسط PI في الشريان الرحمي أعلى بشكل ملحوظ بين حالات مرض PCO مقارنة بمجموعة التحكم.

الكلمات المفتاحية: مؤشر نبض الشريان الرحمي في متلازمة تكيس المبايض. دراسة حالة تحكم ، مؤشر نبض الشريان الرحمي في متلازمة تكيس المبايض

1. INTRODUCTION:

PCOS is a heterogeneous pathological disorders characterized by reproductive abnormality, and usually associated with hyperandrogenism, obesity, hyperinsulinemia, and insulin resistance. It represents the commonly prevalent endocrinopathy in women, and its prevalence is around 6-8% in the reproductive age **[1]**. Though polycystic ovaries can be described in about 33% of the women, they are not essentially related with the typical symptoms and PCOS, which may be presented at some period during the reproductive life span when provoked by, for example, weight gain or insulin resistance **[2, 3]**. A refined definition of PCOS declared by a joint ESHRE/ASRM consensus meeting in 2003, "namely the presence of two out of the following three criteria: (1) oligo- and/or anovulation, (2) hyperandrogenism (clinical and/or biochemical), and (3) polycystic ovaries, with the exclusion of other etiologies "**[4]**. PCO morphology of the PCO was redefined as an ovary with ≥12 follicles of diameter of 2-9 mm in and/or elevated ovarian volume (> 10 cm3) **[5]**. One of the essential methods in PCOS diagnosis and the gold standard for defining polycystic ovary (PCO) is the Ultrasound assessment of ovarian morphology. The women with the polycystic ovary syndrome have the morphological ovarian phenotype this known as the polycystic ovary **[6]**. Transvaginal Doppler sonography has participated greatly to the improvement of ultrasound diagnosis and has provided greatly new information morphologically and pathophysiologically on blood flow dynamics within the female pelvis **[7,8]**. Battaglia and co-workers found that PCOS patients develop obvious ovarian vascularization changes at the level of the intraovarian arteries **[9]**, Zaidi and co-workers **[10]** and Aleem and co-workers **[11]** proved that, in PCOS patients, great

intraovarian vessels changes occur. Additionally, PCOS has increased uterine artery resistance. Doppler analysis of ovarian stromal arteries in PCOS may be helpful in diagnostic improvement, and provision great extra information regarding the evolution & pathophysiology of the PCOS **[9-11]**. Doppler ultrasound Over the last twenty years Doppler has become a reliable and frequently used method to monitor the fetoplacental unit of risk pregnancies in the last two decades **[12-17]**. Pulsatility index measure the increased resistance in the uterine artery measured and it determines a reduced blood flow to the placenta and may be an early sign of placenta pathology and/or hypertensive disorder in pregnancy **[12,17,18]**. PCOS is linked to pregnancy complications, such as gestational diabetes mellitus, preterm delivery, and preeclampsia **[19-21]**. Research of UtAPI in females with PCOS are dispersed, but some of them have documented reduced blood flow in the uterine artery in women with PCOS either non-pregnant or pregnant **[22-25]**. Palomba, et al in 2010 found that a significantly higher rate of PCOS females with abnormal UtAPI measurements during first and mid-second trimesters compared to controls. Only little information exists in the literature regarding the details of ultrasound parameters in women with PCO only and PCOS, which may be important in the understanding of the pathophysiology of PCOS. An understanding of vascular changes in women with PCO may allow us to gain further insights into the underlying pathophysiology of the condition and differences between PCOS and PCO only patients**[26]**.This study aimed to show assess uterine blood flow and whether there is a correlation between these patterns and specific hormonal parameters.

2. Patient and methods:

This is a case control study done in Salah Al-Deen governorate during the period of 1st May 2022 – 1st October. The patients were recruited from the ultrasound clinic of the Department of radiology in Salah Al-Deen general hospital. Sample was collected randomly from the ultrasound clinic, 25 patients with polycystic ovary disease compared with 25 normal healthy women. The inclusion criteria for cases group were "(i) oligomenorrhoea/amenorrhoea for months at least; (ii) Ferrimane- Gallway score >7; (iii) LH: FSH ratio >2; (iv) PCO pattern diagnosed on US showing at least one of the following: either 12 or more follicles measuring ≤ 9 mm in diameter or increased ovarian volume (>10 cm3)". All patients were evaluated for the clinical and biochemical profile to see if the patients meet the Rotterdam criteria. Oligomenorrhoea was defined as cycle length >35 days and amenorrhoea were defined as absence of vaginal bleeding for >3 months in individuals who previously had experienced periodic menstruation at least for 6 months. Hirsutism was evaluated using the modified

Ferriman–Gallwey score, which ranges from 1 to 36; scores of 7 or more indicate hirsutism [27]. Body mass index was calculated, and ultrasound and Doppler analyses were performed by the same physician for all women during the follicular phase of the menstrual cycle (between the third and fifth day) using a 6.5 MHz vaginal transducer equipped with color and pulsed Doppler. Ovarian volume was calculated using the formula for an ellipse (length×width×height×0.523) .

Uterine artery blood flow velocities were analyzed from the ascending branches of both main arteries at the level of the internal cervical os in a longitudinal plane. At least 3 satisfactory blood flow velocity waveforms were obtained and used for statistical analysis of the average from 3 waveforms. The angle of insonation was always changed to obtain maximum color intensity. When good color signals were obtained, blood flow velocity wave forms were recorded by placing the sample volume across the vessel and entering the pulsed Doppler mode. The pulsatility index (PI), defined as the difference between peak-systolic and end diastolic flow divided by the mean maximum flow velocity was determined using calculation software. [28] The research was approved by the Salah Al-Deen research Committee, and every Participant informed about the objectives, benefits, purpose, and risks the study before they agree joining the study. Data analyzed using SPSS version (23), and Excel sheets. Student 't' test was used to test the significance of the relations. p value <0.05 was considered statistically significant.

3. Results

The oligomenorrhea found among 18 (72%) of the patients , clinical/biochemical signs of hyperandrogenism found among 19(76%), Increased ovarian volume of more than 10 cm3 found among 20(80%), and Twelve or more follicles measuring 2-9mm found among 21(84%) of the PCO disease patients, as shown in **Figure 1**. Mean BMI was significantly higher among PCO disease cases 33.1 ± 6.3 than control group 25.4 ±5.7, (P value <0.05). Mean Hirsutism score was significantly higher among PCO disease cases 9.6 ± 3.7 than control group 4.9 ±1.2, (P value <0.05). The mean LH (mIU/L) was significantly higher among PCO disease cases 11.6 ± 1.8 than control group 6.5 ±1.3, (P value <0.05). The mean FSH (mIU/L) was significantly lower among PCO disease cases 4.8±1.2 than control group 7.1 ±2.0, (P value <0.05). Mean prolactin (ng/ml) was significantly higher among PCO disease cases 34.6 ± 3.5 than control group 20.9±5.1 (P value <0.05). Mean ovarian volume was significantly higher among PCO disease cases 11.4±3.4 than control group 7.2 ± 1.5 (P value <0.05). The mean Uterine artery

PI was significantly higher among PCO disease cases 2.3±0.5 than control group 1.8±0.4 (P value <0.05), as shown in **Table 1**.

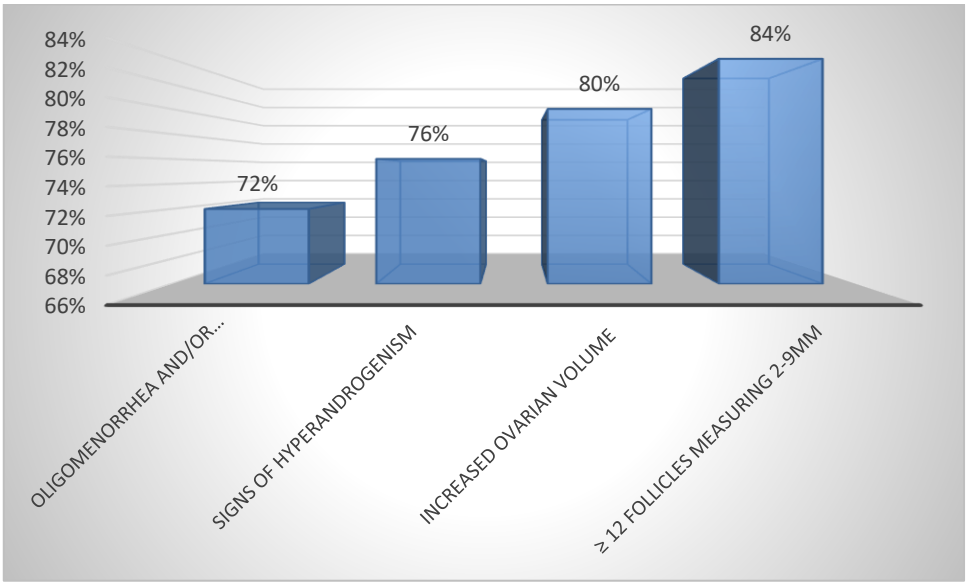

Fig. 1: The signs and symptoms of PCOD patients

Table 1: The mean hormonal and sonographic parameters among study groups.

clinical biochemical and sonographic characteristics	Cases		Controls		
	Mean	Std. Deviation	Mean	Std. Deviation	P value
Age	26.7	7.8	25.9	6.5	>0.05
BMI	33.1	6.3	25.4	5.7	<0.05*
Hirsutism score	9.6	3.7	4.9	1.2	<0.05*
LH (mIU/L)	11.6	1.8	6.5	1.3	<0.05*
FSH (mIU/L)	4.8	1.2	7.1	2.0	<0.05*
LH/FSH ratio	2.1	0.4	1.1	0.1	<0.05*
prolactin (ng/ml)	34.6	3.5	20.9	5.1	<0.05*
Total testosterone, ng/dL	59.7	10.2	41.6	12.3	>0.05
Ovarian volume cm^3	11.5	3.4	7.2	1.5	<0.05*
Uterine artery PI	2.3	0.5	1.8	0.4	<0.05*

***Significant**

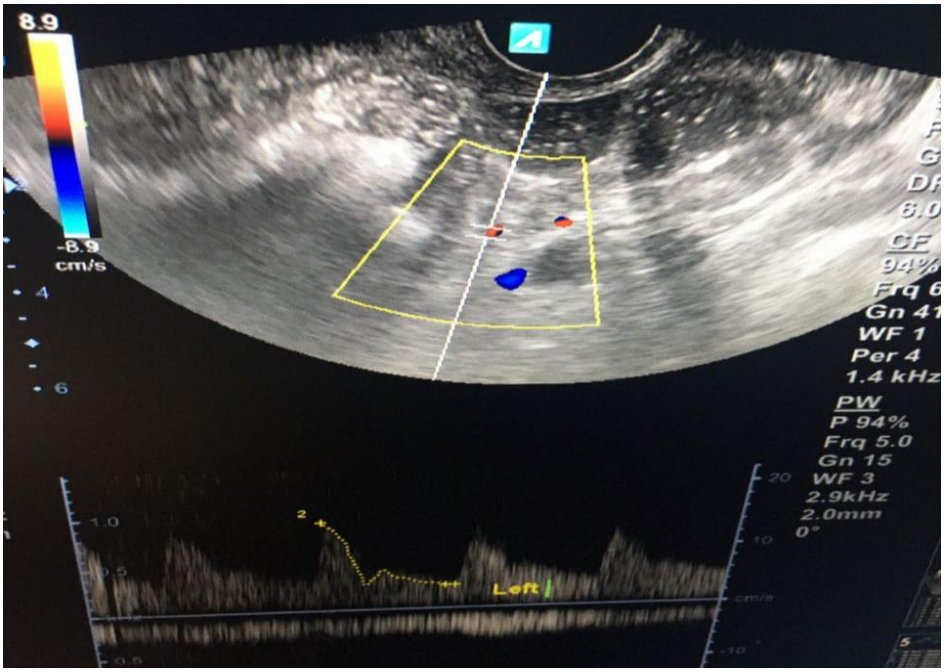

Fig. 2: The Doppler study of uterine artery.

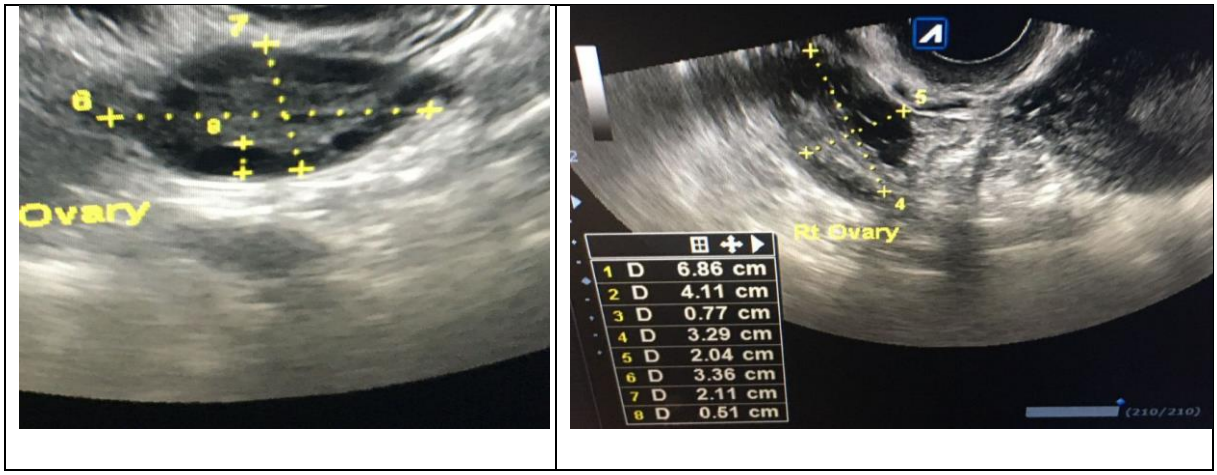

Fig. 3: The ultrasonic features of the ovary in a patient aged 29 years with PCOS and secondary infertility history.

4. Discussion

The current study showed that oligomenorrhea found among (72%) of the patients, clinical/biochemical signs of hyperandrogenism found among (76%). This is like a study carried out by Adams et al in 2004 found that most of the patients with PCOD presented with

oligomenorrhoea (82.5%) followed by infertility (30%) and secondary amenorrhoea (15%) like previous studies[29] .

The current study showed that the mean LH (mIU/L) was significantly higher among PCO disease cases and that the mean FSH (mIU/L) was significantly lower among PCO disease cases than control group. The current study showed that increased ovarian volume of > 10 cm3 found among (80%), and ≥12 follicles measuring 2-9 mm found in (84%) of the PCO disease patients. This may be explained by the fact that the mean ovarian volume in the present study also correlated with the serum LH and explained that the enlarged ovarian volume was under the effect of high LH. This is like Pache et al. also found similar correlation of ovarian volume with LH (r¼0.30, p¼0.003). In the present study, all PCOD patients had multiple follicles. [30] The present study also indicates the high LH:FSH ratio. This is like Vrtacnik-Bokal & Meden-Vrtovec, and Arroyo et al . [31,32]

The current study showed that the mean BMI was significantly higher among PCO disease cases than control group. This is like a study of Franks in 2004 found that more than 50% had obesity. [33] The current study showed that the mean Uterine artery PI was significantly higher among PCO disease cases 2.3 ± 0.5 than control group 1.8 ± 0.4 (P value <0.05). Goswamy and Steptoe first who reported significantly elevated PI values in the uterine arteries of infertile females (Goswamy, R. K., & Steptoe, P. C. 1988) [34].

According to different studies, there are a lot of variations in the pulsatility index and Resistive index of uterine arteries in PCOS patients. Asma, B. et al. in Lahore in 2016 on PCOS found that mean values of pulsatility index of uterine arteries bilaterally were High in PCOS - patients. [35] Maciołek- Blewniewska, G. et al., 1999 observed elevated pulsatility index of uterine arteries in females with PCOS. [36] Dolz, M. et al., 1999 found that that PCOS had greater values of uterine artery pulsatility index and Resistive index (Dolz, M. et al., 1999). [37] Anum S in 2019 found that there is no significant difference of uterine artery resistive index in polycystic ovarian syndrome patients and normal females. [38]

5.Conclusions

The mean Uterine artery PI was significantly higher among PCO disease cases than control group, and its useful in diagnosis of polycystic ovarian syndrome and its differentiation from polycystic like ovary cases. The mean ovarian volume was significantly higher among PCO disease cases than control group.

6. References

[1] Azziz R, Woods KS, Reyna R, Key TJ, Knochenhauer ES, Yildiz BO. The prevalence and features of the polycystic ovary syndrome in an unselected population. J Clin Endocrinol Metab. 2004;89(6):2745-2749.

[2] Norman RJ, Davies MJ, Lord J, Moran LJ. The role of lifestyle modification in polycystic ovary syndrome. Trends Endocrinol Metab. 2002;13(6):251-257.

[3] Homburg R. Polycystic ovary syndrome - from gynaecological curiosity to multisystem endocrinopathy. Hum Reprod. 1996;11(1):29-39. 4-Stein IF,

[4] Leventhal ML. Amenorrhea associated with bilateral polycystic ovaries. Am J Obstet Gynecol 1935; 29:181-188.

[5] Balen AH, Laven JS, Tan SL, Dewailly D. Ultrasound assessment of the polycystic ovary: international consensus definitions. Hum Reprod Update. 2003;9(6):505-514.

[6] Kurjak A, Zalud I, Jurkovic D, et al. Transvaginal color Doppler for the assessment of pelvic circulation. Acta Obstet Gynecol Scand.1989;68(2):131-5.

[7] Kurjak A, Jurkovic D, Alfirevic Z, Zalud I. Transvaginal color Doppler imaging. J Clin Ultrasound. 1990;18(4):227-34.

[8] Battaglia C, Artini PG, D'Ambrogio G, Genazzani AD, Genazzani AR. The role of color Doppler imaging in the diagnosis of polycystic ovary syndrome. Am J Obstet Gynecol. 1995;172(1 Pt 1):108-13.

[9] Zaidi J, Campbell S, Pittrof R, Kyei-Mensah A, Shaker A, Jacobs HS, Tan SL. Ovarian stromal blood flow in women with polycystic ovaries—a possible new marker for diagnosis? Hum Reprod. 1995;10(8):1992-6.

[10] Aleem FA, Predanic M. Transvaginal color Doppler determination of the ovarian and uterine blood flow characteristics in polycystic ovary disease. Fertil Steril. 1996;65(3):510-516.

[11] Ajossa S, Guerriero S, Paoletti AM, Orru M, Floris S, Mannias M, Melis GB. Uterine perfusion and hormonal pattern in patients with polycystic ovary syndrome. J Assist Reprod Genet. 2001;18(8):436-40.

[12] Papageorghiou A. T., Yu C. K. H., Nicolaides K. H. The role of uterine artery Doppler in predicting adverse pregnancy outcome. Best Practice & Research Clinical Obstetrics & Gynaecology. 2004;18(3):383–96.

[13] Gomez O., Figueras F., Martinez J. M., et al. Sequential changes in uterine artery blood flow pattern between the first and second trimesters of gestation in relation to pregnancy outcome. Ultrasound in Obstetrics & Gynecology. 2006;28(6):802–8.

[14] Kalache K. D., Duckelmann A. M. Doppler in obstetrics: beyond the umbilical artery. Clinical Obstetrics and Gynecology. 2012;55(1):288–95.

[15] Stampalija T., Gyte G. M. L., Alfirevic Z. Utero-placental Doppler ultrasound for improving pregnancy outcome. Cochrane Database of Systematic Reviews. 2010;(9, article CD008363).

[16] Alfirevic Z., Stampalija T., Gyte G. M. Fetal and umbilical Doppler ultrasound in high-risk pregnancies. Cochrane database of systematic reviews. 2013;(11, article CD007529).

[17] Eser A., Zulfikaroglu E., Eserdag S., Kilic S., Danisman N. Predictive value of middle cerebral artery to uterine artery pulsatility index ratio in preeclampsia. Archives of Gynecology and Obstetrics. 2011;284(2):307–311.

[18] Papageorghiou A. T., Yu C. K. H., Cicero S., Bower S., Nicolaides K. H. Second-trimester uterine artery Doppler screening in unselected populations: a review. The Journal of Maternal-Fetal & Neonatal Medicine. 2002;12(2):78–88.

[19] Palomba S., de Wilde M. A., Falbo A., Koster M. P. H., La Sala G. B., Fauser B. C. J. M. Pregnancy complications in women with polycystic ovary syndrome. Human Reproduction Update. 2015;21(5):575–592.

[20] Goodman N. F., Cobin R. H., Futterweit W., Glueck J. S., Legro R. S., Carmina E. American Association of Clinical Endocrinologists, American College of Endocrinology, and Androgen Excess and PCOS Society disease state clinical review: guide to the best practices in the evaluation and treatment of polycystic ovary syndrome-part 2. Endocrine Practice. 2015;21(12):1415–1426.

[21] Katulski K., Czyzyk A., Podfigurna-Stopa A., Genazzani A. R., Meczekalski B. Pregnancy complications in polycystic ovary syndrome patients. Gynecological Endocrinology. 2015;31(2):87–91.

[22] Adali E., Kolusari A., Adali F., Yildizhan R., Kurdoglu M., Sahin H. G. Doppler analysis of uterine perfusion and ovarian stromal blood flow in polycystic ovary syndrome. International Journal of Gynaecology and Obstetrics. 2009;105(2):154-7.

[23] Ajossa S., Guerriero S., Paoletti A. M., et al. Uterine perfusion and hormonal pattern in patients with polycystic ovary syndrome. Journal of Assisted Reproduction and Genetics. 2001;18(8):436-40.

[24] Ozkan S., Vural B., Caliskan E., Bodur H., Turkoz E., Vural F. Color Doppler sonographic analysis of uterine and ovarian artery blood flow in women with polycystic ovary syndrome. Journal of Clinical Ultrasound. 2007;35(6):305-13.

[25] Resende A. V., Mendes M. C., Dias de Moura M., et al. Doppler study of the uterine arteries and ovarian stroma in patients with polycystic ovary syndrome. Gynecologic and Obstetric Investigation. 2001;52(3):153-7.

[26] Palomba S., Falbo A., Russo T, et al. Uterine blood flow in pregnant patients with polycystic ovary syndrome: relationships with clinical outcomes. BJOG. 2010;117(6):711–21.

[27] Aswini R, Jayapalan S. Modified Ferriman–Gallwey score in hirsutism and its association with metabolic syndrome. International journal of trichology. 2017 Jan;9(1):7.

[28] Stridsklev S, Salvesen Ø, Salvesen KÅ, Carlsen SM, Vanky E. Uterine Artery Doppler in Pregnancy: Women with PCOS Compared to Healthy Controls. Int J Endocrinol. 2018 Aug 16;2018:2604064.

[29] Adams JM, Taylor AE, Crowley JrWF, et al. Polycystic ovarian morphology with regular ovulatory cycles: insights into the pathophysiology of polycystic ovarian syndrome. J Clin Endocrinol Metab 2004 Sep;89(9):4343e50.

[30] Pache TD, de Jong FH, Hop WC, et al. Association between ovarian changes assessed by transvaginal sonography and clinical and endocrine signs of the polycystic ovary syndrome. Fertil Steril 1993 Mar;59(3):544e9.

[31] Vrtacnik-Bokal E, Meden-Vrtovec H. Utero-ovarian arterial blood flow and hormonal profile in patients with polycystic ovary syndrome. Hum Reprod 1998 Apr;13(4):815e21.

[32] Arroyo A, Laughlin GA, Morales AJ, et al. Inappropriate gonadotropin secretion in polycystic ovary syndrome: influence of adiposity. J Clin Endocrinol Metab 1997 Nov;82(11):3728e33.

[33] Franks S. Controversy in clinical endocrinology: diagnosis of polycystic ovarian syndrome: in defense of the Rotterdam criteria. J Clin Endocrinol Metab 2006 Mar;91(3):786e9.

[34] Goswamy, R. K., & Steptoe, P. C. Doppler ultrasound studies of the uterine artery in spontaneous ovarian cycles. Human Reproduction 1988, 3(6), 721-726.

[35] Asma, B., Asma, T., & Atiq-ur-Rehman. (2016). Diagnosis of PCOS on Doppler based Resistive Index and Pulsatility Index. Journal of rawalpindi medical college (JRMC), 20(4), 305-308. 18.

[36] Maciołek-Blewniewska, G., Kozarzewski, M., Szpakowski, M., Pertyński, T., & Nowak, M. (1999). The evaluation of blood flow in uterine arteries in girls with polycystic ovary syndrome by transvaginal color Doppler ultrasonography. Ginekologia polska, 70(5), 412- 417. 19.

[37] Dolz, M., Osborne, N. G., Blanes, J., Raga, F., Abad-Velasco, L., Villalobos, A., ... & Bonilla- Musoles, F. (1999). Polycystic ovarian syndrome: assessment with color Doppler angiography and three-dimensional ultrasonography. Journal of ultrasound in medicine, 18(4), 303-313.

[38] Anum S, Raham B, Syed Y, et al. Sonographic Correlation Of Polycystic Ovarian Syndrome With Uterine Artery Resistive Index. EAS Journal of Radiology and Imaging Technology 2019; 1 (5):94-100.

https://doi.org/10.32441/kjps.06.02.p3

Al-Kitab Journal for Pure Sciences
ISSN: 2617-1260 (print), 2617-8141(online)
www.kjps.isnra.org

Ferritin level and Hb after covid 19 in the city of Baghdad and Karbala-Iraq

*Hiba Yousef Saleh, Hadeel Ahmed Hasan, Ghaidaa Neamah Kadhim, Sameerah Saadoon Mustafa

Medical Technical Institute, Al- Mansour, Middle Technical University, Iraq

*Corresponding Author: Hiba.yousif.saleh@mtu.edu.iq

Citation: Saleh H. Y., Hasan H. A., Kadhim G. N., Mustsfa S. S. Ferritin level and Hb after covid 19 in the city of Baghdad and Karbala-Iraq. Al-Kitab Journal for Pure Sciences (2022); Doi: https://doi.org/10.32441/kjps.06.02.p3 .

Keyword
Ferritin, Covid 19, hemoglobin, Corona virus

Article History
Received 15 Sep. 2022
Accepted 25 Oct. 2022
Available online 17 Nov. 2022

Abstract:

The study was conducted by taking blood samples from those recovering from the Corona virus, specifically 20-28 days after infection. The number of samples was (54) patients, collected from the period among six months (Mars to September). Blood samples were taken from patients recovering from Covid 19 from the hospitals of Karbala and Baghdad, the information of the samples was recorded, and laboratory analyzes were done to measure the level of ferritin, and the complete blood picture was measured. The data of patients were studied Biochemistry lab with biochemical tests.

The results were obtained and indicated that most of the recovered patients with Corona virus had symptoms of acute anemia , and after conducting a ferritin analysis, it was found that their ferritin level was high, which caused an increase in stored iron and a lack of iron associated

with hemoglobin. The research recommended continues taking vitamins and minerals necessary for the health of the body.

Keywords: Ferritin, Covid 19, hemoglobin, Corona virus.

مستوى الفيريتين ونسبة الهيموجلوبين بعد كوفيد ١٩ في مدينة بغداد وكربلاء – العراق

هبة يوسف صالح*، هديل أحمد حسن، غيداء كاظم نعمه، سميرة سعدون مصطفى

المعهد الطبي التقني المنصور/ الجامعة التقنية الوسطى – العراق

Hiba.yousif.saleh@mtu.edu.iq / hadeelahmed@mtu.edu.iq / ghaidaanehma@mtu.edu.iq / samira.sadoon13@gmail.com

*Corresponding Author: Hiba.yousif.saleh@mtu.edu.iq

الخلاصة:

أجريت الدراسة بأخذ عينات دم من المتعافين من فيروس كورونا وتحديدا بعد ٢٠-٢٨ يوما من الإصابة. وبلغ عدد العينات (٥٤) مريضا جمعت من فترة ما بين ستة أشهر (أذار حتى أيلول). وأخذت عينات الدم من المرضى المتعافين من كوفيد ١٩ من مستشفيات كربلاء وبغداد ، وسجلت معلومات العينات ، وأجريت التحاليل المختبرية لقياس مستوى الفيريتين وقياس صورة الدم الكاملة. تم دراسة بيانات المرضى من خلال الاختبارات البيوكيميائية

وأوضحت النتائج أن معظم المتعافين من فيروس كورونا ظهرت عليهم أعراض فقر الدم الحاد ، وبعد إجراء تحليل الفيريتين تبين أن مستوى الفيريتين لديهم مرتفع مما تسبب في زيادة مخزون الحديد ونقص الحديد المرتبط بالهيموغلوبين. وأوصى البحث بمواصلة تناول الفيتامينات والمعادن الضرورية لصحة الجسم

الكلمات المفتاحية: فيريتين ، كوفيد ١٩ ، هيموجلوبين ، فيروس كورونا.

1. INTRODUCTION:

Coronavirus disease -19 (COVID-19) is seen as an infectious inflammatory disease that mainly affects the lungs [1]. Recently, the involvement of multiple organs, with different pathways to injury [2], has been highlighted. Hemoglobinopathy, hypoxia and cellular iron overload may have an additional potential role. The scientific literature has indicated Corona virus causes an increase in the percentage of white blood cells than normal [3], a sharp decrease in the percentage of red blood cells and hemoglobin in the body, and an increase in the level of iron in the blood; excess iron in the cell/tissue (hyperferrinemia) [4].

Ferritin is a major mediator of immune deregulation, and it helps to understand the amount of iron stored in the body, ferritin can activate (macrophages) type of white blood cell in the immune system [5].

When they are activated, they begin to secrete cytokines that regulate immunity [6], when it is secreted in low concentrations, it is considered safe for the body and helps protect it from viruses and bacteria. When it is secreted in high concentrations, called 'cytokine storm' develops, which can be fatal for half of patients, especially the elderly [7]. Ferritin normal ratio is from 20-300 nm/ml for women and 20-350 for men. Severe hyperferritinemia indicates, through direct immunosuppressive and inflammatory effects, the fatal outcome of COVID-19 has been reported [8].

2. Methods:

Blood samples were taken from patients recovering from Covid 19, from three public hospitals in Iraq. Data were recorded 21-28 days after infection [9].

Blood samples are clinically examined by a set of tests, including a complete blood test, and the level of ferritin in the blood in the medical laboratories by advanced laboratory equipment photometer 5010 by the turbidimeter method; the data of patients were studied Biochemistry lab with biochemical tests [10]. All patient data were examined and analyzed according to the results in Table 1.

3. Results and Discussion:

Table(1) evidence and results of ferritin and haemoglobin tests for control sample

Descriptive Statistics						
	N	Minimum	Maximum	Mean	Std. Error	Std. Deviation
Hb	30	12.20	16.00	14.0633	.21028	1.15176
Ferritin	30	43.00	210.00	116.2333	8.13545	44.55967

Table (2) Evidence and results of ferritin and haemoglobin tests for those recovering from Covid 19

	N	Minimum	Maximum	Mean	Std. Error	Std. Deviation
Hb	54	9.60	14.70	12.2000	.19580	1.43882
Ferritin	54	308.00	580.00	429.7037	8.22757	60.46007

N: represents the size of the studied sample and is equal to (54) and for the two statistics (HB) and (FIRRITIN)

RANG: shows us its value for (HB) equal to (5.1) and for (FIRRITIN) equal to (272).

MEAN: shows us the arithmetic mean value of (HB) equal to (12.2) and of (FIRRITIN) equal to (429.7).

S.D: The value of the standard deviation is equal to (HB) equal to (1.438) and for (FIRRITIN) equal to (60.46).

S(2): the variance value for (HB) is (2.07) and for (FIRRITIN) is (3655.42).

When looking at the studied values (range), it appears to us, and by reading the data of the two tables above and comparing them, that the greater the percentage of dispersion in the data, the greater the percentage or probability of developing symptoms **[11]**. (1.151), which is less than its value in the case of infected people, which was equal to (1.438) and the same case for (FIRRITIN), where its value appeared for healthy people equal to (44,559) and for the injured (60.46), and the difference is clear between the two values, and this means that the natural dispersal ratio should be close about the standard limit **[12]**, and whenever the value of the person studied is close to the standard value, the probability of him suffering from symptoms is few or close to zero.

Also, for the purpose of simple clarification, the subject of the largest value and the smallest value was touched upon. When studying the affected persons , the largest value was (14.7) and (580) and the smallest value was (9.6) and (308) for each of (HB) and (FIRRITIN), respectively, When studying healthy people, the results (HB) and (FIRRITIN) had the largest value (16) and (210) and the smallest value (12.2) and (43), respectively, and it also indicates that (FIRRITIN) its value for the injured is very large for healthy people and the same for the case of (HB) **[11]**.

Recent studies of COVID-19 have shown that infection depends on cytokine storm syndrome **[13]**. Many people with diabetes have elevated levels of ferritin in their blood and may experience serious complications from COVID-19 **[14]**. The results of the study showed that the recovered suffer from an increase in the level of ferritin, and this indicates the possibility of bacterial infection during infection with the virus because of the immune system's preoccupation with fighting the virus **[15]**.

And this indicates that the Corona virus participates during infection by binding to the iron stored in the human body, which reduces its association with the "globulin protein" **[16]**. These results in a lack of hemoglobin, which carries oxygen **[17]**, which may cause a decrease in the level of oxygen in the body of the infected person, and these symptoms continue for a period of 30-40 days from the beginning of the infection **[18]**.

This confirms that Covid 19 patients decreased in hemoglobin levels and resulted in anemia even after recovery from the disease **[19, 20]**.

4. Recommendation:

The study recommends following up the cases of patients after recovering from the Covid 19 virus, especially patients who have a family history of chronic diseases such as diabetes and high blood pressure and following up on those recovering for anemia analyzes. It is advised to continue taking vitamins and minerals necessary for the health of the body and strengthening immunity.

5. References

[1] Cavezzi, Attilio, Emidio Troiani, and Salvatore Corrao. "COVID-19: hemoglobin, iron, and hypoxia beyond inflammation. A narrative review." Clinics and practice 10.2 (2020): 24-30.

[2] Varga Z, Flammer AJ, Steiger P, et al. Endothelial cell infection and endothelitis in COVID-19. Lancet 2020;395: 1417-8.

[3] Lithanatudom P, Leecharoenkiat A, Wannatung T, et al. A mechanism of ineffective erythropoiesis in β-thalassemia/Hb E disease. Haematologica 2010;95:716-23.

[4] Majeed A, Shajar MA. Is hemoglobin the missing link in the pathogenesis of COVID-19? Anaesth Pain Intensive Care 2020;24:9-12.

[5] Hariyanto, Timotius Ivan, and Andree Kurniawan. "Anemia is associated with severe coronavirus disease 2019 (COVID-19) infection." Transfusion and apheresis science 59.6 (2020).

[6] Abobaker, Anis. "Reply: iron chelation may harm patients with COVID-19." European Journal of Clinical Pharmacology 77.2 (2021): 267-268.

[7] Habib, Hosam M., et al. "The role of iron in the pathogenesis of COVID-19 and possible treatment with lactoferrin and other iron chelators." Biomedicine & Pharmacotherapy (2021): 111228.

[8] Bikdeli B, Madhavan MV, Jimenez D, et al. COVID-19 and thrombotic or thromboembolic disease: implications for prevention, antithrombotic therapy, and follow-up (Epub 2020 Apr 15). J Am Coll Cardiol 2020;S0735-1097(20) 35008-7.

[9] Wenzhong L, Hualan L. COVID-19: Attacks the 1-beta chain of hemoglobin and captures the porphyrin to inhibit human heme metabolism. ChemRxiv 2020.11938173.v8.

[10] Ulrich, H, Pillat M. CD147 as a Target for COVID-19 Treatment: Suggested Effects of Azithromycin and Stem Cell Engagement. Stem Cell Rev Rep 2020.

[11] Qu R, Ling Y, Zhang YH, et al. Platelet-to-lymphocyte ratio is associated with prognosis in patients with coronavirus disease-19. J Med Virol. 2020.

[12] Snijders D, Schoorl M, Schoorl M, Bartels PC, van der Werf TS, Boersma WG. D-dimer levels in assessing severity and clinical outcome in patients with community-acquired pneumonia. A secondary analysis of a randomised clinical trial. Eur J Intern Med. 2012;23(5):436-441.

[13] Han H, Yang L, Liu R, et al. Prominent changes in blood coagulation of patients with SARS-CoV-2 infection. Clin Chem Lab Med. 2020.

[14] Lippi G, Favaloro EJ. D-dimer is associated with severity of coronavirus disease 2019: a pooled analysis. Thromb Haemost. 2020;120(05): 876-878.

[15] Huang C, Wang Y, Li X et al (2020) Clinical features of patients infected with 2019 novel coronavirus in Wuhan, China. Lancet 395(10223):497–506. https://doi.org/10.1016/s0140-6736(20) 30183-5.

[16] Burcelin R, Amar J (2015) Diabetes: antibiotics or prodiabetics? Nat Rev Endocrinol 11(7):385–386. https://doi.org/10.1038/ nrendo.2015.75.

[17] Bonow RO, Fonarow GC, O'Gara PT, Yancy CW. Association of coronavirus disease 2019 (COVID-19) with myocardial injury and mortality. JAMA Cardiol 2020 Mar 27.

[18] Saleh, Hiba Yousef, Ghaidaa Neamah Kadhim, and Hadeel Ahmed Hasan. "Cadmium and Selenium Levels in Blood Smokers of Water Pipe (Hookah) in Baghdad." Systematic Reviews in Pharmacy 11.11 (2020): 1818-1820.

[19] Lee N, Hui D, Wu A, et al. A major outbreak of severe acute respiratory syndrome in Hong Kong. N Engl J Med. 2003;348(20):1986- 1994.

[20] Witt DM, Nieuwlaat R, Clark NP, et al. American Society of Hematology 2018 guidelines for management of venous thromboembolism: optimal management of anticoagulation therapy. Blood Adv. 2018;2 (22):3257-3291.

Al-Kitab Journal for Pure Sciences
ISSN: 2617-1260 (print), 2617-8141(online)
www.kjps.isnra.org

Green Hospitals for the Future of Healthcare: A Review

Athra Alkaabi, Mohammad Aljaradin*

Hamdan Bin Mohammed Smart University, School of Health & Env. Studies, Dubai, UAE.

*Corresponding Author: m.aljaradin@hbmsu.ac.ae

Citation: Alkaabi A., Aljaradin, M., Green Hospitals for the Future of Healthcare: A Review. Al-Kitab Journal for Pure Sciences (2022); 6(2): 31-45. DOI: https://doi.org/10.32441/kjps.06.02.p4

Keyword: Green hospital, future hospital, green building, and patient-centered concepts.

Article History

Received	15 Dec. 2022
Accepted	04 Jan. 2023
Available online	15 Jan. 2023

Abstract:

Hospitals are essential for preserving and enhancing both human and environmental health. The "green hospital" concept seeks to redefine how medical facilities are constructed to preserve human life while protecting the environment. The concept of a "green hospital" and its potential benefits are discussed in this paper. It also discusses the "green hospital" concept in the United Arab Emirates as an example for future hospitals. The paper also discusses various aspects of green hospitals, such as facility design, energy efficiency, green procurement, and patient-centered concepts. Finally, the provided discussion and examples demonstrated the benefits of using the green hospital concept as a model for future hospitals, as well as the drawbacks and barriers to adopting the green hospital concept.

Keywords: Green hospital, future hospital, green building, and patient-centered concepts.

المستشفيات الخضراء لمستقبل الرعاية الصحية

عذرا الكعبي ، محمد الجرادين*

جامعة حمدان بن محمد الذكية، دبي، الإمارات العربية المتحدة

*m.aljaradin@hbmsu.ac.ae

الخلاصة:

تعد المستشفيات ضرورية للحفاظ على صحة الإنسان وصحة البيئة. يسعى مفهوم المستشفى الأخضر إلى إعادة تعريف كيفية إنشاء المرافق الطبية من أجل الحفاظ على حياة الإنسان بالإضافة الى حماية البيئة. في هذا البحث تم مناقشة مفهوم المستشفى الأخضر وفوائده المحتملة. كما يناقش ايضا مفهوم المستشفى الأخضر في دولة الإمارات العربية المتحدة كمثال لمستشفيات المستقبل. يناقش البحث أيضًا جوانب مختلفة من المستشفيات الخضراء، مثل تصميم المرافق، وكفاءة الطاقة، والمشتريات الخضراء، والمفاهيم التي تركز على المريض. أخيرًا، أظهرت المناقشة والأمثلة المقدمة فوائد استخدام مفهوم المستشفى الأخضر كنموذج للمستشفيات المستقبلية، بالإضافة إلى عوائق وتحديات اعتماد مفهوم المستشفى الأخضر.

الكلمات المفتاحية: المستشفى الأخضر، المستشفى المستقبلي، المباني الخضراء، العناية المركزة للمريض .

1. INTRODUCTION:

Hospitals make a significant contribution to their communities by providing a wide range of services. Hospitals, on the other hand, operate 24 hours a day, seven days a week, leaving a significant environmental footprint in many cities [1]. Hospitals have some environmental impacts, according to the US EPA (2022). Every day, hospitals generate approximately 7,000 tons of waste, which includes medical waste, hazardous waste, and municipal waste. PVC, DEHP, cleaning materials, heavy metals in electronics, insecticides, and batteries are all used in hospitals. Water is used extensively in hospitals for domestic purposes, heating/cooling, and gardening. Hospitals use massive amounts of energy in their buildings and automobile fleets, resulting in massive greenhouse gas emissions. According to Garg and Dewan (2022), healthcare facilities typically use resources such as water, energy, petroleum products, chemicals, food, building materials, gases, and so on. Because of their carbon footprint, all of these things harm the environment. Although hospitals cannot provide excellent care without the use of natural resources, hospitals can significantly reduce their carbon footprint if these

resources are distributed and exploited in a simple, clever, and sustainable manner. Green building is being promoted all over the world as a means of improving the environment [2].

Green building principles are revolutionizing building practices and emerging as a growing concern about environmental degradation, increased awareness and understanding of climate change, depleting resources, rising energy costs, and growing demands for sustainable building design and construction [3]. A green hospital has no universal definition; however, it can be defined as a facility that is designed and built to use as many natural resources as possible in an efficient and environmentally friendly manner [2]. A green hospital must meet requirements for waste, environment, water, energy, hazardous material management, material properties, and efficient building layout [4]. Green building concepts not only serve to create environmentally sensitive designs, but also to protect the natural balance while meeting the required satisfaction and medical conditions [5]. Because hospitals and healthcare facilities are intended to be places of healing and rehabilitation, the influence of the environment on users is more essential than in offices or other commercial settings [6]. Ensuring universal health coverage requires that healthcare facilities operate in a safe and sustainable environment. Only when adequate water, sanitation, hygiene, and waste management are offered, as well as environmental adaptability to disasters and climate change, can patient safety be attained [7].

2. Literature review

Health care has worldwide environmental consequences that, depending upon what indicator is used, vary between 1% and 5% of overall global effects, with certain country impacts exceeding 5% [8]. Poor management of waste, extended and excessive usage of hazardous materials, dangerous chemicals, and medical technology emitting dangerous radiation in healthcare organizations, according to research, are gradually and surely hurting the environment [9]. The healthcare industry, including hospitals, health systems, and the supply chain for medical supplies, can increase emissions over the whole lifespan of their operations [10]. Because hospitals are a significant source of pollution, the Green Hospital principles have begun to play a significant role in hospital administration. To solve some environmental issues, several hospitals have attempted to implement the "green hospital" idea [11].

2.1 Green hospital's significance to the environment and human beings

According to Erdede et al. 2021, adopting the green building concept has numerous environmental, social, and economic benefits, such as reducing CO2 emissions, minimizing

environmental damage during construction, minimizing operational expenses, enabling the use of renewable energy, enabling recycling, enabling harvested rainwater (green roofs), and allowing for the use of ambient daylight (helps in saving energy and decreasing heating and cooling expenses) [4, 12]. Green roofs, for example, have the potential to improve stormwater management, reduce the urban heat island effect, increase biodiversity, and filter the air to absorb poisons and pollutants [13].

A "green hospital" considers the environment to be an essential component of providing excellent care. It has characteristics such as a strategic position, efficient use of resources such as water, electricity, and air pollution, and the use of high-quality materials. It can produce more goods, maintain interior quality, and provide healthy meals and a natural environment. It promotes environmentally friendly practices, non-toxic environments, green cleaning, and trash reduction, as well as providing a therapeutic garden [14].

According to Allen et al. (2015), green buildings minimize their negative effects on the environment by conserving energy and water, as well as by minimizing side effects close to the construction site. The goal of green design, on the other hand, is typically to improve people's health. Public health is significantly impacted by green buildings on two levels: directly at the individual level by providing ideal indoor environmental conditions, and indirectly at the population level by lowering energy consumption and thereby reducing harmful emissions that cause illnesses and contribute to global climate change, which is linked to a number of detrimental health effects [15].

According to Danilov et al. (2020), designing healthcare facilities in accordance with green standards has a number of benefits, including quicker patient recovery (resulting in a shorter hospital stay), a reduction in sick building syndrome (SBS) for both patients and staff, and lower stress levels among hospital staff (which improves the quality of patient care) (which improves their work quality and overall hospital performance). Furthermore, a green hospital improves patient medical care while utilizing environmental resources efficiently, effectively, and sustainably [2]. Green hospitals had 3.6% higher overall patient satisfaction than non-green hospitals, according to Golbazi and Aktas (2020). Patients were 5.6% more likely to recommend green hospitals to others [16]. According to one study, the benefits of using a green hospital approach include reduced hospital stays by 8.5%, 15% faster healing times, a 22% reduction in the need for painkillers, and an 11% reduction in secondary infections [17].

Other approaches and instruments, such as "Towards a carbon-neutral hospital," "Health Care Without Harm," and an Environmental Thermometer, have been developed specifically for the healthcare industry, and hospitals in particular. One of these strategies is illustrated by the international nongovernmental organization (NGO) Health Care Without Harm (HCWH), which strives to transform health care globally in order to leave a smaller environmental footprint, grow into a social anchor for sustainability, and become a leader in the global movement for environmental health and justice [19].

2.2 Examples of green hospitals and their advantages

Deviyanti (2022) reports that between 2016 and 2021, the RSUP Dr. Sardjito hospital was able to recycle 8.08–14.61% of 900 kg of medical waste per day and 34.35–62.2% of 9,606 kg of solid waste per month. Composting organic waste further boosts the hospital's efficiency. RSUP Dr. Sardjito will be able to save nearly $24,000 as a result in 2022. Beyond waste management, the hospital is dedicated to creating a healthier environment for guests, staff, and patients. Its green hospital initiative is carried out across all operational aspects and infrastructures, from creating environmentally friendly patient amenities like healing gardens, bike lanes, and pedestrian walkways to promoting energy efficiency [7].

The Green Hospital Scorecard (GHS) is a Canadian program that helps strengthen environmental activities, inspires behavioral modification for future conservation efforts, raises hospital awareness, and evaluates a hospital's corporate leadership, planning, and administration, as well as its energy and water saving, waste management, and pollution control efforts, according to Shi et al (2021). GHS revealed a total energy usage of 13,293,297 GJ among all participants in 2019. (83 hospitals participate in the GHS program in Canada). While the overall average energy usage intensity (EUI) for all hospitals was determined to be 2.8 GJ/m2/year, hospitals consumed a total of 8,543,242 cubic meters of water in 2018; participants' average water usage intensity (WUI) was 1.84 m3/m2/year. A total of 101,898 metric tonnes (MT) of waste were produced by hospitals, yet 39,946 MT of recyclables and other non-disposable waste were kept out of landfills. With an average waste volume of 3.15 MT/bed, participants kept around 39% of their garbage out of landfills [20].

In 2017, the Mayo Clinic in Eau Claire, Wisconsin, saved enough water to fill 50 Olympic-sized swimming pools, and renewable energy accounted for 25% of its electricity. The hospital implemented green practices by reusing 7.3 tons of plastic and 3.3 tons of surgical instruments, recycling 2.9 tons of batteries, and composting food waste [21].

One of HCWH's achievements is the successful 15-year campaign to phase out mercury-based medical equipment and replace it with safe, affordable, and accurate substitutes. The campaign was started in 1996 at a single hospital in Boston and spread to other hospitals around the globe. The WHO and other organizations collaborated on this international campaign, which was successful in getting language mandating the phase-out of mercury-containing thermometers and blood pressure devices by 2020 [19].

2.3 United Arab Emirates (UAE) & green hospitals

According to Todorova (2013), in the UAE, the Cleveland Clinic Abu Dhabi is a green hospital that meets Estidama's two-pearl standards. In addition, The MedHealth Medical Centre in Dubai uses a paperless method and is housed in a water and energy efficient structure. It has an irrigation system that uses condensation from air conditioners and a solar-powered hot water system that can produce 1,000 liters per day. The hospital is 50% more energy-efficient than comparable-sized structures, according to the architects, and has significant insulation to reduce heat gain while maximizing the use of natural sunlight. The building's construction method, which used roughly 30% locally made materials and 14% recycled content, adds to the facility's environmental credentials. The selection of paints and materials that don't contain a lot of volatile organic compounds—a group of chemicals, some of which are thought to be carcinogenic—was done with great care [22]. Green hospitals are definitely part of a recent sustainability initiative in the UAE. However, there is little information available in the UAE about green hospitals. Furthermore, the International Hospital Federation's 45th World Hospital Congress (WHC) was recently held in Dubai, with a focus on developing "green hospitals." During the conference, participants and decision-makers had ample opportunity to discuss potential solutions to global health concerns, particularly sustainability in healthcare. It also provides an excellent opportunity for all attendees to network, exchange knowledge, and discuss potential new areas of collaboration [23].

3. Methodology

The methodology for the study was based on a review of scholarly work in the field. The discussion centered on the main aspects of the green hospital: Green hospital facility design, green hospital energy efficiency, green hospital and patient-centered approach, green procurement in hospitals, as well as disadvantages and barriers to implementing the green hospital concept.

4. Discussion

4.1 Green hospital facility design

The "green hospital" approach refers to hospitals that meet at least one of the following criteria: selecting an environmentally friendly settlement design, purchasing sustainable construction products and materials, becoming environmentally conscious during hospital construction, and remaining environmentally conscious throughout the service production process [24]. This approach is based on environmental management knowledge in a variety of areas, including waste and hazardous material management, water management, energy management, emission control systems, and innovative environmental designs.

A healthcare center's planning and design process must consider a number of factors, including energy conservation, the use of renewable energy sources, water efficiency, indoor environmental quality, the efficiency of heating and cooling systems, chemical management, waste management, environmental protection, food services, greener purchasing, greener structural materials, pharmaceutical management, and reduced transportation [2].

Green grading systems for assessing and evaluating a building's environmental performance are gaining popularity around the world. As people become more aware of the benefits of "going green," various green building grading systems have emerged. Around the world, more than six building grading systems are in use, including LEED in the United States, Canada, China, and India, Green Star in Australia, New Zealand, and South Africa, and CASBEE in Japan [25].

For example, the Leadership in Energy and Environmental Design (LEED) grading system for green buildings, which includes green healthcare facilities and structures, has grown to become the most widely recognized accreditation system in the United States [16]. The primary goals of the rating system are divided into six categories: transportation and location, sustainable site planning, water sustainability, energy and air, resources and materials, and environmental quality (indoor) [26].

Both inpatient and outpatient healthcare facilities and accredited long-term care facilities can earn the LEED for Healthcare certification. The grading scheme incorporates specialized healthcare-related tactics and is tailored to healthcare contexts [16]. Hospital administrations have collaborated with designers, architects, and construction companies to obtain the LEED certification [27].

4.2 Green hospital energy efficiency

Standard operating procedure for the majority of large western-style hospitals requires significant energy use for water heating, indoor environmental temperature and humidity controls, lighting, ventilation, and various medical procedures, with correspondingly high financial costs and greenhouse gas emissions [28]. Hospitals frequently have an energy usage intensity (EUI) that is roughly three times higher than the national average for commercial buildings [29].

Improvements in the energy economy, on the other hand, do not have to come at the expense of patient care [30]. Green designers prioritize energy conservation, particularly in ventilation and lighting. Increasing the use of natural lighting throughout the day can reduce energy costs while also improving the environment for building occupants. The importance of natural light availability and its influence on building users, particularly how it can drastically affect behaviors, has been demonstrated [6].

It may be possible to significantly reduce energy waste by taking steps like switching to compact fluorescent and light-emitting diode (LED) light bulbs, adjusting thermostats seasonally, purchasing energy-efficient items, limiting "standby" energy consumption, and upgrading buildings [31]. A program was started in 2003–2004 by Companhia Paulista de Força e Luz (CPFL), a Brazilian energy holding company, to help 101 hospitals and clinics in the state of So Paulo reduce their energy costs and greenhouse gas emissions. The simple energy-saving initiatives, which included repairing compact fluorescent lights and improving light circuits, resulted in a 25% decrease in energy consumption (and energy costs) at the 101 healthcare facilities [32].

A number of guidelines have been developed to assist in designing energy-efficient healthcare facilities. For instance, Arub 2021 presented a guide titled Energy and Resource Efficiency in Hospitals and Healthcare Facilities. The Guide offers cost-effective efficiency techniques for the design and construction of new healthcare facilities, the renovation and modernization of existing healthcare facilities, the reduction of operating costs for healthcare facilities and the technology systems that support them, and discussion of waste management and fire safety as the two most important infrastructure elements in healthcare institutions [33].

4.3 Green procurement in hospitals

According to CHEO (2016), green procurement is the practice of purchasing more environmentally friendly goods and services and incorporating environmental performance

measures into all phases of the procurement process, including design, purchasing, using, and disposing. Environmentally preferable goods and services have less of an impact on the environment over the course of their useful lives when compared to competing products or services performing the same function. Green purchasing eliminates negative effects on health, reduces resource consumption and waste production, and might even result in cost savings. It also encourages sustainability [34]. **Figure 1** shows the main tenets of green procurement.

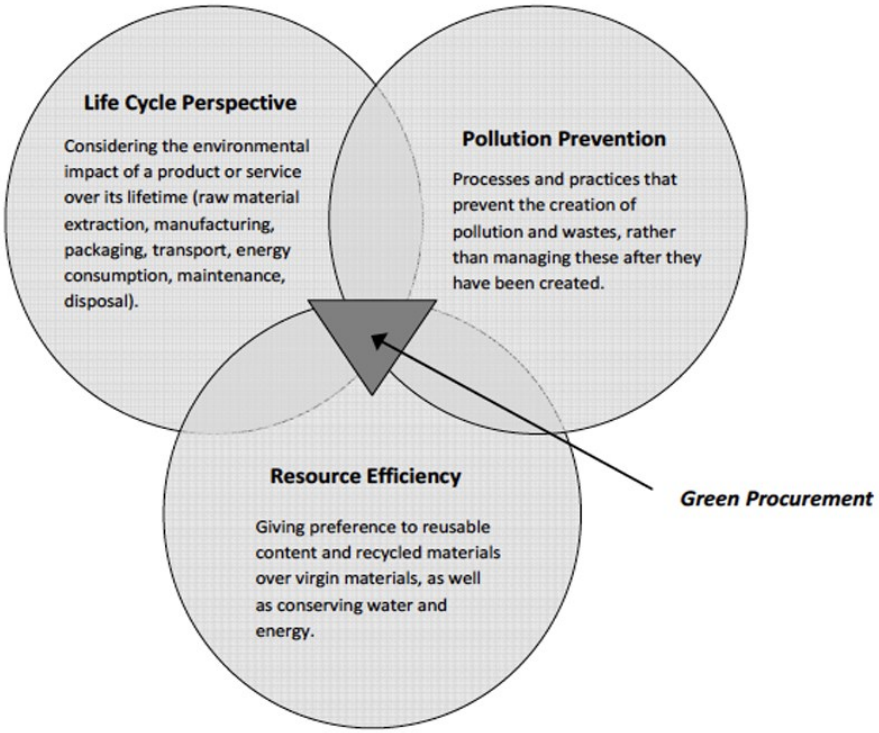

Figure 1:Green procurement principles. Adopted from [33].

In the majority of healthcare organizations, supply chain teams frequently make purchases on behalf of various departments. Healthcare product safety and quality must always come first, but procurement staff are increasingly concentrated on other aspects of a product, such as its packaging and the efficient use of water and energy [35].

Manufacturers and healthcare providers have made significant progress in adopting and integrating environmental, social, and financial sustainability throughout the industry over the past 20 years. The products' manufacturing processes and materials are being assessed by suppliers [36]. According to a study, 35% of healthcare organizations globally acknowledged switching suppliers in order to obtain more environmentally friendly products and supplies [37]. CHEO (2016) cites the following instances of green purchasing in healthcare facilities:

- Purchasing energy-efficient appliances.
- Purchasing long-lasting/durable materials and goods.

- Dealing with companies who use environmentally friendly technology and procedures.
- Applying techniques to reduce pollution or water usage.
- Purchasing materials and items that have preferable choices for recycling, remanufacturing, and/or disposal.

The United Nations Development Programme (UNDP) and Health Care Without Harm launched Sustainable Health in Procurement Project (SHiPP). The Sustainable Health Procurement program offers instructions and a plan for creating a program and governance structure that promotes sustainable health procurement [36].

4.4 Green hospital and patient-centered approach

According to Shepley et al. (2009), while the first significant document to shift hospital design toward sustainable practices (i.e., Green Guide for Healthcare) was published in 2002, the Evidence-Based Design movement has been driven by the creation of patient-centered institutions that have improved patient care for the last 25 years. On a practical level, these two design philosophies do, however, largely overlap, and because they both have a goal associated with human health, their relationship is frequently synergistic. As was already mentioned, implementing a green hospital approach has numerous direct and indirect advantages for patients [38].

According to Delgado et al. (2021), the interaction of technological advancement, economic market forces, rising healthcare costs, patient and staff safety, and changing governmental regulations is leading to a shift toward patient-centered care. This change is encouraging the deliberate implementation of healthy building practices that improve lighting and air quality [39].

4.5 Green hospital drawbacks and Barriers

Adoption of green hospitals may face some challenges. There is no universal plan for green hospitals, and many countries employ a variety of models based on their geographical location and individual needs [40]. The Bureau of Energy Efficiency (BEE) has several green building grading systems, such as Star Rating, ECBC Compliance, Green Rating for Integrated Habitat Assessment (GRIHA), and others. These systems overlap in terms of energy efficiency, water efficiency, and waste management patterns, which may be related to geographic variations, and various companies supplying organizations must be mentioned [41]. Due to health and safety laws and construction regulations, hospitals are unable to adopt sustainable practices. Furthermore, hospitals must adhere to stringent infection control procedures, which may conflict with long-term business viability [42]. Compliance with federal, state, and accrediting

criteria may make it difficult to make environmentally responsible decisions [42]. The exteriors of hospital buildings can last for a long time, but interior upgrades are required every few years [42]. Green hospitals are expensive to build at first [5]. According to one study, the most pressing issues are the lack of green procurement regulations, financial assistance from senior management, government incentives for green purchases, and senior management support for green purchases [43].

5. Conclusion

Healthcare systems are critical to maintaining and improving human health, but they have environmental consequences that contribute to environmental degradation and have an impact on human health. Although the hospital's primary goal is to improve human health, it cannot be considered to exist in a bubble separate from the city. "Green Hospital" is a strategy that has emerged as an effort to improve health, which is its primary goal, as well as to address environmental issues and community needs in health issues. The green hospital concept has the potential to be a game changer for more sustainable health care. Green hospitals can be achieved through green design, energy efficiency, and green procurement. Several pieces of evidence demonstrated how the green building concept benefits both the environment and people. Even though there are obstacles, they can be overcome through innovative thinking and technology.

It is sincerely hoped that by cooperating on all levels, from the individual to the organizational, we will be able to transform the healthcare facility from a major energy consumer to an environmental advocate. More hospitals should join environmental sustainability efforts and strive for a healthy, environmentally sustainable workplace. The following are some ideas for increasing the adoption of the green hospital concept. Thinking outside the box and presenting creative, interdisciplinary design techniques that consider innovative solutions [44]. Incentives must be provided to encourage the development of innovative, sustainable healthcare facilities. When making sustainable procurement of goods and services, the entire lifecycle of healthcare delivery must be considered. This includes the manufacture and distribution of goods such as pharmaceuticals and medical devices, the actual delivery of healthcare through the efficient and sustainable procurement of services for resources such as water and energy, and the proper disposal of used products at the end of their useful lives, such as waste, packaging materials, food waste, etc. [10]. Establish an infrastructure for action and form a committee to oversee hospital-wide sustainability initiatives by assessing baseline emissions, establishing priorities, and drafting environmental initiative

regulations [33]. In the healthcare industry, the government must support, legislate, and adopt green building concepts. Through research and the examination of best practices, hospitals must constantly broaden their green initiatives in the following areas: environmentally friendly purchasing, chemical management, sustainable building and renovation, energy and water conservation, and waste management strategies, objectives, and action plans.

6. References

[1] US EPA. (n.d.). Sustainable Healthcare. United States Environment Protection Agency. Retrieved Nov 27, 2022, from https://archive.epa.gov/region03/green/web/html/healthcare.html

[2] Garg, A. & Dewan, A. (2022). Green Hospitals. Manual of Hospital Planning and Designing .485-498.10.1007/978-981-16-8456-2_48.

[3] Howard, J. (2003). The federal commitment to green building: experiences and expectations. Federal Executive, Office of The Federal Environmental Executive, Washington.

[4] Konakoğlu, Z. & Kurak, F. (2021). Assessment Of Green Hospital Criteria: Case of Trabzon. Social Mentality and Researcher Thinkers Journal. 7. 3512-3522.

[5] Danilov, A. , Benuzh, A. , Yeye, O., Compaore, S. & Rud, N. (2020). Design of healthcare structures by green standards. E3S Web of Conferences. 164. 05002. 10.1051/e3sconf/202016405002.

[6] Wood, L., Wang, C., Abdul-Rahman, H., & Abdul-Nasir, N. (2016). Green hospital design: integrating quality function deployment and end-user demands. Journal of Cleaner Production, 112, 903-913.

[7] Deviyanti, I (2022). Green hospitals for a healthier future. World Health Organization. Retrieved Dec 3, 2022, from https://www.who.int/indonesia/news/detail/15-08-2022-green-hospitals-for-a-healthier-future

[8] Lenzen, M., Malik, A., Li, M., Fry, J., Weisz, H., Pichler., & Pencheon, D. (2020). The environmental footprint of health care: a global assessment. The Lancet Planetary Health, 4(7), 271-279.

[9] Kapoor, R., & Kumar, S. (2011). Energy Efficiency in Hospitals Best Practice Guide. United States Agency for International Development, 41-52.

[10] Wilburn, S., Jharia, I., & Prabhakaran, P. (2021). Sustainable procurement in healthcare. Climate Change and the Health Sector, 183-191.

[11] Intraruangsri, J., & Mateekul, C. (2018). The Evolution of Green Hospital Concept for Thailand's Hospital, Thammasat University,1-66.

[12] Farzianpour, F., Hosseini, S.H. & Hosseini, S. (2014) .Global Change and Human Health. 2nd International Congress on Energy Efficiency and Energy Related Materials Libery Hotels Lykia, Oludeniz, 16-19 October 2014, 365.

[13] O'Hara, A. C., Miller, A. C., Spinks, H., Seifert, A., Mills, T., & Tuininga, A. (2022). The Sustainable Prescription: Benefits of Green Roof Implementation for Urban Hospitals. *Frontiers in Sustainable Cities*, *4*, 798012.

[14] Suwasono, E., Suman, A. and Yanuwiadi, B. (2013) Creating a Green Hospital Concept through the Management of Non-Medical Waste. International Journal of Advances in Engineering & Technology, 6.

[15] Allen, J., MacNaughton, P., Laurent, J ., Flanigan, S.., Maitland, E ., & Spengler, J. (2015). Green Buildings and Health. *Current Environmental Health Reports*, 2(3), 250-258. 10.1007/s40572-015-0063-y

[16] Golbazi, M., & Aktas, C.(2020). LEED Certification and Patient Wellbeing in Green Healthcare Facilities. *Journal of Green Building*, 15(4), 3-18.

[17] GBCA (n.d.). *Why design or build a green hospital?* Green Building Council of Australia. Retrieved Dec 3, 2022, from https://www.gbca.org.au/green-star/why-design-or-build-a-green-hospital/

[18] Kras, I.(2011). Sustainable hospital buildings. A Research Project Submitted in Fulfilment of master's degree in Urbanism and Building Sciences, Department of Real Estate and Housing, Technical University of Delft.

[19] HCWH. (2022). About: Health Care Without Harm. Health Care Without Harm. Retrieved Nov 30, 2022, from https://www.noharm.org/content/global/about

[20] Shi, S., Ritchie, D., Akella, k., & Varangu, L. (2021). Green Hospital Scorecard 2019. *The Canadian Coalition for Green Health Care*. 1-81.

[21] Lee, S. & Lee, D. (2022). Developing Green Healthcare Activities in the Total Quality Management Framework. *International journal of environmental research and public health*, *19*(11), 6504. https://doi.org/10.3390/ijerph19116504

[22] Todorova. V (2013). *Dubai's new hospital is a green light for energy efficiency*. The National. Retrieved Dec 3, 2022, from https://www.thenationalnews.com/uae/environment/dubai-s-new-hospital-a-green-light-for-energy-efficiency-1.388699

[23] Saseendran.S (2022). *World Hospital Congress in Dubai opens with a call for 'green hospitals' to fight climate change*. Uae – Gulf News. Retrieved Dec 3, 2022, from https://gulfnews.com/uae/world-hospital-congress-in-dubai-opens-with-call-for-green-hospitals-to-fight-climate-change-1.91878529

[24] Aydın ,D., Yaldız, E.,& Buyuksahin , S. (2017). Sustainable Hospital Design for Sustainable Development. 8th International Conference on Urban Planning, Architecture, Civil and Environment Engineering(UPACEE-17), Dubai (UAE) Dec. 21-22 AEBMS-2017, ICCET-2017, BBMPS-17, UPACEE-17, LHESS-17, TBFIS-2017, IC4E-2017, AMLIS-2017 & BEFM-2017. https://doi.org/10.15242/HEAIG.H1217804

[25] Wu, Z.(2011). Evaluation of a sustainable hospital design based on its social and environmental outcomes [Dissertation]. A Thesis Presented to the Faculty of the Graduate School of Cornell University in Partial Fulfilment of the Requirements for the Degree of Master of Science, Cornell University,1-228.

[26] USGBC. (2018). LEED rating system-U.S. Green Building Council. Retrieved Nov 25, 2022, from https://www.usgbc.org/leed.

[27] Corporate Wellness Magazine. (n.d.). *Redefining Healthcare with Design of the Green Hospital*. Retrieved Dec 3, 2022, from https://www.corporatewellnessmagazine.com/article/redefining-healthcare-design-green-hospital

[28] Dhillon, V., & Kaur, D. (2015). Green Hospital and Climate Change: Their Interrelationship and the Way Forward. *Journal of clinical and diagnostic research*: JCDR, 9(12), 1-5. https://doi.org/10.7860/JCDR/2015/13693.6942

[29] Della Barba, M. (2014). Optimizing Energy Use in a Healthcare Setting. 22nd National Conference on Building Commissioning.

[30] Karliner, J., & Guenther, R. (2011). Global green and healthy hospitals. Health Care Without Harm,1-31.

[31] HCWH. (2009). Addressing climate change in the health care setting: opportunities for action. Health Care Without Harm, Arlington, 3-11.

[32] WHO. (2009). Health Care Without Harm. Healthy hospitals, healthy planet, healthy people—addressing climate change in health care settings: discussion draft. World Health Organization,1-32.

[33] Arup. (2021). Energy and Resource Efficiency in Hospitals and Healthcare Facilities,1-86.

[34] CHEO.(2016).Green Hospital Procurement Policy and Procedure Manual, and Implementation Guide. Children's Hospital of Eastern Ontario,1-42.

[35] Mwacharo, F. (2015). Green procurement in Kenyan hospitals: exploring the awareness and opportunities for Kenyan hospitals to implement green procurement. A Research Project Submitted in Partial Fulfilment of the Requirements for the Award of the Degree of Master of Business Administration, School of Business, University of Nairobi.

[36] Lindstrom, A.& Coronado-Garcia, L. (2020). Sustainable Health in Procurement Guidance Note. United Nations Development Programme (UNDP),1-58.

[37] Johnson & Johnson. (2012). The growing importance of More Sustainable Products in the Global Health Care Industry,4-19.

[38] Shepley, M., Baum, M., Ginsberg, R., & Rostenberg, B. (2009). Eco-effective design and evidence-based design: Perceived synergy and conflict. HERD: Health Environments Research & Design Journal, 2(3), 56-70.

[39] Delgado, A., Keene, K. M, & Wang, N. (2021). Integrating Health and Energy Efficiency in Healthcare Facilities (No. PNNL-31040). *Pacific Northwest National Lab.(PNNL)*, Richland, WA (United States),1-15.

[40] Shaabani, Y., VafaeeNajar, A., & Hooshmand, E. (2016). Investigation and comparison of available models for green hospitals. Journal of Healthcare Management, 7(1), 15-24.

[41] Tarkar, P. (2022). Role of green hospitals in sustainable construction: Benefits, rating systems, and constraints. Materials Today: Proceedings. 60. 10.1016/j.matpr.2021.12.511.

[42] Roberts, G. (2011). Shades of green. Health Facilities Management. Retrieved Dec 2, 2022, from https://www.hfmmagazine.com/articles/813-shades-of-green

[43] Ahsan, K. & Rahman, S. (2017). Green public procurement implementation challenges in the Australian public healthcare sector. *Journal of cleaner production, 152*, 181-197. DOI: 10.1016/j.jclepro.2017.03.055

[44] Chias, P. & Abad, T. (2017). Green hospitals, green healthcare. *International Journal of Energy Production and Management*. 2. 196-205. 10.2495/EQ-V2-N2-196-205.

Al-Kitab Journal for Pure Sciences (2022); 6(2): 46-64.

https://doi.org/10.32441/kjps.06.02.p5

Al-Kitab Journal for Pure Sciences
ISSN: 2617-1260 (print), 2617-8141(online)
www.kjps.isnra.org

Diagnosing the Effect of Misalignment on a Rotating System using Simulation and Experimental Study

Luay Majid Hassan *, Jaafar Khalaf Ali

University of Basrah, Iraq.

*Corresponding Author: engpg.luay.majid@uobasrah.edu.iq

Citation: Hassan, L., Ali, J. Diagnosing the Effect of Misalignment on a Rotating System using Simulation and Experimental Study. Al-Kitab Journal for Pure Sciences (2022); 6(2): 46-64. DOI: https://doi.org/10.32441/kjps.06.02.p5

Keyword
Diagnosis, FFT Analyzer, Parallel Misalignment Vibration Spectrum, Ansys software.

Article History

Received	01 Jan.	2023
Accepted	21 Jan.	2023
Available online	30 Jan.	2023

Abstract:

Misalignment is one of the common causes of machine vibration. Understanding and practicing the fundamentals of rotating shaft parameters is the first step in reducing unnecessary vibration, reducing maintenance costs, and increasing machine uptime. In the industrial setting, misaligned machines account for 50% of all machine downtime. The most frequent issue with rotating machinery that affects every industry is rotor shaft misalignment. Consequently, misalignment defects can be qualitatively identified using condition monitoring based on vibration measurements. The present study employs vibration measurement method by Building a model that contains suggested defects and then using it in advanced simulation programs such as Ansys. and Validation of the results by comparing them with the results of experimental methods Validation results show that both numerical and experimental data are in good match regarding amplitude and frequency. The verification results proved that the frequencies that were extracted by using finite element techniques (simulation reading) agree with the frequencies that were extracted by the experimental (experimental reading) (100%).

Keywords: Diagnosis, FFT Analyzer, Parallel Misalignment, Vibration Spectrum, Ansys software.

تشخيص تأثير المحاذاة الخاطئة على نظام دوار باستخدام المحاكاة والدراسة التجريبية

لؤي ماجد حسن*، جعفر خلف علي

جامعة البصرة، كلية الهندسة، العراق.

*engpg.luay.majid@uobasrah.edu.iq

الخلاصة:

يعد الاختلال في المحاذاة أحد الأسباب الشائعة لاهتزاز الماكينة. يعد فهم وممارسة أساسيات معلمات عمود الدوران الخطوة الأولى في تقليل الاهتزاز غير الضروري وتقليل تكاليف الصيانة وزيادة وقت تشغيل الماكينة. في البيئة الصناعية ، تمثل الآلات المنحرفة ٥٠٪ من كل وقت تعطل الماكينة. المشكلة الأكثر شيوعًا في الآلات الدوارة التي تؤثر على كل صناعة هي اختلال محاذاة عمود الدوران. وبالتالي ، يمكن التعرف على عيوب المحاذاة الخاطئة نوعياً باستخدام مراقبة الحالة بناءً على قياس الاهتزاز. تستخدم الدراسة الحالية طريقة قياس الاهتزاز من خلال بناء نموذج يحتوي على عيوب مقترحة ثم استخدامه في برامج المحاكاة المتقدمة مثل ANSYS. والتحقق من صحة النتائج من خلال مقارنتها مع نتائج الطرق التجريبية. أظهرت نتائج التحقق أن كل من البيانات العددية والتجريبية متطابقة بشكل جيد من حيث السعة والتردد. كما أثبتت نتائج التحقق أيضا" أن الترددات التي تم استخلاصها باستخدام تقنيات العناصر المحدودة (قراءة المحاكاة) تتفق مع الترددات التي تم استخلاصها بالقراءة التجريبية بنسبة ١٠٠٪.

الكلمات المفتاحية: تشخيص العيوب، محلل FFT ، اختلال متوازي، طيف الاهتزاز، برنامج محاكاة متقدم.

1. INTRODUCTION:

Rotor systems have been widely used in mechanical engineering. The dynamics of rotor systems have been studied for over a century. With the high-speed demand of today's machinery, it becomes more important than ever. Misalignment is one of the predominant failures of rotating machines driven by induction motors, this leads to economic losses. Also misaligned machinery is more prone to failure due to increased load on bearings, seals, and couplings. Shaft misalignment has major implications for modern day rotating equipment's reliability. Even though many efficient alignment methods have been put into place, alignment nevertheless may deteriorate because of changes in equipment operating conditions. Vibration issues have become more complicated due to the increasing sophistication of rotating machinery. In extreme circumstances presence of shaft misalignment can greatly influence machinery vibration response. All devices, such as motors and turbines, develop unique effects which can be analyzed to improve the design and decrease the possibility of failure [2,3].

Therefore, engineering judgments based on understanding of physical phenomenon are essential to provide diagnosis and method for correcting such faults. Anecdotal evidence suggests that as much as 50% of machine breakdown can be directly attributed to incorrect shaft alignment [1]. A large payback is always seen by regularly aligning the machine. Therefore, machine's operating life increases and as a result, process condition optimization takes place. There is widespread promotion of vibration signatures as a useful tool for studying machine malfunctions. However, the literature on this topic does not provide a clear picture of signature characteristics attributable exclusively to misalignment. Different authors report different signatures for misalignments using different types of couplings. Khot and Khaire [1] studied the effect of misalignment with flexible flange connections with the help of an FFT analyzer to obtain the frequency spectrum using the experimental setup that was developed for their work. The study was done by experimental work distortion work (displacement by an amount of 1.5mm). Between the two rotating shafts. Then simulate the rotary system using the Ansys program. within a specified speed range of (250 rpm to 1500 rpm). The vibration spectrum is gathered by modeling and testing with various stimulation frequencies, and it is observed that they are tightly connected. The results revealed that in second harmonics, or for parallel misalignment, the shaft should operate at 2X its normal speed, and for angular misalignment, at 1X its normal speed. Mohanty [2] presented a work that, the resulting vibration was studied by the presence of two types of problems in the mechanical system prepared for this purpose (unbalance and misalignment). The theoretical part was based on a proposed system consisting of equations that were used in calculating the forces in the three directions (X, Y, Z) resulting from these faults, and the results were identical in both cases. The method may be useful for large systems such as turbine shafts, gearboxes, and the like. Dere and Dhamande [3], proposed a work that uses misalignment of a rotating shaft by using the Ansys program, and good results were obtained by comparing them with the experimental side, and the results obtained by the researcher. Overall vibrational magnitude, as measured by root-mean-square acceleration values, is found to be greater at bearing support-2 (the point away from the motor) than at bearing support-1 (the point near the motor) with respect to both the horizontal and vertical axes for a variety of misalignment conditions, Including parallel or angular misalignment, or both. Babar and Utpat [4], to forecast the vibration spectrum of shaft misalignment, a rotary bearing system was analyzed in their work. An accelerometer and the Fast Fourier Transform (FFT) Analyzers were both employed. To measuring vibration. By modeling the rotating system and identifying the frequencies that signify the existence of the issue, the theoretical findings were discovered using the Ansys software (misalignment). in both the horizontal and

vertical directions, angular misalignment is found to be higher at bearing housing2 (the point away from the motor) and lessen at bearings housing1 (the point near the motor). It is also shown that for both bearing supports, the maximum total RMS acceleration for vibration is larger in the horizontal direction and increases as misalignments become more severe. Mogal and Lalwani [5] the problem of unbalance and misalignment was studied experimentally by analyzing orders in a direct examination method for the laboratory apparatus prepared for their work. The results showed that. When there is an unbalance, the total RMS value is higher in the horizontal than in the vertical direction, the amplitude is of the first order and dominates (1X), and the degree of phase changes and ranges between (by 90°±30°) on the drive end bearing and non-drive end bearing. While in the case of angular misalignment, the phase difference is between (180°±30°) and the value of RMS is greater in the axial direction compared to the vertical and horizontal directions. While it was discovered that in the case of parallel misalignment, the phase difference is between (180°±30°) measured via the coupling, and the RMS value is of the second order (2X) and is very large.

In this research, a study was done investigated the effect of parallel misalignment on a rotor shaft with a rigid as well as flexible flange coupling have 2 and 4, nuts and bolts and rubber coupling. Where it was noted that the use of rubber coupling helps in vibrations reduction by 98%. It is also revealed from the literature review that above, it is important to detect the fault at earlier stage, so that the machine life can be enhanced with less cost. Hence, it is proposed to investigate the effect of parallel misalignment of the rotating machinery by using experimental and simulation study.

2. Faults modeling

2.1 Coupling misalignment

Misalignment of the coupling in modern manufacturing, shaft misalignment in the rotor-bearing system is a typical and primary source of vibration in rotating machinery. In a system with misalignment, the parts are not coaxial because of their individual purposes. When two shafts aren't perfectly aligned, couplings are employed to make up the difference. Coupling is an often overlooked yet crucial aspect of any rotor system despite being relatively inexpensive in comparison to the whole. Complete lineouts may use either rigid or flexible couplings to join the individual shafts. In the case of stiff couplings, the link is modeled as the union of two beam elements. Flexible couplings are frequently employed in rotating machinery because they permit some misalignment between the axis of rotation of any two adjacent shafts. [2].

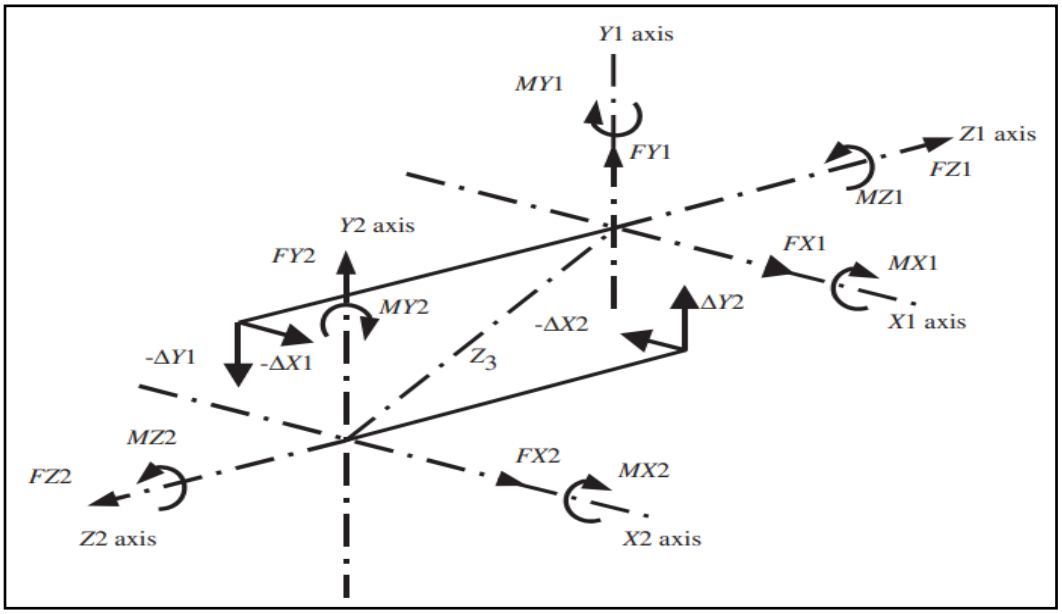

Fig. 1: Coupling coordinate system – parallel misalignment [2].

acts as follows on the shaft of the machine:

For parallel misalignment [2].

$$MX1 = T_q \sin\theta_1 + k_b\phi_1 \quad , \quad MX2 = T_q \sin\theta_2 + k_b\phi_2 \tag{1}$$

$$MY1 = T_q \sin\theta_1 + k_b\phi_1 \quad , \quad MY2 = T_q \sin\theta_2 + k_b\phi_2 \tag{2}$$

$$FX1 = (-MY1 - MY2)/Z3 \quad , \quad FX2 = -FX1 \tag{3}$$

$$FY1 = (MX1 + MX2)/Z3 \quad , \quad FY1 = FY2 \tag{4}$$

3. Experimental details

3.1 Faults Simulator Tests

Faults Simulator Tests To get more robust and approval for this work, many faults have been simulated at the machinery faults simulator. In these tests, The Data Acquisition (IDAC-6C) device was used with two sensor accelerometer type (B&K 4338) of a serial No. (442068) & (B&K 4338) of serial No. (540553) to transfer the data and then analyzed in the MATLAB program to detect fault cases misalignment. The machinery faults simulator can be shown in **Figure (2)** below. The main experimental part used in the generation of vibration signals are:

1. AC-motor controller
2. Tachometer

3. The Motor

4. Flexible coupling

5. Experimental bearing

6. Disc

7. Accelerometer.

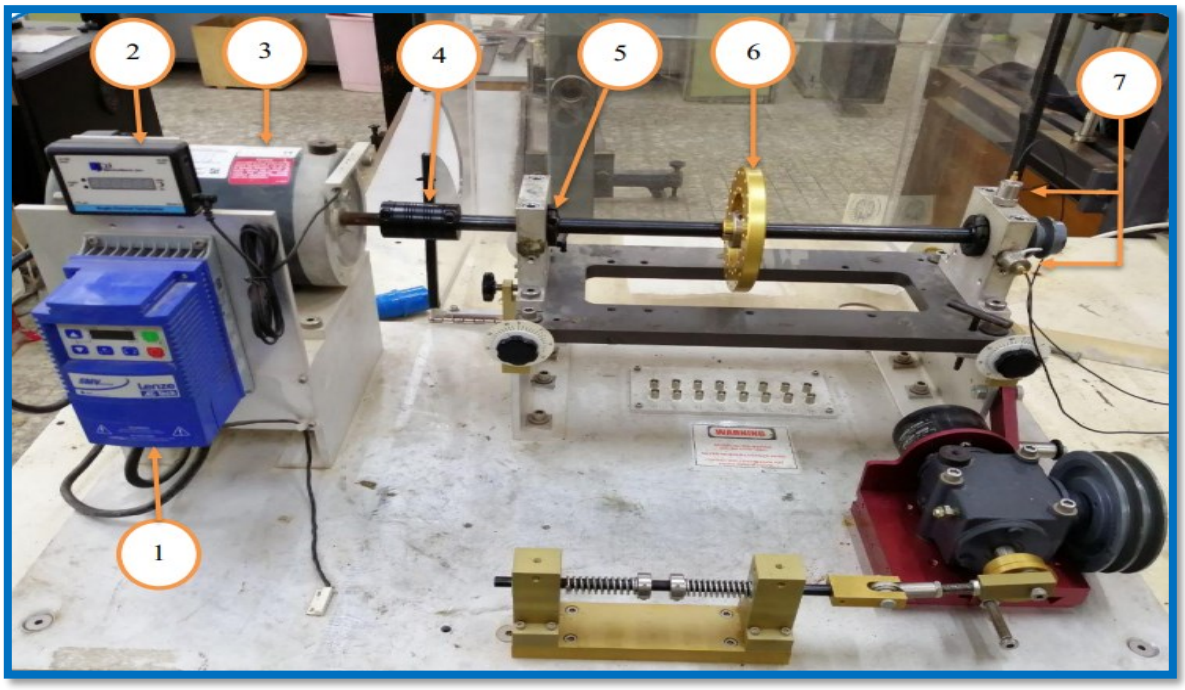

Fig.2: Machinery faults simulator

In these tests, the used rotor was already balanced. It has been used to show its vibration data, vibration spectrum, and phase difference at certain points on it. The shaft of the rotor has a diameter of (0.75 inches or 19.05 mm), and the distance between the supports was (407 mm). fault cases have been tested.

3.2 Experimental Procedure

Initially, the accelerometer is attached to the bearing housing and connected to the FFT analyzer. An FFT analyzer and a computer are used to record the vibration data. Bearings are subjected to a typical vibration spectrum. Vibration frequency spectrum behavior was investigated at a speed of (1500) rpm in the experiment. the laboratory workflow diagram is shown in **Figure (3)**. Data acquisition device is used to collect the raw vibration signal generated by MFS at speed value (1500 rpm), take new data for diagnosis **[9]**.

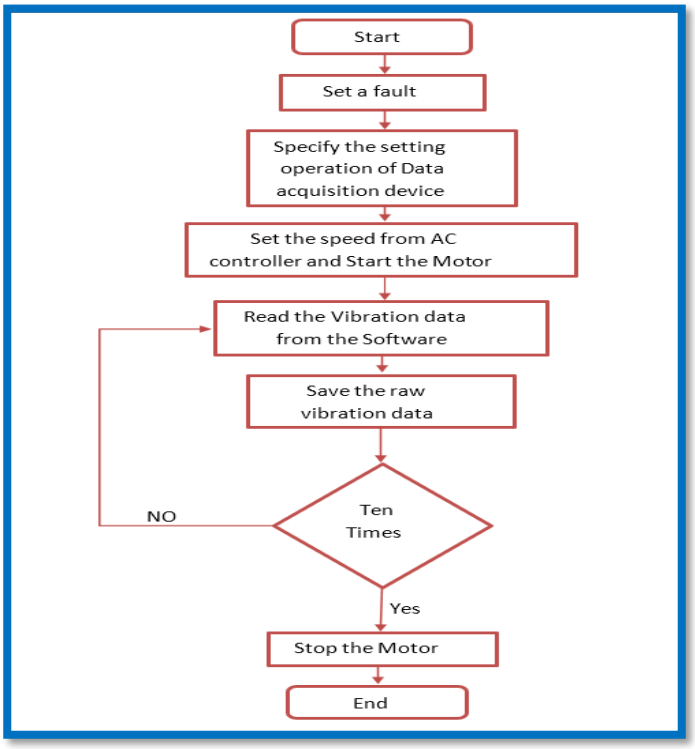

Fig. 3: Experimental Lap Procedure [9]

The setting operation for the IDAC-6C software interface for the speed(1500rpm) are:

• for speed (1500 rpm or 25 Hz) the sample rate is 2048 sample/sec, and the number of samples is 8192 and the low-pass filter is 800 sample/sec, and the high-pass filter is 0.3[9].

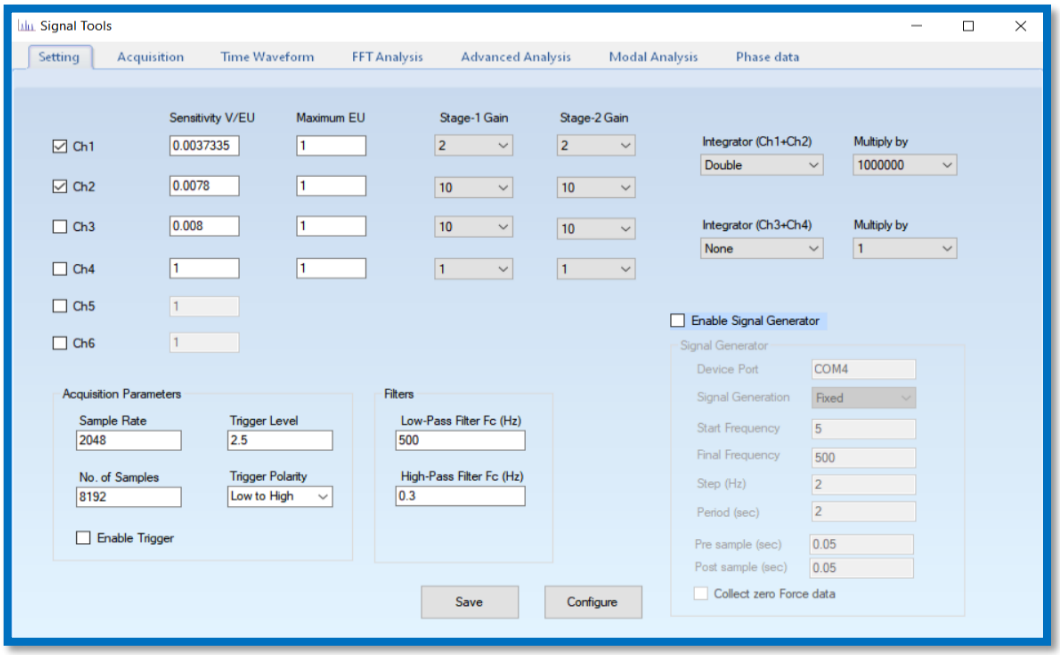

Fig. 4: setting operation for IDAC-6c software interface at speed (1500 rpm).

By Using MATLAB programming on the data that we obtained from the data acquisition device. This is done by writing a code in MATLAB, is possible to obtain vibration spectrum FFT with time waveform diagrams.

3.3 fault tested experimentally parallel Misalignment.

(1) Misalignment using Flange coupling at two-pins

The misalignment fault has been done Where the two shafts are connected using a Flange coupling at two-pin. And then it was given by giving a displacement of (1mm) to each of the main supports of the rotating shaft. The speed of (1500 r.p.m. or 25 HZ). was as shown in **Figure (5)**.

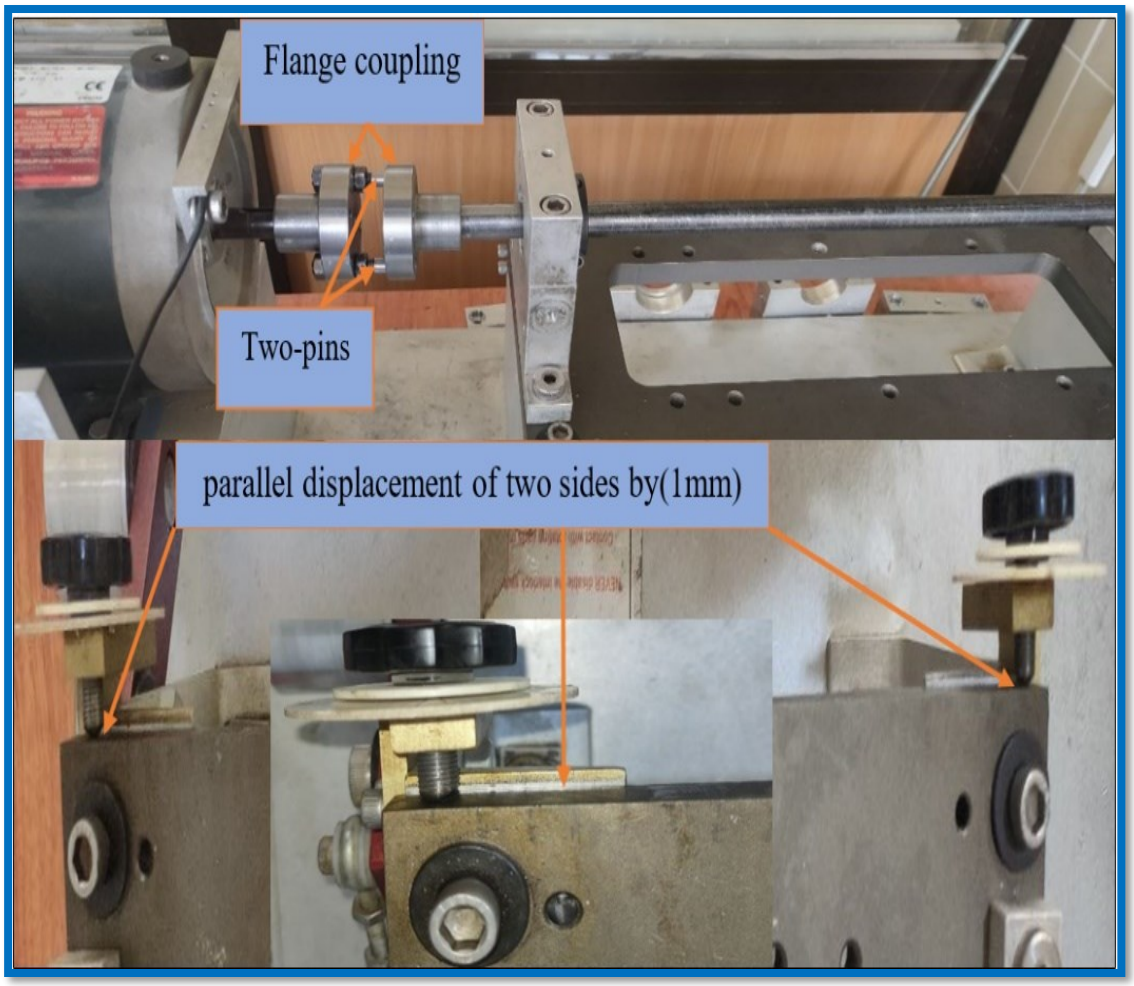

Fig. 5: shows the experimental parallel misalignment (using Flange coupling at two-pins).

(2) Misalignment using Flange coupling at four-pins

It has been accomplished in the same way as in the above case (Misalignment using Flange coupling at two-pin). But it was completed by changing the coupling. using Flange coupling at four-pin. was as shown in the **Figure (6)**.

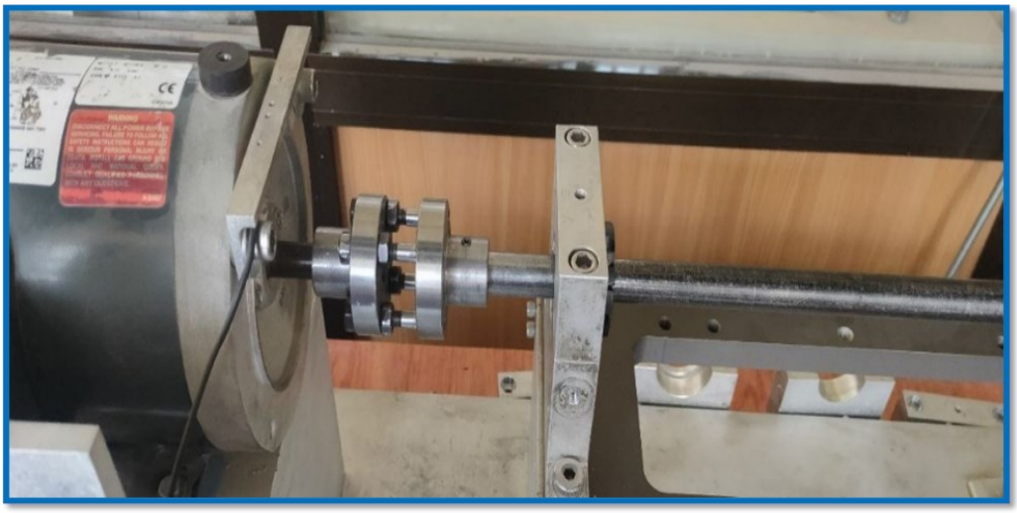

Fig. 6: shows the experimental parallel misalignment (using Flange coupling at four-pins)

(3) Misalignment using Rubber coupling

It has been accomplished in the same way as in the above case (Misalignment using Flange coupling at two-pin). But it was completed by changing the coupling. using Rubber coupling. The two ends of the coupling tool are tied with a rubber band of diameter(50mm) and length (20). With certain specifications. was as shown in the **Figure (7)**.

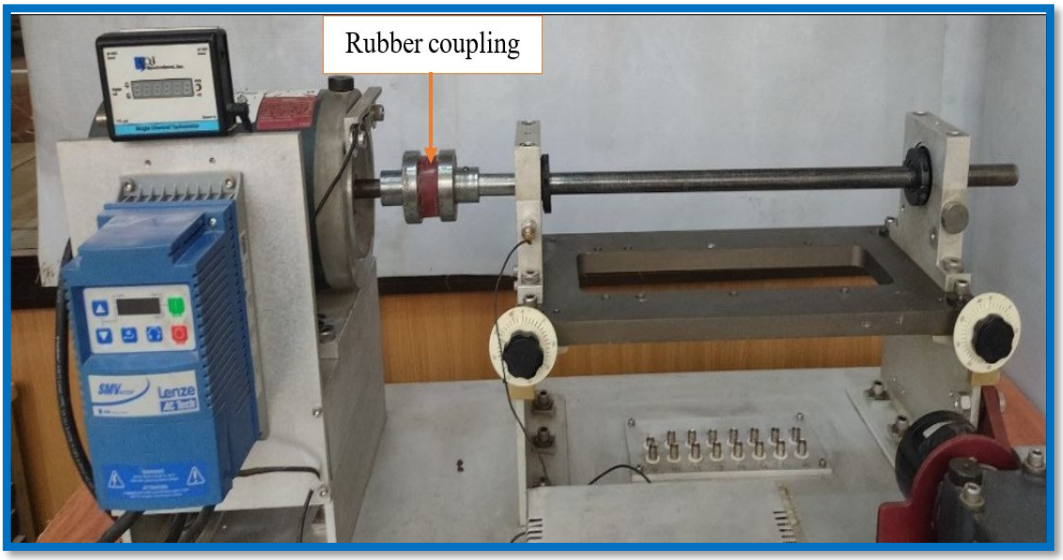

Fig. 7: shows the experimental parallel misalignment (using Rubber coupling)

4. Simulation Study

4.1 Modeling and mesh

Numerical analysis is carried out in this work by using FEA tool-ANSYS (2020R2) to determine the modal frequencies, mode shapes, and steady-state response of the system operation under parallel Misalignment, And the speed of the test was1500rpm (25HZ).

Figure (8) shows the 3-D model created, for the three misalignment cases with bearings specified in the FEA tool, for the numerical analysis of the system **[10]**. The automatic mesh method was used to mesh the structural model of the system as shown in **Figure (9)**. The material specified is structural steel with properties of elastic modulus E=210GPa, Poisson ratio=0.3, and Density=7850 kg/m^3.

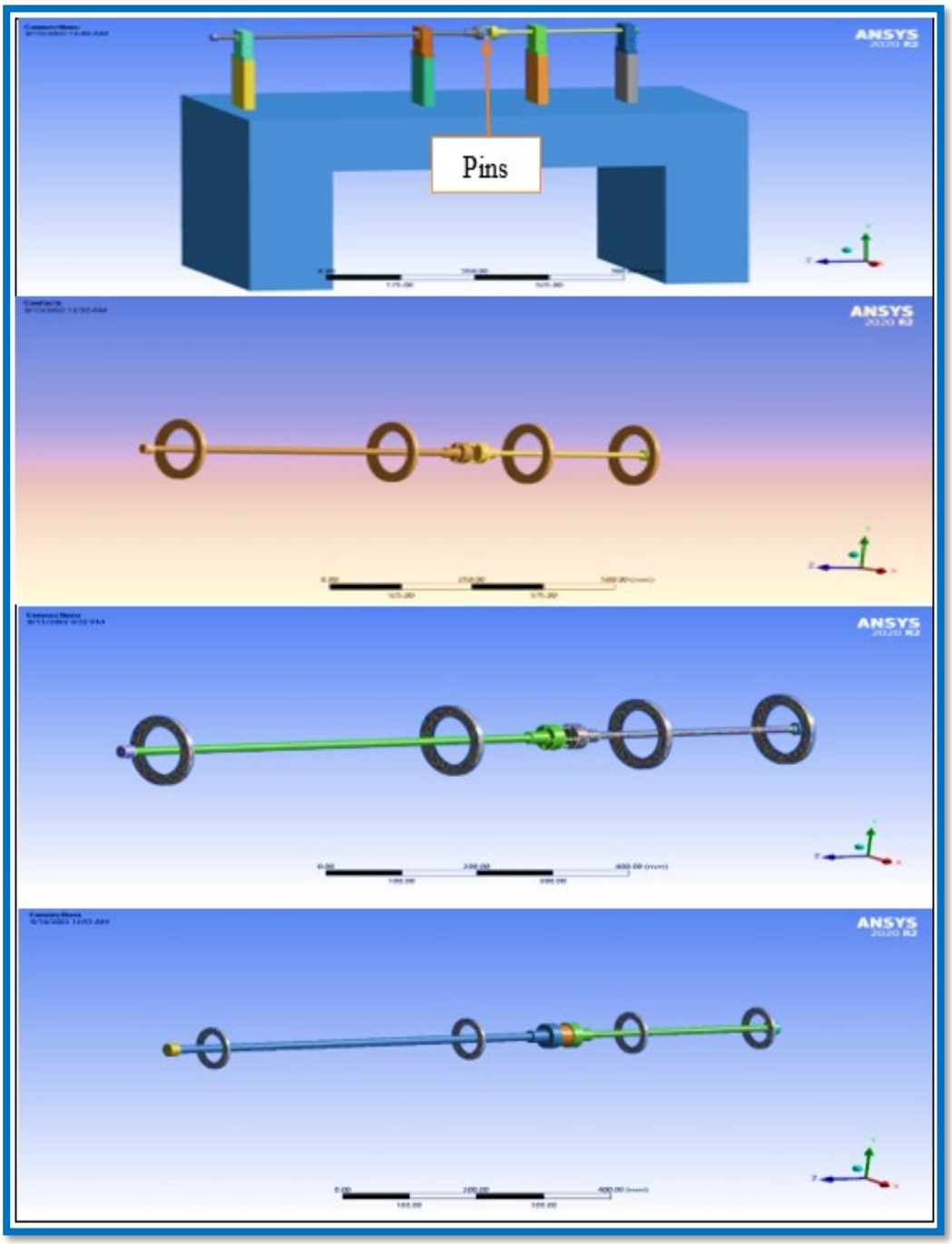

Fig.8: 3-D model for the three misalignment cases

Fig. 9: The automatic mesh using to mesh the structural model of the system.

4.2 Boundary condition and loading

• The bearing stiffness(K) was set to a constant value of 5000 N/mm because the bearing load and influence of rotation speed on bearing stiffness were not considered. Where the value of the velocity was 1500 RPM, and its direction was in the direction of the Z axis.

• The rotational velocity is added by writing commands in APDL in the Ansys program. Where the first command is for the first rotating shaft, which represents driving. While the second command is for the second rotating shaft, which represents the driven shaft. As shown below:

ICROTATE, SPOOL1,157,0,0,0,0,0,1,0,0,0,0

ICROTATE, SPOOL2,157,1,0,0,1,0,1,0,0,0,0

• Use flexible fixation from the edge of the left shaft to create thrust bearing (elastic support value =10 N/mm^3).

•Type of analysis in ANSYS: Transient Structural.

• A displacement of (1mm) was given in the direction of the axis (X), with the offset of the two axes fixed (Y and Z). The displacement was entered on the form of data. This data was produced by writing code in the MATLAB program. To be converted by the Excel program into a table consisting of two columns, it first represents the displacement, and the second column represents the time. Then they are entered into the Ansys program within the displacement condition and in the direction of the axis X.

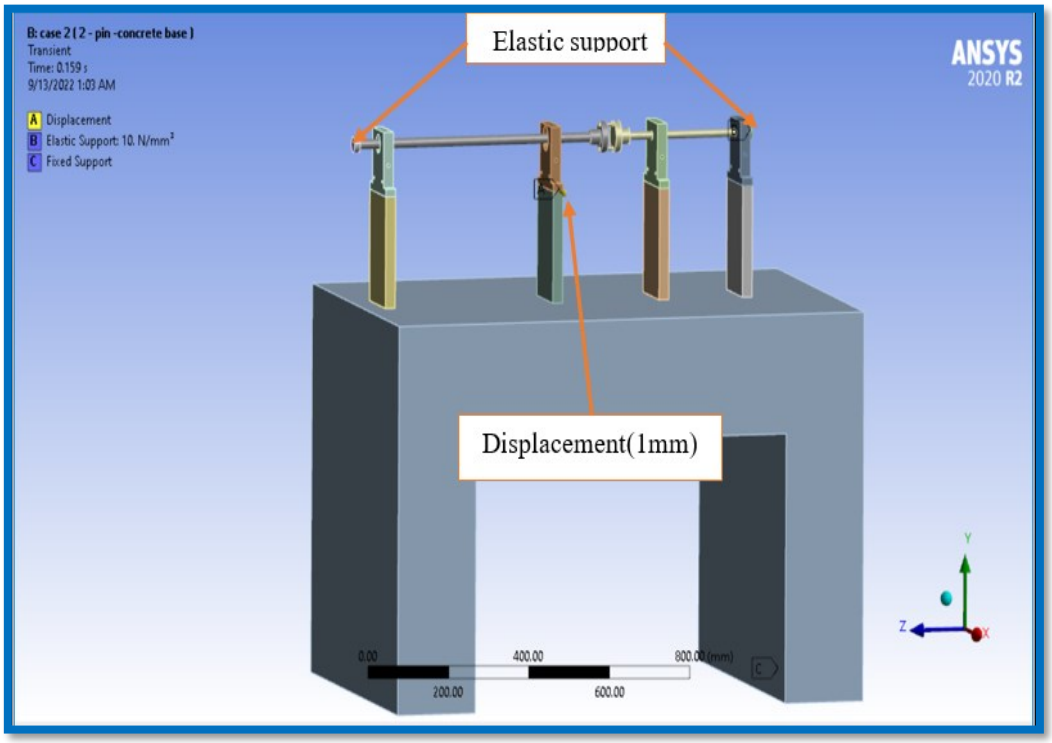

Fig. 10: Use boundary conditions in model of rotor bearing system (the direction of the displacement and elastic support)

• The code used to generate the displacement data using the MATLAB program.

```
t=0:0.001:0.16
y= (1/0.01) *(0:0.001:0.01)
y1=repmat (1, [1,150]);
yt= [y y1]
plot (t, yt)
ylim ([0 1.2])
```

• Convert data from MATLAB to Excel using the formula below.

```
k=table (t', y t','variable Names', {'time','dis'});
>> MS='mytrue.xlsx';
```

>> writetable (k, MS);

>> winopen (MS)

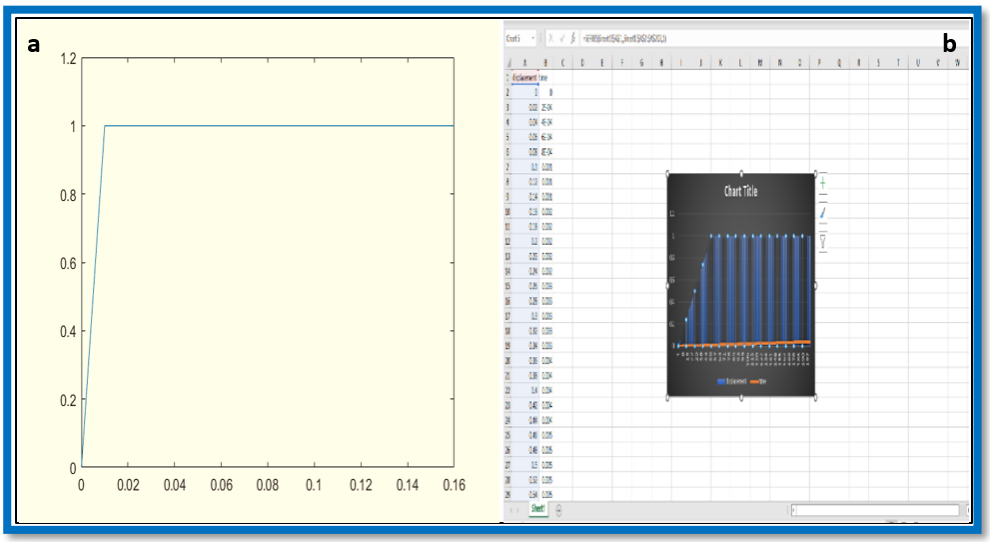

Fig.11: (a) Represents the displacement in MATLAB; (b) Represents the displacement in Excel.

5. Results and discussions

The vibrations are measured at the Drive end (DE) bearing in, horizontal directions, for the misalignment cases The above-mentioned. This work agrees with some of the research that was mentioned in the literature review. Where Some of them used the method of the empirical study to prove the validity of their work, and others used the simulation study (Ansys) and the empirical study to prove the validity of their work as well. Where they both extracted the diagrams of vibration spectrum (FFT) and time waveforms. Therefore, we can refer to some researchers whose research has been helpful to complete the results [1,2].

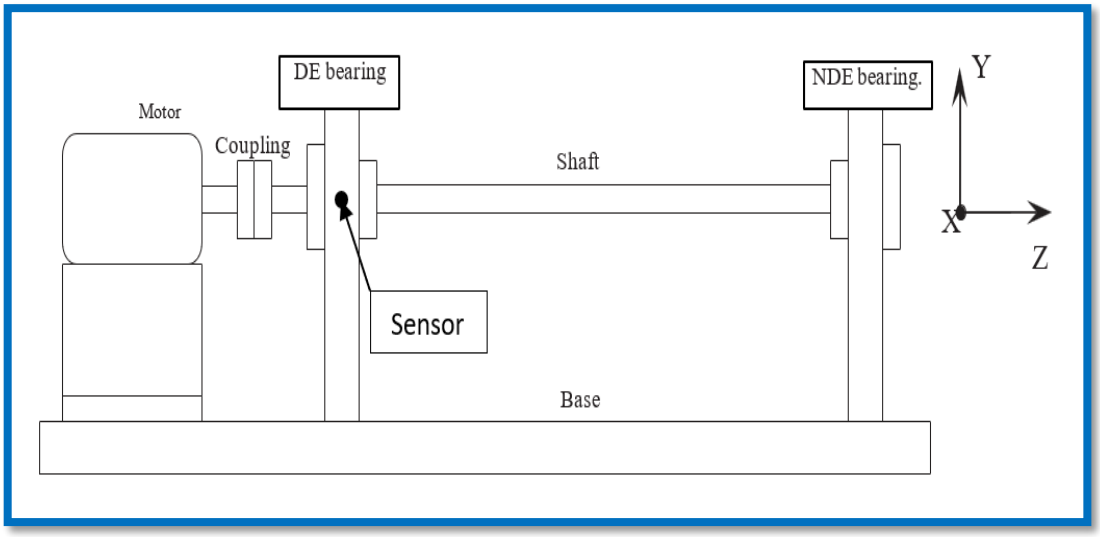

Fig. 12: Rotor–coupling–bearing test rig.

(A) Misalignment using Flange coupling at two-pins

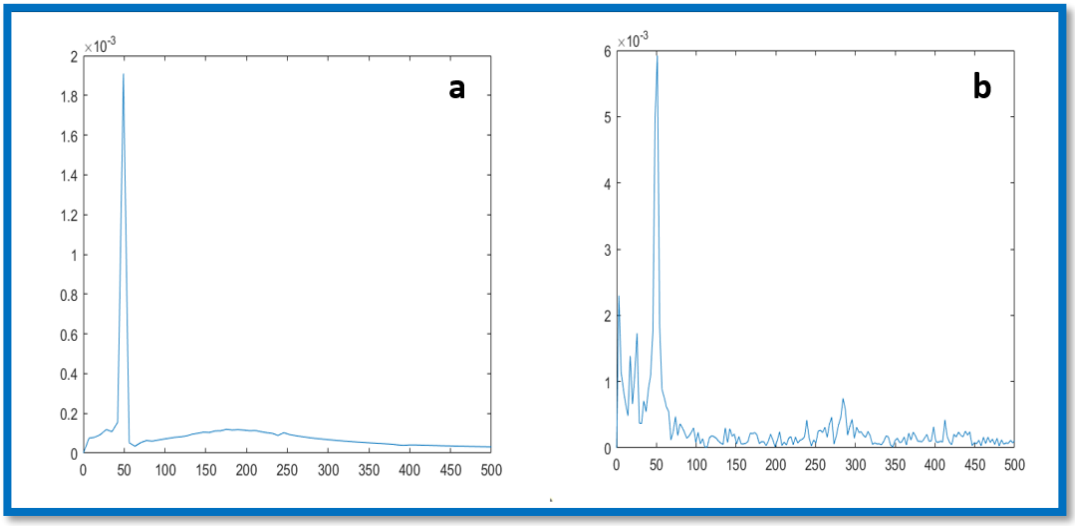

Fig.13: FFT of parallel misalignment (using flange coupling at two-pins for speed 1500rpm) at the Drive-end in the horizontal direction (DE-H). (a) Simulation study; (b) Experimental study.

Table 1: Overall amplitude for parallel Misalignment using Flange coupling at two-pins in horizontal direction at Drive-end (DE) bearings of the rotor.

Speed (RPM)	Amplitude (mm)		
	Bearing end	Simulation study	Experimental study
		Horizontal (H)	Horizontal (H)
1500 RPM (25HZ)	Drive-end (DE)	0.00190	0.00582

Observed through the experiment and simulation the vibration spectrum acquired on end bearings (Drive-end (DE) at a frequency of 25 Hz, it is found that the maximum vibration amplitudes observed are (0.00582mm) and (0.00190mm) for the experimental and simulation respectively. This indicates that the amplitude of vibration in the simulations is less than it is in the experiment. And this is possible because the theoretical model is not completely similar to the practical one in terms of the type of the pin's material and the space between the pin and the coupling, and also because of inaccurate manufacturing and the presence of deviations in the coupling itself that hinder movement more and cause a higher force. Also, other vibration sources contribute to the experimental data. However, the simulation and experimental results are in close agreement regarding dominant frequency since the peak amplitude is seen at 50 Hz which is 2X the shaft speed. As shown above, in **Figure (13)** and **Table (1)**.

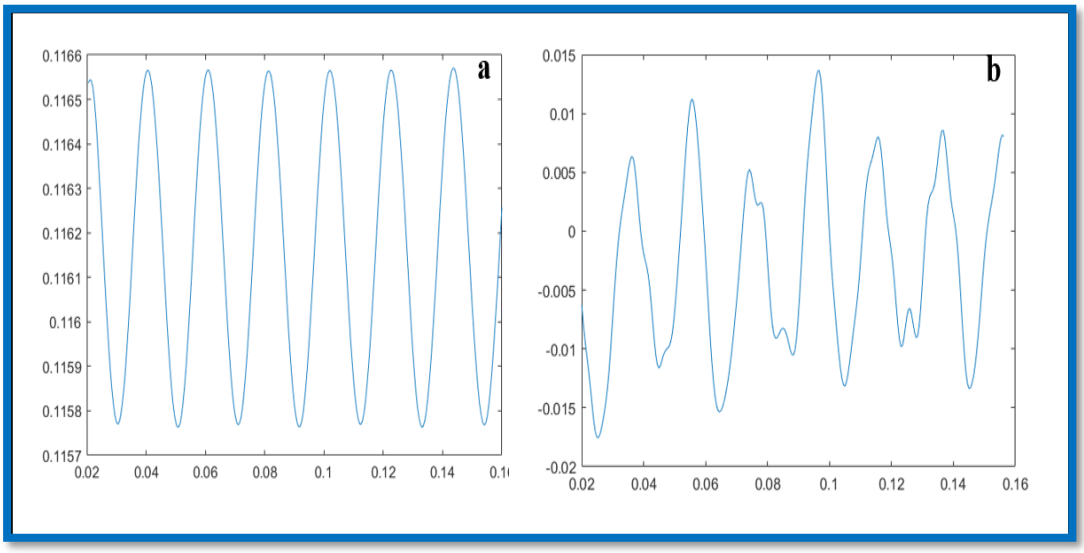

Fig. 14: Parallel misalignment (using Flange coupling at two-pins) responses at the time domine at bearings (DE) in the horizontal direction. [(a) Simulation study; (b) Experimental study at speed 1500rpm].

We note when excitation frequency is increased, the magnitude of vibrational amplitudes increases, **Figure (14)** above shows the responses in the time domain, for machine bearings. for the two studies (Experimental and simulation).

(B) Misalignment using Flange coupling at four-pins.

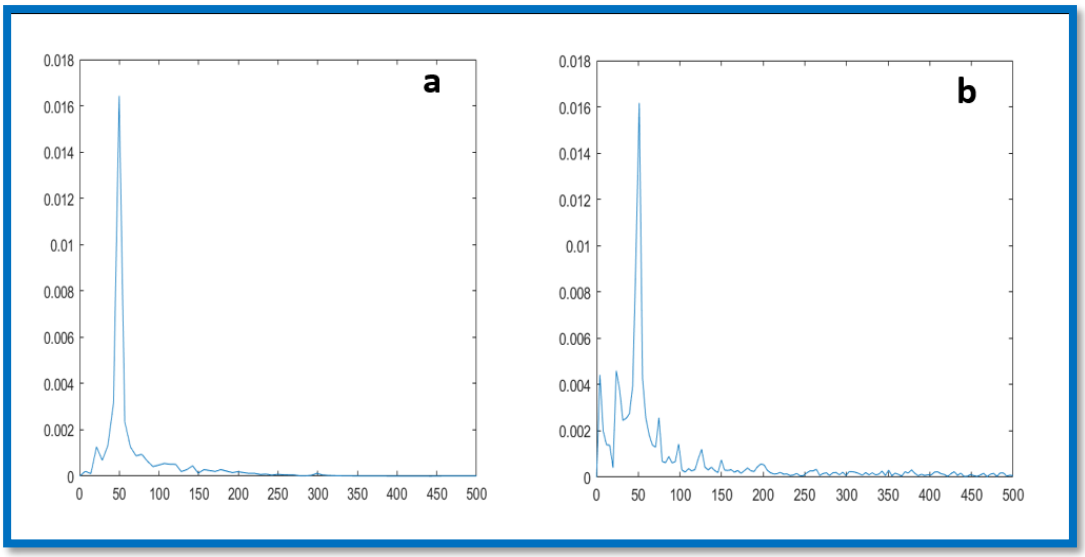

Figure 15: FFT of Parallel misalignment (using flange coupling at four-pins for speed 1500rpm) at the Drive-end in the horizontal direction (DE-H). (a) Simulation study; (b) Experimental study.

Table 2: Overall amplitude for Parallel misalignment using Flange coupling at four-pins in horizontal direction at Drive-end (DE) bearings of the rotor.

Speed (RPM)	Amplitude (mm)		
	Bearing end	Simulation study	Experimental study
		Horizontal (H)	Horizontal (H)
1500 RPM (25HZ)	Drive-end (DE)	0.01612	0.01646

It can be seen from the **Figure (15)** and **Table (2)** the vibration spectra are obtained through experimental and simulation for various excitation frequencies and found to be in close agreement. Results from both the experimental and simulated studies showed that the second harmonics (2X), or twice the shaft running speed in the case of parallel misalignment, best characterize the misalignment.

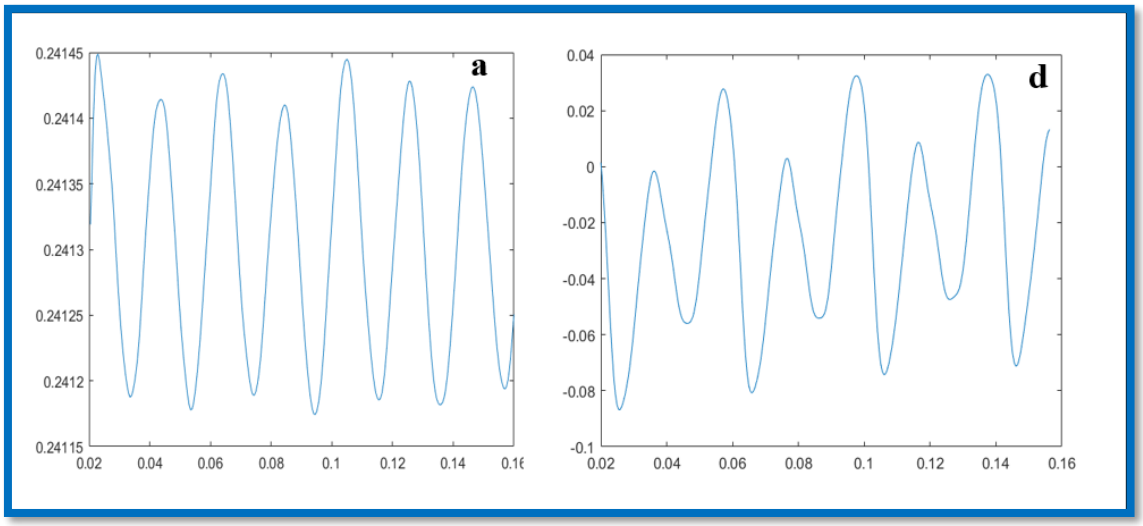

Figure 16: Parallel misalignment responses (using Flange coupling at four-pins) at the time domine at bearings (DE) in the horizontal direction. [(a) Simulation study; (b) Experimental study at speed 1500rpm].

It can also be concluded from the time-domain diagrams shown in **Figure (16)** that the magnitude of the vibrational amplitudes increases with the increase in the excitation frequency. with the prevailing peak remaining (2X). (i.e., 2X the shaft speed).

(C) Misalignment using a Rubber coupling

It can be concluded from the experiment and simulation the vibration spectrum acquired on end bearings (Drive-end (DE)) at a frequency of 25 Hz that the results are in good agreement. Through the FFT diagram shown in the **Figure (17)**, it was found that when using the rubber

material in the coupling tool between the drive shafts of the machine, the frequency did not appear clearly. meaning that the absence of the peak prevailing (2X) as in the previous cases of misalignment. And the reason for that goes back to that the rubber material absorbs the forces of vibration and reduces them to the minimum possible.

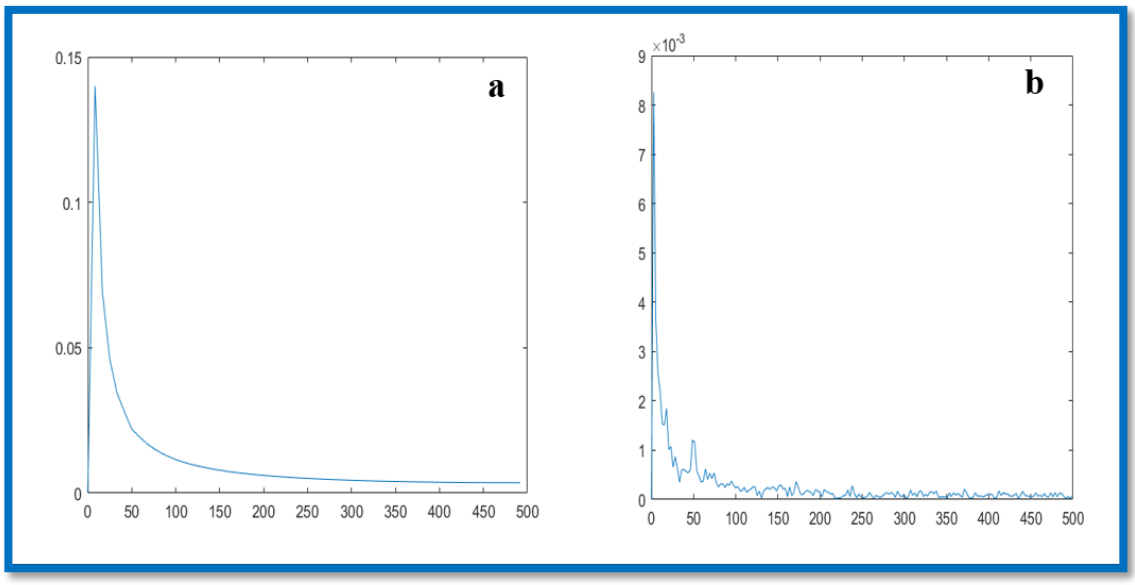

Fig.17: FFT of Parallel misalignment (using a Rubber coupling for speed 1500rpm) at the Drive-end in the horizontal direction (DE-H). (a) Simulation study; (b) Experimental study.

6. Conclusions

the following conclusions can be obtained as a result of the experimental analysis and the theoretical analysis that was used to verify the operating conditions of the vibration characteristics of the rotating mechanical system:

1. For the misalignment case, the vibration spectra are obtained through experimental and simulation for various excitation frequencies and found to be in close agreement. Results from both the experimental and simulated studies showed that the second harmonics (2X), or twice the shaft running speed in the case of parallel misalignment, best characterize the misalignment. In contrast, the amplitude of vibration was much lower in the case of an aligned system. In addition, it can be seen that the amplitude of vibration grows in tandem with the excitation frequency.

2. By conducting the two studies, it was proved that when using rubber material in coupling tool with certain specifications commensurate with the size of the machine and operating conditions, the machine can work without the misalignment defect for a longer period of time

than if the rubber was not used. meaning that the absence of the peak prevailing (2X) as in the previous cases of misalignment.

7. Acknowledgments

sincerely express my deep sense of gratitude to Dr. Jaafar Khalaf Ali for rendering valuable guidance, advice and encouragement in this work. I am thankful to for valuable support and advice.

8. Reference

[1] Khot, S. M., and Pallavi Khaire. "Simulation and experimental study for diagnosis of misalignment effect in rotating system." *Journal of Vibration Analysis, Measurement, and Control* 3.2 (2015): 165-17.

[2] Jalan, Arun Kr, and A. R. Mohanty. "Model based fault diagnosis of a rotor–bearing system for misalignment and unbalance under steady-state condition." *Journal of sound and vibration* 327.3-5 (2009): 604-622.

[3] Dere, Sachin D., and Laxmikant Dhamande. "Rotor bearing system FEA analysis for misalignment." (2017).

[4] Babar, A. C., and A. A. Utpat. "Vibration analysis of misaligned rotating shaft." International Journal of Mechanical Engineering and Information Technology (IJMEIT) 2.6 (2014): 287-294.

[5] Mogal, S. P., and D. I. Lalwani. "Experimental investigation of unbalance and misalignment in rotor bearing system using order analysis." Journal of Measurements in Engineering 3.4 (2015): 114-122.

[6] Gibbons, C. B. "Coupling misalignment forces." Proceedings of the 5th Turbomachinery Symposium. Texas A&M University. Gas Turbine Laboratories, 1976.

[7] Hujare, Deepak P., and Madhuri G. Karnik. "Vibration responses of parallel misalignment in Al shaft rotor bearing system with rigid coupling." *Materials Today: Proceedings* 5.11 (2018): 23863-23871.

[8] Xie, Zhongliang, et al. "Theoretical and experimental investigation on the influences of misalignment on the lubrication performances and lubrication regimes transition of water lubricated bearing." *Mechanical Systems and Signal Processing* 149 (2021): 107211.

[9] Abdulrazzaq A. Abdulrazzaq and Jaffer K. Ali.," Diagnosis of Rotating Machines Faults Using Intelligent Methods "Basrah Journal for Engineering Sciences (2019)

[10] Ameen, Yahya Muhammed, and Jaafar Khalaf Ali. "Flexible rotor balancing without trial runs using experimentally tuned FE based rotor model." *Basrah Journal for Engineering Sciences* 21.1 (2021).

[11] Babar, A. C., and A. A. Utpat. "Vibration analysis of misaligned rotating shaft." International Journal of Mechanical Engineering and Information Technology (IJMEIT) 2.6 (2014): 287-294.

[12] Khot, S. M., and Pallavi Khaire. "Simulation and experimental study for diagnosis of misalignment effect in rotating system." Journal of Vibration Analysis, Measurement, and Control 3.2 (2015): 165-17.

[13] Azeem, Naqash, et al. "Experimental condition monitoring for the detection of misaligned and cracked shafts by order analysis." Advances in Mechanical Engineering 11.5 (2019): 1687814019851307.

[14] Zhang, Hong-xin, et al. "Shaft orbit analysis based on LabVIEW for fault diagnosis of rotating machinery." 2016 11th International Conference on Computer Science & Education (ICCSE). IEEE, 2016.

[15] Smirnova, Tatiana. Analysis, "Modeling and Simulation of Machine Tool Parts Dynamics for Active Control of Tool Vibration". Diss. Blekinge Institute of Technology, 2010.

Al-Kitab Journal for Pure Sciences (2022); 6(2): 65-78.

https://doi.org/10.32441/kjps.06.02.p6

Al-Kitab Journal for Pure Sciences
ISSN: 2617-1260 (print), 2617-8141(online)
https://isnra.net/index.php/kjps

Effect of dual trigger with chorionic gonadotropin hormone and follicle-stimulating hormone on endometrial thickness in infertile women who had superovulation with an aromatase inhibitor

Salwa Sadoon Mustafa[1*], Enas Thamer Mousa[2]

[1]Kirkuk Health Directorate, Iraq

[2]College of Medicine, Al-Nahrain University, Iraq

*Corresponding Author: salwa_sadoon484@yahoo.com

Citation: Mustafa, S. S., Mousa, E. T. Effect of dual trigger with chorionic gonadotropin hormone and follicle-stimulating hormone on endometrial thickness in infertile women who had superovulation with an aromatase inhibitor. Al-Kitab Journal for Pure Sciences (2022); 6(2): 65-78.
DOI: https://doi.org/10.32441/kjps.06.02.p6

Keyword
Dual trigger, Beta HCG, Endometrial thickness, Infertility, an Aromatase inhibitor.

Article History

Received	15 Oct. 2022
Accepted	25 Nov. 2022
Available online	30 Jan. 2023

Abstract:

Beginning in October 2020 and ending in April 2021, researchers from Al-Nahrain University's High Institute for Infertility Diagnosis and Assisted Reproductive Technologies compared the success rates of two different methods of diagnosing and treating infertility. The major purpose of the research was to assess the impact of a combined trigger (follicle-stimulating hormone [FSH] and human chorionic gonadotropin [hCG]) on endometrial receptivity (endometrial thickness, endometrial pattern, sub-endometrial blood flow). A total of 100 females took part in the study. All patients gave their informed written consent, and the study was approved by the Al-Nahrain University Ethics Committee. Procedure Time To confirm ovulation, measure and analyze the endometrial pattern, and examine the sub-endometrial blood flow, a vaginal ultrasound was done 36 to 48 hours following trigger

ovulation. All four hormones (FSH, LH, Progesterone, and E2) were tested in the blood at the same time to determine whether a couple was fertile, a complete medical history, and physical examination whereas performed on each member of the pair. An ultrasound vaginal probe was used to do the transvaginal examination. Patients were placed in the dorsal lithotomy position with an empty bladder for early follicular US (CD 2-3) to assess the number of antral follicles, measure endometrial thickness, and rule out ovarian cysts or other pathology. A second ultrasound was performed during the middle of the cycle (CD9-14) to determine whether a mature follicle had been found. A multiplanar image of the uterus was acquired after an ultrasound scan was swept across the mid-sagittal plane. Endometrial thickness in the median longitudinal plane of the uterus was calculated as the largest distance from one basal endometrial interface via the endometrial canal to the opposite endometrial-myometrial interface of the anterior-posterior uterine wall. A statistically significant difference was found between Group A's average E2 concentration of 69.62 pg/mL and Groups B and C's concentrations of 53.32 and 36.65 pg/mL. (P 0.001). In group C, there was a statistically significant difference in E2 levels on the day of the trigger and the day of the IUI (P = 0.036). On the day of IUI compared to the day of trigger, no statistically significant differences were seen between the study groups for any of the other hormonal indicators (P > 0.05). There were no significant differences (P > 0.05) in any of the baseline clinical measures between the research groups. All clinical indicators were comparable across groups (P > 0.05). There were no statistically significant differences (P > 0.05) between the research groups on any other clinical indicators. When comparing groups, A, B, and C on the decline in RI between the trigger and IUI days, group A significantly outperformed the others (P = 0.003). There was no statistically significant difference (P > 0.05) in any of the other clinical parameters between the IUI and trigger groups on the day of IUI.

Keywords: Dual trigger, Beta HCG, Endometrial thickness, Infertility, an Aromatase inhibitor.

تأثير الزناد المزدوج مع هرمون موجهة الغدد التناسلية المشيمية والهرمون المنبه للجريب على سمك بطانة الرحم لدى النساء المصابات بالعقم اللائي لديهن إباضة مفرطة مع مثبطات أروماتيز

سلوى سعدون مصطفى*[1]، إيناس ثامر موسى[2]

[1]دائرة صحة كركوك العراق

[2]جامعة النهرين العراق

*salwa_sadoon484@yahoo.com

الخلاصة:

بدءًا من أكتوبر ٢٠٢٠ وانتهى في أبريل ٢٠٢١ ، قارن باحثون من المعهد العالي لتشخيص العقم والتقنيات المساعدة على الإنجاب في جامعة النهرين معدلات نجاح طريقتين مختلفتين لتشخيص وعلاج العقم. كان الغرض الرئيسي من البحث هو تقييم تأثير المحفز المركب (الهرمون المنبه للجريب [FSH] والغدد التناسلية المشيمية البشرية [HCG]) على تقبل بطانة الرحم (سمك بطانة الرحم ، نمط بطانة الرحم ، تدفق الدم تحت بطانة الرحم). شارك في الدراسة مجموع ١٠٠ أنثى. أعطى جميع المرضى موافقتهم الخطية المستنيرة ، وتمت الموافقة على الدراسة من قبل لجنة الأخلاقيات بجامعة النهرين. وقت الإجراء لتأكيد الإباضة وقياس وتحليل نمط بطانة الرحم وفحص تدفق الدم تحت بطانة الرحم ، تم إجراء الموجات فوق الصوتية المهبلية بعد ٣٦ إلى ٤٨ ساعة من بدء الإباضة. تم اختبار الهرمونات الأربعة (FSH وLH وPROGESTERONE وE٢) في الدم في نفس الوقت. من أجل تحديد ما إذا كان الزوجان يتمتعان بالخصوبة أم لا ، تم إجراء تاريخ طبي كامل وفحص جسدي لكل فرد من الزوجين. تم استخدام مسبار الموجات فوق الصوتية المهبلي لإجراء الفحص المهبلي. تم وضع المرضى في وضع استئصال الحصاة الظهرية مع وجود مثانة فارغه مع فحص الجريبات في جهاز الموجات فوق الصوتية(CD 2-3) لتقييم عدد البصيلات الغارية ، وقياس سمك بطانة الرحم ، واستبعاد أكياس المبيض أو غيرها من الأمراض. تم إجراء الموجات فوق الصوتية الثانية خلال منتصف الدورة (CD9-14) لتحديد ما إذا كان قد تم العثور على جريب ناضج أم لا. تم العثور على فرق معتد به إحصائيًا بين متوسط تركيز E2 للمجموعة A البالغ ٦٩,٦٢ بيكوغرام / مل وبين تركيزات المجموعتين B وC البالغة ٥٣,٣٢ و ٣٦,٦٥ بيكوغرام / مل. (ص ٠,٠٠١). في المجموعة C ، كان هناك فرق ذو دلالة إحصائية في مستويات E2 في يوم المشغل ويوم IUI (P = 0.036). في يوم IUI مقارنة بيوم التحفيز، لم تُلاحظ فروق ذات دلالة إحصائية بين مجموعات الدراسة لأي من المؤشرات الهرمونية الأخرى (P> 0.05). لم تكن هناك فروق ذات دلالة إحصائية (P> 0.05) في أي من التدابير السريرية الأساسية بين مجموعات البحث. كانت جميع المؤشرات السريرية قابلة للمقارنة عبر المجموعات (P> 0.05). لا توجد فروق ذات دلالة إحصائية (P> 0.05) بين مجموعات البحث على أي مؤشرات سريرية أخرى. عند مقارنة المجموعات A وB وC عند الانخفاض في RI بين أيام التحفيز وأيام IUI ، تفوقت المجموعة A بشكل كبير على المجموعات الأخرى (P = 0.003). لم يكن هناك فرق ذو دلالة إحصائية (P> 0.05) في أي من المعلمات السريرية الأخرى بين IUI ومجموعات التحفيز في يوم IUI.

الكلمات المفتاحية: التحفيز المزدوج. HCG بيتا ؛ سمك بطانة الرحم العقم. مثبط أروماتيز.

1. INTRODUCTION:

Despite merely providing exposure equivalent to LH, HCG is an effective oocyte maturation inducer, indicating that the mid-cycle FSH surge ordinarily present in the natural cycle is not necessary for successful oocyte maturation. Comparing the benefits of GnRHa and kisspeptin to those of hCG and rLH, one is that they may promote the concurrent synthesis of FSH as well as LH-like activity. FSH may promote nuclear tissue maturation, cumulus expansion, and the synthesis of LH receptors in luteinizing granulosa cells [1]. Positive and negative feedback mechanisms are responsible for the regulation of the ovulatory cycle. The pattern of secretion of kisspeptin, gonadotrophin-releasing hormone (GnRH), follicle-stimulating hormone (FSH), and luteinizing hormone (LH) is regulated by steroid sex hormones generated by the ovaries. These hormones in turn affect how ovarian hormones are released. The rupture and release of the dominant follicle from the ovary into the fallopian tube, where it has the potential to be fertilized, is what is known as ovulation. Ovulation is a physiological process. Ovulation is the process through which the dominant follicle is discharged into the fallopian tube. Throughout the ovulation process, the gonadotropic hormones (FSH and LH) are what regulate when an egg is released [2]. The consequences of a midcycle increase in FSH include induction of plasminogen activity, promotion of LH receptor synthesis in luteinizing granulosa cells, nuclear maturation, and cumulus expansion. Research conducted on animals has demonstrated that FSH is capable of stimulating ovulation. Ovulation was produced in hypophysectomized rats using LH-free recombinant FSH, and as a result, a dose-dependent ovulation rate of one hundred percent was achieved [3]. The follicle-stimulating hormone also contributes to the preservation of open gap junctions between the cumulus cells and the oocyte. This hormone may thus be essential to the signaling cascades [4]. It is believed that FSH collaborates with other hormones to set the stage for ovulation to occur once an egg has fully matured [2]. An intrauterine insemination is a treatment option for couples with moderate to severe male factor infertility when the female spouse has at least one intact tube. The effectiveness of this kind of assisted reproduction is limited by several parameters, which have been the subject of decades' worth of study. Semen quality, female etiology, synchronization with ovulation, evaluation of follicle rupture, number of inseminations each cycle, and the impact of uterine contractions are some of these criteria. These elements must be present for a good result. When all other factors are considered, satisfactory outcomes can be achieved using intrauterine insemination, which is a method that is both less intrusive and less expensive than in vitro fertilization [5]. To evaluate if endometrial receptivity indicators might be enhanced by

using a dual trigger (FSH and hCG) (endometrial thickness, endometrial pattern, sub-endometrial blood flow).

2. Materials and Methods

A prospective comparative study was conducted at the High Institute for Infertility Diagnosis and Assisted Reproductive Technologies, Al-Nahrain University, from October 2020 to April 2021. A hundred women were included in this study. Every patient gave her written informed consent before taking part in the study, which was approved by the Ethics Committee, Al-Nahrain University. One hundred and one women were recruited from the patient population of the consultant clinic at the High Institute for Infertility Diagnosis and Assisted Reproductive Technologies for this research.

Exclusion criteria: All medical disorders that are incompatible with pregnancy, such as endometriosis, ovarian cysts, bilateral tubal obstructions, and acute genital tract infection in either parent or others, are prohibited.

Methods.

All The women who participated in the research were asked detailed questions about their obstetrical and gynecological histories, as well as information on their experiences with infertility and loss in the past. One should have a complete physical and a gynecological checkup. investigation of tubal patency through hysterosalpingogram or laparoscopy; vaginal ultrasound; hormonal test in CD3; infertility workup. The spouse was also given a complete medical history and his seminal fluid was analyzed; the results of the seminal fluid examination were evaluated by WHO 2010 standards. The aromatase inhibitor pill (Gynotril 2.5 mg), which was administered orally twice daily at intervals of 12 hours starting on day 3 and continuing for a total of five days, was given to the women who participated in the trial. At CD3, a hormonal test (including FSH, LH, Progesterone, prolactin, E2, and AMH), as well as an evaluation of antral follicle counts and endometrial thickness using ultrasound, were performed. Starting on day 9, a serial ultrasound was performed every other day until at least one developed follicle measuring less than 17 millimeters in diameter was found. On the day before the trigger, every patient has another round of hormonal testing, including LH, FSH, E2, and progesterone. Another evaluation for sub-endometrial blood flow, endometrial pattern, and endometrial thickness Patients are divided into three categories according to the kind of triggers they experience:

1 .Group A: women in the research group were given injections of both a dual trigger and an (Ovitrelle 250 mg plus FSH 150 IU Gonal f).

2 .Group B: On the day of the trigger, women in the trial group were given an injection containing both Ovitrelle (250 mg) and follitropin-stimulating hormone (75 IU).

3 .Group C: Only female participants were given Ovitrelle (250 mg).

To confirm ovulation on the day of the IUI, vaginal ultrasound was carried out between 36 and 48 hours after the ovulation trigger was administered This was done by measuring the endometrium and analyzing its significance as well as by determining how much blood is flowing outside of the uterine lining. A blood sample was taken that day to do a hormonal assay to identify FSH, LH, progesterone, and E2. The normal hormonal levels that were employed in the investigation are listed in **Table 1**. On the day of the IUI, the patient started using a progesterone vaginal suppository with 400 mg daily to aid in the luteal phase. This treatment lasted for two weeks. (In the United Kingdom, Cyclogest® 400mg is sold under the name "Cyclogest"). Beta human chorionic gonadotropin estimation 14 days after in vitro fertilization.

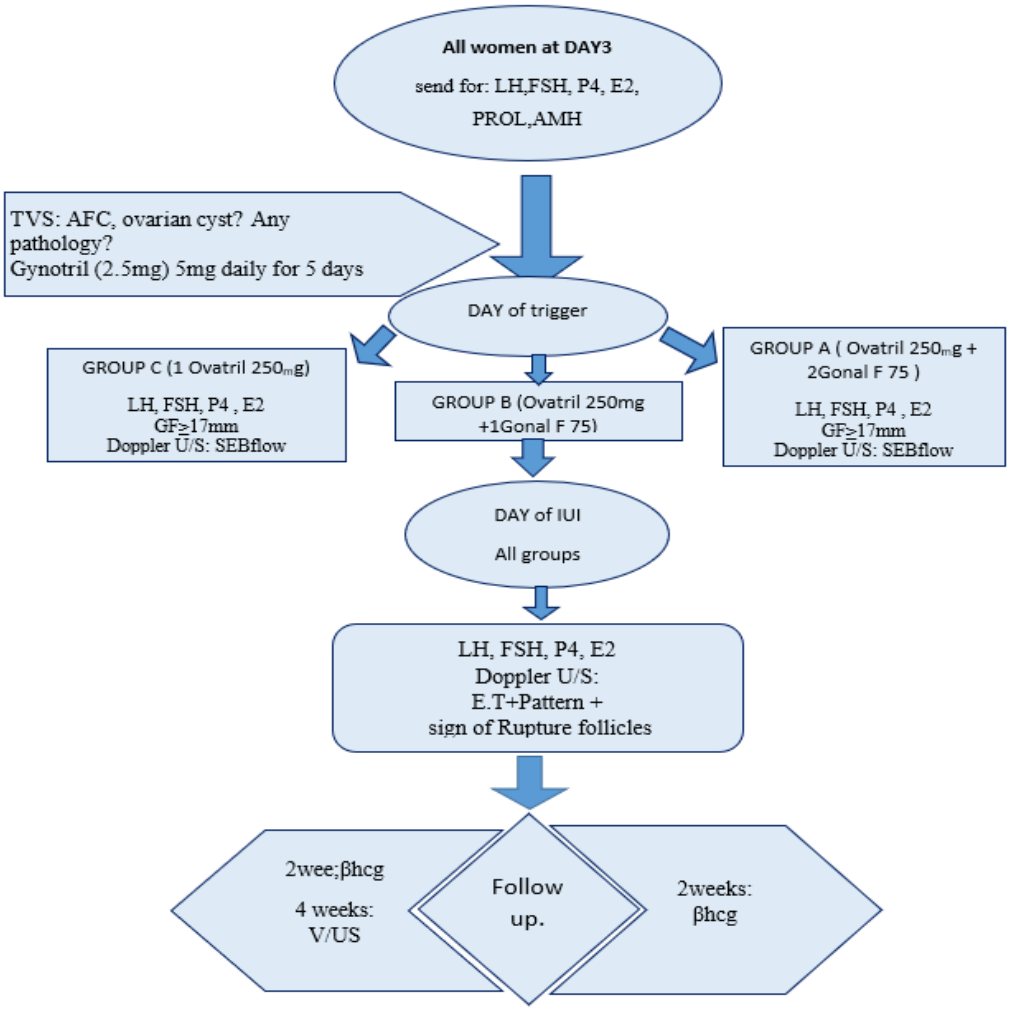

Figure 1: Study design

Before being accepted into the study, every pair was given an infertility test that included a careful history and physical examination, as well as the age of the female and the male spouse. The length of infertility and its underlying reason, menstruation history, prior pregnancies and losses, history of illnesses, use of cigarettes, medicines, or surgery, and any previous infertility diagnoses or treatments, such as IUI or IVF. Knowing the person's sexual history, including how often they have sexual encounters and if they have ever used birth control, is also crucial. Then, we obtained the patients' duly written informed permission.

On cycle day 3, a blood sample was taken from each woman as part of the workup to get a baseline measurement of the hormones FSH, LH, E2, progesterone, AMH, and prolactin. As part of the workup, this was completed. Additionally, a thyroid function test, often referred to as TSH, will be carried out as a screening for thyroid function. Serum LH, FSH, E2, and progesterone levels were assessed on the day when ovulation was triggered (days 11–14). When the ovulation was verified, a second blood sample was taken on the day of the IUI (36–48 hours after the triggering) and utilized for hormonal analysis (FSH, LH, Progesterone, E2).

The transvaginal scan was completed by using the ultrasound device's vaginal probe (vinno35, china). After placing patients in the dorsal lithotomy posture with an empty bladder, an early follicular ultrasound (CD 2-3) was carried out to count the number of antral follicles, gauge the thickness of the endometrium, and rule out the presence of ovarian cysts or other pathologies. The ultrasound was then performed once again in the middle of the cycle (CD9–14) to see whether a mature follicle had been discovered. A sweep of the mid-sagittal plane of the uterus was performed after employing an ultrasound device to provide a multiplane display. The greatest distance from one basal endometrial interface through the endometrial canal to the opposing endometrial-myometrial interface of the anterior to the posterior wall of the uterus was used to determine the endometrial thickness, which was measured in the median longitudinal plane of the uterus. This measurement was made between the uterus' anterior and posterior walls). There must be at least one dominant follicle that is greater than 17 millimeters in diameter for an IUI procedure to be successful. Additionally, as shown in **Figure 1**, a triple-line pattern and an ET of less than 8 millimeters are strongly associated with successful implantation. (3.4). Depending on how it appeared, the pattern of the endometrium was classified as multilayered or non-multilayered. A Type A triple-line pattern, with hyperechogenic outer lines, a distinct core echogenic line, and hypoechogenic or dark patches in between these lines, represented a multilayered endometrium. It was observed that the center echogenic line was well delineated. neutral in attitude (same reflectivity of the endometrium as

the surrounding myometrium and poorly defined central echogenic line-Type B), A homogeneous endometrial pattern that is either hyperechogenic or echogenic makes up one kind of endometrium, called a non-multilayered endometrium.

For endometrial assessment, a sonographic examination of endometrial thickness and texture has been employed. Every ultrasound exam I've seen has included switching to color Doppler once a longitudinal picture of the uterus has been taken. Our ability to identify the sub-endometrial blood flow distribution pattern was made possible using pulsating color signals shown in the sub-endometrial and endometrial regions. those patients who have vascularization that has penetrated the sub endometrium. Zone 1 included vessels that entered the outer hypoechogenic area surrounding the endometrium but did not penetrate the hyperechogenic outer margin; Zone 2 included vessels that entered the hyperechogenic outer margin but did not penetrate the hypoechogenic inner area; Zone 3 included vessels that entered the hypoechogenic inner area; and Zone 4 included vessels that reached the central echogenicity of the endometrium.

After that, Doppler sonography was done on the blood vessels that had the most prominent coloration within the innermost part of the endometrial and sub-sub-endometrial. After ensuring that there were no gaps in the waveforms, a cardiac cycle average of three to five beats was selected to calculate the resistance index (RI) and the pulsatility index (PI). We took three separate readings for each parameter, and then we calculated the average of those readings. The resistance index (RI) and pulsatility index (PI) of the sub-endometrial arteries were automatically calculated by ultrasonography. The sub-endometrial zone was regarded to be within 1 mm of the myometrial–endometrial contour when it was first described. When a patient's medical history or physical examination revealed evidence of previous damage to the Fallopian tube as a result of pelvic inflammatory disease (PID) or previous surgery, endometriosis, hysterosalpingography, and/or laparoscopy were performed to evaluate the tube's patency, and determine whether or not it was intact. In addition, congenital deformities of the uterus, such as a bicornuate uterus, were not taken into consideration.

3. Results

All hormonal markers (**Table 1**) showed no statistically significant differences ($P>0.05$) between research groups.

Table 1: Indicator-day clinical parameter comparisons between study groups

Clinical parameter On the day of the trigger	Study group			P - Value
	A Mean ± SD	B Mean ± SD	C Mean ± SD	
LH (IU/L)	15.49 ± 10.6	14.11 ± 8.5	17.96 ± 14.5	**0.386**
FSH (IU/L)	5.92 ± 2.6	6.05 ± 3.3	6.2 ± 4.7	**0.954**
Progesterone (ng/mL)	0.38 ± 0.38	0.35 ± 0.36	0.55 ± 0.38	**0.073**
E2 (pg/mL)	195.33 ± 98.7	183.78 ± 99.5	160.54 ± 79.8	**0.271**

The table below compares the hormonal parameters of the study groups on the day of IUI (2). With a median of 6.98 IU/L, group C's FSH was significantly lower than groups A and B's (9.06 and 9.3 IU/L, respectively; P=0.031). A statistically significant difference was found between Group A's average E2 concentration of 69.62 pg/mL and Groups B and C's concentrations of 53.32 and 36.65 pg/mL. (P 0.001). No significant changes between groups were seen for any of the other hormonal variables (P> 0.05).

Table 2: Clinical parameters on the day of IUI compared across research groups.

Clinical parameter On the day of IUI	Study group			P - Value
	A Mean ± SD	B Mean ± SD	C Mean ± SD	
LH (IU/L)	19.96 ± 11.1	24.65 ± 11.5	22.01 ± 12.4	**0.24**
FSH (IU/L)	9.06 ± 3.7	9.3 ± 4.3	6.98 ± 3.02	**0.031**
Progesterone (ng/mL)	1.78 ± 1.4	1.87 ± 1.7	2.14 ± 1.6	**0.655**
E2 (pg/mL)	69.62 ± 45.0	53.32 ± 33.1	36.65 ± 24.0	**0.001**

When comparing E2 levels on the day of the trigger to the day of the IUI, we found that in group C, the difference was statistically significant (P=0.036). All other hormonal markers showed no statistically significant variation between research groups on the day of IUI compared to the day of trigger (P> 0.05).

Table 3: Clinical parameter comparison between IUI and trigger day in terms of % change

What difference between IUI day and trigger day as a percentage	Study group			P - Value
	A Mean ± SD	B Mean ± SD	C Mean ± SD	
LH	72.45 ± 104.8	124.75 ± 138.6	89.88 ± 138.8	**0.22**
FSH	70.29 ± 74.2	80.57 ± 83.9	47.68 ± 79.9	**0.247**
Progesterone	734.66 ± 865.7	629.07 ± 609.9	455.08 ± 506.6	**0.271**
E2	- 61.23 ± 24.2	- 67.17 ± 19.2	- 74.13 ± 18.2	**0.036**

The comparison in baseline clinical parameters between study groups is shown in **Table 4**. No statistically significant differences (P≥ 0.05) between study groups regarding all baseline clinical parameters.

Table 4: Comparison in baseline clinical parameters (at cycle day 2) between study groups

Baseline clinical parameter	Study group			P - Value
	A Mean ± SD	B Mean ± SD	C Mean ± SD	
AFC (Count)	12.31 ± 3.9	13.81 ± 3.8	12.1 ± 2.9	**0.099**
Endometrial thickness (mm)	4.73 ± 0.9	4.56 ± 1.0	4.78 ± 1.2	**0.665**

The comparison in clinical parameters between study groups on the day of the trigger is shown in **Table 8**. No significant differences between study groups (P ≥ 0.05) in all clinical parameters.

Table 5: Comparison between study groups in clinical parameters on the day of the trigger

Clinical parameter on the day of the trigger	Study group			P - Value
	A Mean ± SD	B Mean ± SD	C Mean ± SD	
Endometrial thickness (mm)	8.06 ± 1.5	8.15 ± 1.5	8.23 ± 2.0	**0.919**
Resistance Index	0.62 ± 0.07	0.59 ± 0.04	0.59 ± 0.06	**0.092**
Pulsatile Index	1.07 ± 0.2	1.04 ± 0.2	1.01 ± 0.2	**0.553**
S/D	2.65 ± 0.5	2.52 ± 0.3	2.53 ± 0.3	**0.311**
Follicle number	1.28 ± 0.5	1.51 ± 0.5	1.34 ± 0.5	**0.145**
Endometrial pattern No. (%) No. (%) No. (%)				
hypoechoic endometrium A	25 (71.4)	24 (64.9)	20 (69.0)	**0.694**
Isoechoic endometrium B	10 (28.6)	13 (35.1)	9 (31.0)	

Clinical parameters comparing research groups on the day of IUI are shown in **Table 6**. All other clinical measures showed no significant group differences (P > 0.05).

Table 6: Clinical parameters on the day of IUI compared across study groups.

Clinical parameters on the day of IUI	Study group			P - Value
	A Mean ± SD	B Mean ± SD	C Mean ± SD	
Endometrial thickness (mm)	9.76 ± 1.5	9.32 ± 1.6	8.9 ± 1.8	**0.115**
Resistance Index	0.58 ± 0.07	0.61 ± 0.06	0.57 ± 0.06	**0.074**
Pulsatile Index	1.0 ± 0.19	1.03 ± 0.18	0.95 ± 0.2	**0.286**
S/D	2.51 ± 0.5	2.6 ± 0.4	2.35 ± 0.4	**0.067**
Endometrial pattern No. (%) No. (%) No. (%)				
B	33 (94.3)	34 (91.9)	27 (93.2)	**0.542**
A	2 (5.7)	3 (8.1)	2(6.8)	

Table 7 shows the percentage change between the day of IUI and the day of the trigger for each research group. Also, in comparison to the day of the trigger, RI was lower in group A on the day of IUI (P= 0.003) than in either of the other two groups (B and C). All other clinical parameters showed no statistically significant difference between research groups on the day of IUI compared to the day of trigger (P> 0.05).

Table 7: A cross-sectional research comparing several clinical parameters on the day of IUI and the day of trigger across the study groups.

Difference between IUI day and trigger day as a percentage	Study group			P - Value
	A Mean ± SD	B Mean ± SD	C Mean ± SD	
Endometrial thickness	22.98 ± 18.6	15.94 ± 17.5	9.43 ± 11.3	**0.006**
Resistance Index	- 6.21 ± 9.4	- 3.14 ± 13.3	3.13 ± 11.5	**0.003**
Pulsatile Index	- 4.91 ± 14.3	1.77 ± 21.0	- 3.36 ± 24.1	**0.337**
S/D	- 3.17 ± 21.1	4.08 ± 18.6	- 6.27 ± 16.0	**0.073**

4. Discussion

Baseline hormonal parameters for each study group are shown in **Table 1** below. All the studied groups showed similar levels of FSH, LH, progesterone, and estradiol at baseline, with no statistically significant differences (P values 0.05) between the groups. Similar research conducted by **[6]** Younis et al. and Mahajan et al. **[7]** found no statistically significant differences in demographics (age, BMI, baseline FSH, LH, and AMH levels) or infertility risk factors (causes). Baseline variables including age, BMI, basal FSH, and LH did not vary substantially across groups, demonstrating this. Declare et al. **[8]** found no statistically significant difference in the time course of hormone changes between the two groups when comparing estradiol and progesterone levels on a triggering day. Both hormones shared this property. This can be explained by the fact that all the participants in the research took the same drug during the induction phase. Our findings agreed with those found in a different study carried out by Lamb, **[2]**. Women who underwent a prolonged GnRHa regimen were included in this trial, and an FSH supplement was administered around the time of the hCG trigger. Increased blood FSH levels were reported in both investigations, however, one research did so before oocyte extraction and the other after. Researchers in this research took into account the fact that women often have greater FSH levels in their blood on the day of oocyte extraction than they do on the day before the procedure. Another study found that a decrease in E levels after hCG administration did not alter pregnancy outcomes. The number of eggs that were

recovered, the number of mature oocytes, and the fertilization rates were all unaffected by the decrease in E. [9]. According to the findings of Chiasson [10], a drop in E2 levels following the injection of hCG for 24 hours did not affect the results of the pregnancy. The number of eggs that were recovered, the number of mature oocytes, and the fertilization rates were all unaffected by the decrease in E2. As no significant difference in implantation rates was revealed with either an increase or decrease in E levels following hCG injection, it seems that estradiol levels do not play a role in priming the endometrium for implantation. In addition, there was no correlation between endometrial receptivity priming and estrogen concentrations.

According to the findings of morad [11], letrozole is an effective second-line therapy for women with poor endometrial response to CC. This is because letrozole enhanced endometrial thickness in a trilaminar pattern and improved endometrial perfusion. When comparing the endometrial thickness of group A to that of groups B and C on the day of IUI, group A demonstrated a considerably greater rise (P = 0.006) and a significantly greater drop (P = 0.003) in endometrial thickness than group B and C did. This may be understood by considering the simultaneous rise in the E2 level that was discovered previously in this study. It was discovered by Ciechanowska et al. [12] that many different variables had been evaluated as potential predictors of endometrial thickness. In women, these variables include age, BMI, total exogenous FSH/highly purified human menopausal gonadotrophin dosage, ovarian stimulation time, and oestradiol and progesterone levels during the late follicular phase. This explains why our research indicated that there was an increase in endometrial thickness when the fish bolus dose was detected at the time of the trigger.

When comparing the RI in Group A on the day of IUI to the RI in Groups B and C on the day of the trigger, the researchers observed that Group A had a statistically significant drop in sub-endometrial blood flow (P = 0.003). To explain this finding, Ng et al. demonstrated that increased blood E2 concentration during ovarian stimulation causes vasodilation, particularly in the myometrium (2007). Blood flow in the uterus, endometrium and sub-endometrium are all linked during normal, stimulated menstrual cycles. The endometrium and sub-endometrium get less blood supply during ovarian stimulation. It was discovered that monitoring uterine blood flow is not an accurate surrogate for endometrial blood flow[13], even during stimulated cycles found that rFSH and uFSH were able to differently influence the gene expressions in human endometrial stromal cells that were cultivated in vitro[14]. According to the findings of their research, fsh has several beneficial effects on the expression of genes involved in implantation, including an increase in endometrial receptivity. Aromatase transcription was

also found in the endometrium of individuals who were unable to conceive, even though the levels were quite variable between samples. As a result, FSH may affect endometrial aromatase, leading to an increase in local estrogen production. After using the FSH/LH trigger, endometrial receptivity indicators were found to have greatly increased, despite an increase in endometrial thickness and a large reduction in resistance index. Since it considerably increases endometrial thickness, the dual trigger FSH / LH might be a viable alternative therapy for individuals who have a thin endometrium. Both the examination of sub-endometrial blood flow by 2D ultrasonography and the determination of follicle development are important aspects of the procedure. More studies are required to compare the success rate of pregnancy in women with normal endometrial thickness to those in women with thin endometrium when using the dual triggerfish/lh.

5. Reference

[1] Thurston L, Abbara A, Dhillo WS. Investigation and management of subfertility. Journal of clinical pathology. 2019 Sep 1;72(9):579-87.

[2] Lamb JD, Shen S, McCulloch C, Jalalian L, Cedars MI, Rosen MP. Follicle-stimulating hormone administered at the time of human chorionic gonadotropin trigger improves oocyte developmental competence in vitro fertilization cycles: a randomized, double-blind, placebo-controlled trial. Fertility and sterility. 2011 Apr 1;95(5):1655-60.

[3] Dosouto C, Haahr T, Humaidan P. Gonadotropin-releasing hormone agonist (GnRHa) trigger–state of the art. Reproductive biology. 2017 Mar 1;17(1):1-8.

[4] Erb TM, Vitek W, Wakim AN. Gonadotropin-releasing hormone agonist or human chorionic gonadotropin for final oocyte maturation in an oocyte donor program. Fertility and sterility. 2010 Jan 15;93(2):374-8.

[5] Huang J, Lu X, Lin J, Wang N, Lyu Q, Gao H, Cai R, Kuang Y. A higher estradiol rise after dual trigger in progestin-primed ovarian stimulation is associated with a lower oocyte and mature oocyte yield in normal responders. Frontiers in endocrinology. 2019 Oct 9;10:696.

[6] Younis JS, Soltsman S, Izhaki I, Radin O, Bar-Ami S, Ben-Ami M. Early, and short follicular gonadotropin-releasing hormone antagonist supplementation improves the meiotic status and competence of retrieved oocytes in vitro fertilization–embryo transfer cycles. Fertility and sterility. 2010 Sep 1;94(4):1350-5.

[7] Mahajan N, Sharma S, Arora PR, Gupta S, Rani K, Naidu P. Evaluation of dual trigger with gonadotropin-releasing hormone agonist and human chorionic gonadotropin in improving oocyte maturity rates: a prospective randomized study. Journal of human reproductive sciences. 2016 Apr;9(2):101.

[8] Decleer W, Osmanagaoglu K, Seynhave B, Kolibianakis S, Tarlatzis B, Devroey P. Comparison of hCG triggering versus hCG in combination with a GnRH agonist: a

prospective randomized controlled trial. Facts, views & vision in ObGyn. 2014;6(4):203.

[9] Kondapalli LA, Molinaro TA, Sammel MD, Dokras A. A decrease in serum estradiol levels after human chorionic gonadotrophin administration predicts significantly lower clinical pregnancy and live birth rates in vitro fertilization cycles. Human reproduction. 2012 Sep 1;27(9):2690-7.

[10] Chiasson MD, Bates GW, Robinson RD, Arthur NJ, Propst AM. Measuring estradiol levels after human chorionic gonadotropin administration for in vitro fertilization is not clinically useful. Fertility and sterility. 2007 Feb 1;87(2):448-50 .

[11] Mustafa SS, Mousa ET. Effect of Dual Trigger with Follicle Stimulating Hormone and Chorionic Gonadotropin Hormone on Ovulation Rate in Infertile Women received Aromatase Inhibitor Superovulation in Kirkuk City, Iraq.

[12] Ciechanowska, M., Łapot, M., Antkowiak, B., Mateusiak, K., Paruszewska, E., Malewski, T., Paluch, M. and Przekop, F., 2016. Effect of short-term and prolonged stress on the biosynthesis of gonadotropin-releasing hormone (GnRH) and GnRH receptor (GnRHR) in the hypothalamus and GnRHR in the pituitary of ewes during various physiological states. Animal reproduction science, 174, pp.65-72.

[13] O'neill KE, Senapati S, Dokras A. Use of gonadotropin-releasing hormone agonist trigger during in vitro fertilization is associated with similar endocrine profiles and oocyte measures in women with and without polycystic ovary syndrome. Fertility and sterility. 2015 Jan 1;103(1):264-9.

[14] Qiu Q, Huang J, Li Y, Chen X, Lin H, Li L, Yang D, Wang W, Zhang Q. Does an FSH surge at the time of hCG trigger improve IVF/ICSI outcomes? A randomized, double-blinded, placebo-controlled study. Human Reproduction. 2020 Jun 1;35(6):1411-20.